Characteristics of Freestanding Self-written Polymer Waveguides Fabricated between Single Mode Optical Fibres

Mohammed, Pshko

Award date:
2017

Awarding institution:
University of Bath

Characteristics of Freestanding Self-written Polymer Waveguides Fabricated between Single Mode Optical Fibres

Pshko A. Mohammed

Submitted for the degree of Doctor of Philosophy

2017

Centre for Photonics and Photonic Materials
Department of Physics
University of Bath

For Derin,

&

Elan.

Abstract

Freestanding self-written polymer waveguides were fabricated between two single mode fibres by using free radical photopolymerization technique. Photo curing enables modification of the initial liquid monomer at the illuminated part of the photopolymerizable system to form a permanent solid polymer waveguide between the cores of the fibres. Three compound acrylate based monomer (PETA) and Norland optical adhesives (NOA) were used to fabricate polymer bridges. The two systems are cured by visible and UV respectively. The optical, mechanical and nonlinearity properties of freestanding self-written polymer waveguides were investigated.

Polymer waveguides up to 600 µm long between two fibres were fabricated by unidirectional illumination. The optical power required for photopolymerization is sufficiently low that it is possible to use incoherent light source instead of laser, which also allows investigation of the optical transmission over a wide range of wavelengths from visible to NIR. Optical characterization showed that PETA waveguides have better optical transmission and insertion loss of about 1.2 dB was measured for the bridges up to 600 µm long at 1550nm. Some limitations prevented us to extend waveguide's length beyond 600 µm, the bridges also showed poor adhesion quality particularly at the polymer/fibre interfaces which needed an action. In order to improve mechanical properties of polymer waveguides also to overcome bonding failure between fibre and polymer, the fibres were treated with adhesion promoter. The treatment together with bidirectional curing from both fibres improved mechanical and optical properties of the polymer waveguides. The insertion loss was reduced to 0.6 dB associated with bi-directionally cured 600 µm long waveguide.

Nonlinear response of polymer waveguides was measured by coupling a high power ultra short pulse laser. Using bidirectional curing and inserting fibre ends into capillaries millimeter long waveguides with minimum loss of 1.1dB were fabricated. A long interaction length of polymer waveguide allows spectral broadening and self-phase modulation features to occur in response to the high power laser propagation through the polymer bridge. The spectral broadening in polymer waveguide was much broader than that of 1.5m plain fibre. The comparison of the results associated with maximum phase shift occurs in polymer with plain fibre revealed that the nonlinear coefficient of polymer material is about 1000 times larger than that of silica fibre.

Acknowledgement

I would first like to express my gratitude to my wife Derin and my adorable son Elan. I dedicate this thesis to them. I never forget her support and encouragement when times were tough, and little Elan who inspired me especially in the final year of my research and during writing up.

I would like to thank my supervisor Prof. William Wadsworth, for giving me opportunity to work with him and his sincere supervision. I would also like to thank Stephanos for making some devices used in the fabrication processes, and all the other members of the CPPM, who have made working here enjoyable.

Finally my everlasting gratitude goes to my mum, sisters and brothers for their love and support throughout my study. Also to my friends here in UK and in Kurdistan for their support and encouragement. I would also like to express my appreciation to Kurdistan Regional Government for funding my study here in such a great university

Publications

- P. A. Mohammed, S. Yerolatsitis, and W. Wadsworth, "High Optical Transmission of Polymer Waveguides Fabricated Between Two Fibers," in Opto Electronics and Communications Conference (OECC) PWe.45. 2015.

- P. A. Mohammed, and W. Wadsworth, "Long, free-standing polymer waveguides fabricated between single mode optical fiber cores," *Journal of Lightwave Technology*, vol. 33, no. 20, pp. 4384-4389, 2015.

- P. A. Mohammed, and W. Wadsworth, "Improvement in optical and mechanical properties of self-written polymer waveguides bridged single mode fibers," In preparation 2017.

List of Acronyms

3-TPM	:	3-(Tri-methoxysilyl) Propyl Methacrylate
A	:	Absorption
AP	:	Adhesion Promoter
coI	:	co-Initiator
CW	:	Continuous Wave
F	:	Fluorescence
FWHM	:	Full Width at Half Maximum
GVD	:	Group Velocity Dispersion
IC	:	Internal Conversion
ID	:	Internal Diameter
ISC	:	Inter-System Crossing
KDP	:	Potassium Dihydrogen Phosphate
KTP	:	Potassium Titanyl Phosphate
LED	:	Light Emitting Diode
LP	:	Linearly Polarized
M	:	Monomer
MDEA	:	Methyldiethanolamine
MMF	:	Multi-Mode Fibre
mPOF	:	micro-structured Polymer Optical Fibre
NA	:	Numerical Aperture
NIR	:	Near Infrared
NOA	:	Norland Optical Adhesive
OD	:	Output Diameter

OSA	:	Optical Spectrum Analyzer
P	:	Phosphorescence
PETA	:	Pentaerythritol Triacrylate
PI	:	Photoinitiator
PMMA	:	Polymathic Methacrylate
POF	:	Polymer Optical Fibre
SEM	:	Scanning Electron Microscope.
SMF	:	Single Mode Fibre
SPM	:	Self-Phase Modulation
TE	:	Transverse Electric
THG	:	Third Harmonic Generation
TM	:	Transverse Magnetic
TPA	:	Two Photon Absorption
UV	:	Ultraviolet
VR	:	Vibrational Relaxation
WG	:	Waveguide

List of Mathematical Symbols

a	:	Radius of core
$A(z,t)$	:	Slowly varying pulse envelope
$\tilde{A}(z,\omega-\omega_o)$	:	Fourier transform of slowly varying pulse envelope
A_{eff}	:	Effective area of mode
b	:	Normalized propagation constant
c	:	Speed of light in vacuum
d	:	Optical curing depth
$\vec{D}$	:	Electric flux density
$\vec{E}$	:	Electric field vector
$E(r,t)$	:	Slowly varying amplitude
$\tilde{E}(z,\omega-\omega_o)$	:	Fourier transform of slowly varying amplitude
E_{exp}	:	Total exposure energy
E_{ph}	:	Energy of photon
$F(r,\varphi)$	:	Transverse field of propagating pulse
$F(x,y)$	:	Transverse field in Cartesian coordinate system
h	:	Plank's constant
$H_m(\xi), H_n(\eta)$	:	Hermit polynomials of orders *m* and *n*
I	:	Intensity
I_o	:	Peak value of light intensity
$J_l(Ur/a),\ Y_l(Ur/a)$	:	Bessel functions
k_o	:	Free space wave number
$K_l(Wr/a),\ I_l(Wr/a)$	:	Modified Bessel functions
L	:	Physical length of waveguide
L_{eff}	:	Effective length of waveguide
L_D	:	Dispersion length
L_{NL}	:	Nonlinear length
$\bar{M}_n$	:	Average molecular weight

n	:	Refractive index
$\acute{n}$	:	Refractive index of rare medium
n_2	:	Nonlinear refractive index
n_{axis}	:	Refractive index on waveguide axis
n_{clad}	:	Refractive index of cladding
n_{core}	:	Refractive index of core
P	:	Polarization
P_{L}	:	Linear polarization
P_{NL}	:	Nonlinear polarization
P_{curing}	:	Curing beam power
P_o	:	Peak power of pulse
$\mathrm{R}^{\bullet}$	:	Free radical
S_0	:	Grounded state singlet state
S_1	:	Excited singlet state
t	:	Time
T	:	Time reference of moving pulse
T_1	:	Triplet state
v_g	:	Group velocity
V	:	Waveguide parameter (normalized frequency)
w_o	:	Gaussian beam radius
$w(z)$	:	Spot size of a Gaussian beam
z	:	Longitudinal position coordinate (direct of propagation)
z_R	:	Rayleigh range
α	:	Absorption coefficient (Loss)
β	:	Propagation constant
β_o	:	Propagation constant of pulse
β_1	:	Inverse of group velocity
β_1	:	Group velocity dispersion
γ	:	Nonlinearity coefficient
δ	:	Molar extinction coefficient
$\mathcal{C}$	:	Photoinitiator concentration
ϵ	:	dielectric constant

ϵ_o	:	Permittivity of free space
ϵ_{NL}	:	Nonlinear dielectric constant
θ_c	:	Critical angle
θ_i	:	Incident angle
θ_t	:	Transmitted angle
μ_o	:	Permeability of free space
λ	:	Wavelength
ν	:	Frequency
$\mathcal{T}_{exp}$	:	Exposure time
χ	:	Electric susceptibility
$\chi^{(1)}$	:	First order nonlinear optical susceptibility tensor
$\chi^{(2)}$	:	second order nonlinear optical susceptibility tensor
$\chi^{(3)}$	:	Third order nonlinear optical susceptibility tensor
ϕ_{NL}	:	Nonlinearity phase shift
$\Psi(r, \phi, z, t)$	:	Scalar field in wave equation
$\psi(r, \phi)$	:	Transverse component of scalar field
ω	:	Angular frequency
ω_o	:	Angular frequency at centre of pulse spectrum

Table of contents

Chapter One

Introduction

The first generation of glass optical fibre was successfully deployed in the mid-seventies of the last century, and since then, it has steadily provided a unique way to connect the entire world. Glass needed concerted development to become an efficient material in optical fibre communication system. In long haul communication systems, up to date there is no material to compete with silica fibre. However, in local area networking and short interconnection systems polymer fibres could be a potential candidate to replace silica fibre as polymer fibres showed acceptable optical transmission after some modifications [1]. In the same context, polymer waveguides have drawn significant attention in integrated optical systems, sensing and interconnection applications. With the consistent development of material processing and fabrication technologies over the last three decades, the optical transmission of polymer fibre has been greatly improved. Diversity, easy to process, transparency and low cost motivates researchers' attention toward polymer materials. Photopolymer devices enable us to tailor solid polymer structures including polymer waveguides from liquid monomer by photopolymerization. The technique also gives flexibility to fabricate integrated polymer microstructures with optical fibres. The technique was initially used to fabricate a polymer waveguide extended from an optical fibre by immersing the fibre end into a photopolymerizable liquid container [2]. Then it was implemented to grow a small polymer tip on the optical fibre, for coupling [3], imaging [4] and microscopy [5] applications. In the beginning of this century, the idea was implemented to construct self-written polymer waveguides between two single mode fibres [6, 7] also between two multimode fibres [8, 9].

This thesis considers polymer waveguides integrated with optical fibre using the light emerging from the fibre to polymerize liquid monomer deposited on the end of fibre. The gap that motivated us to investigate in this field is lack of long free-standing polymer waveguides between two single mode optical fibres. Therefore this work tries to present some improvement in optical transmission of free-standing self-written polymer

waveguide and extend the waveguide length beyond 1 mm. Furthermore, to improve mechanical properties and investigate optical nonlinearity of polymer bridges.

Chapter 2 begins with general introduction of photopolymerization, and then presents a comprehensive background of free radical photopolymerization including microscopic modification in the monomer state during polymerization. The reaction stages are described from light absorption, chain formation, and termination deactivation inhibition processes, which accompany polymerization reaction. Finally, physicochemical parameters are discussed which effect the polymerization and the optical and mechanical properties of the polymer structure at both pre- and post-polymerization stages. In chapter 3 a general description of optical waveguide and light guiding mechanism is discussed in both step-index and graded-index optical waveguides. Then the chapter focuses on polymer waveguides integrated with optical fibres and the physics of light confinement throughout photopolymerization. The materials used for polymer waveguide fabrication, their structure and preparation methods are also presented.

Chapter 4 to 6 cover the experimental work conducted during my PhD. Chapter 4 presents polymer waveguide fabrication between two single mode fibres and its optical characteristics. The waveguide fabrication was started with short bridges then it was extended to about 600 μm as the longest possible waveguide with unidirectional illumination. For each bridge device, low loss (below 1 dB) was targeted and the process showed high reproducibility, although the device showed fragility particularly at the polymer/fibre interfaces. Some fabrication and structural parameter effect on the waveguide were investigated such as oxygen diffusion, curing beam intensity and photoinitiator concentration. To improve adhesion at the polymer/fibre interfaces, the fibre ends were treated with adhesion promoter. This fibre modification is presented in chapter 5. The treatment was very effective to improve bonding at the interfaces. To assess the polymer waveguide mechanical properties, the channel was put under shear and tensile stresses. Chapter 6 describes nonlinear optical effects which have been generated by propagating high intensity ultra-short pulsed laser in polymer waveguides. The dominant nonlinear effect is self-phase modulation which is mathematically outlined by analyzing nonlinear Schrödinger equation. In order to see the nonlinear effect more clearly via spectral broadening a new technique was introduced to elongate polymer waveguide to 1.2 mm with optical loss about 1 dB. Then the experimental result of spectral broadening in polymer waveguide is shown, and the nonlinear coefficient of the

polymer waveguide is calculated by comparison of the results with that of plain silica fibre. The final chapter gives a summary of the results which achieved in this research work also some possible further work that could be done in this field.

Chapter Two

Free radical photo-induced polymerization

2.1 Photopolymerizartion

Photopolymerization is a process of formation of solid polymer structures with higher molecular weight from lower molecular weight liquid monomer or oligomer under exposure of light. The structural development is based on the monomer system's ability to absorb appropriate wavelength to form primary reactive species and then form a solid structure [10]. Light beams in the spectral region of ultraviolet, visible and infrared are widely used in photocuring techniques [11], although in some special cases, it may include wavelength in the range of X-rays [12]. Also some advanced techniques for instance electron beam writing and atom beam writing are used to build desired 3D patterns [13]. The reactive materials that are most commonly used in photo curing technology are low molecular weight fast curable unsaturated acrylate or methacrylate monomers that can be developed into crosslinked structure in a post polymerization process. Photopolymeraization is therefore a polymer chain formation whereas photocrosslinking relates to crosslinked network created by attaching polymer chains via covalent bonds. It is important for polymer to possess crosslinking characteristics that gives polymer rigidity and hardness to handle post curing conditions. On the other hand, non-crosslinked polymers are soft and subjected to deformation under heat application [14, 15].

The rapid conversion of a photopolymer from the liquid state to a solid polymeric material provides a number of technical and economical advantages over thermal polymerization operations that give photo curing an extensive and wide application in industrial scale during last three decades [16]. Photoplolymerization is a very rapid reaction, and more importantly it only happens in the illuminated part while the non-irradiated part of the liquid is not affected and can be easily washed out by a suitable solvent [17, 18]. It does not need high temperature and can be performed at room

temperature or even below. Also, some functional groups are not stable at high temperature. To simplify the manufacturing processes it is desirable to conduct polymerization at room temperature [19, 20]. Moreover, this technology consumes low power and it needs inexpensive manufacturing equipment, low overall costs, and good reproducibility [21]. Ecologically, the reaction does not release volatile gases [22]. Such advantages of photopolymerization resulted in the development and rapid growth of advanced highly sensitive materials and processes that led to microelectronic photoresists. Without such photopolymer materials, there would be no microelectronics revolution, and consequently no microprocessors and no high capacity data storage systems [23].

Over last three decades UV radiation curing has been a well-accepted technology that has enabled an increasingly large number of industrial uses. These encompassed both high volume applications such as protective and decorative coatings as well as advanced high technology uses such as microelectronic and electronic materials [24, 25]. But nowadays, the development of superior laser sources facilitate the new compelling applications in the direct laser writing of complex and advanced patterns such as holographic optical elements, the recording and storage of information, laser printing, microelectronic machining of three dimensional objects [14]. In addition, taking advantage of precisely curing sources modern photolithography has succeeded to push the resolution of written patterns to sub -100 nm regime which eased the precise tasks in microelectronic technology [13].

2.2 Free radical photopolymerization

Free radical polymerization is an efficient method to convert liquid monomer into a permanent solid polymer by means of light. It occurs at functional groups in monomer units which have double bonds (for instance vinyl groups in acrylate monomers). Polymer molecules of high molecular weight (~ 1000 repeat units) can be constructed from single reactive species during a short time (in the range of one second). In a single component photocurable system which consists of the monomer alone, short wavelength UV photons may have sufficient energy to cleave a bond at functional groups. These types of systems do not need a special photoinititor to initiate photopolymerization. After bond cleavage free radicals $R^{\bullet}$ are derived in the illuminated part of the solution where the intensity is

highest. Subsequently, the reactive species adds to another monomer molecule by opening the π-bond to form a combined free radical [26]. The process repeatedly occurs as many more monomer molecules are successively added to continuously propagate the reactive center as illustrated in Fig. 2-1. One photoinitiated free radical can form a chain of several thousands of monomer units, thus the quantum yield of the reaction is much bigger than 1.

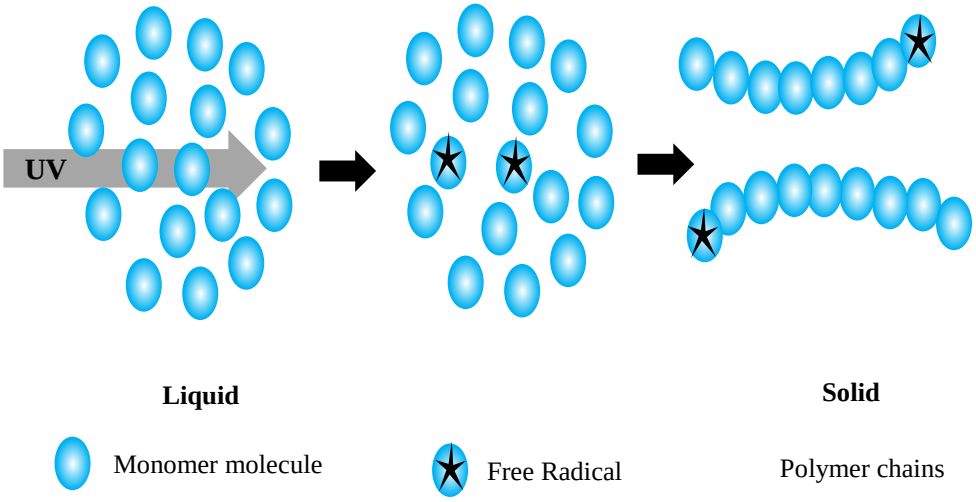

Fig. 2-1: Free radical polymerization in plain monomer system under high energetic UV illumination.

To extend a photopolymerizable monomer system's sensitivity to near visible UV and visible, a new element must be added to the monomer, which called a photoinitiator (PI). In the two compound systems consisting of a monomer and a photoinitiator, free radicals initially form as a result of PI absorption of incident light and they are excited then they react with a nearby monomer molecule to form a combined free radical as shown in Fig. 2-2. A remarkable advantage of extending curing light to visible is using a coherent laser beam instead of UV incoherent light sources such as mercury arc lamp [27]. A visible laser enables better spatial monitoring at the curing site and so it can be used in high resolution applications such as laser direct imaging, graphics arts, holography, and dental materials. The latter requires irradiation in the visible light region to benefit from laser technologies or simply to avoid UV damaging effects [28].

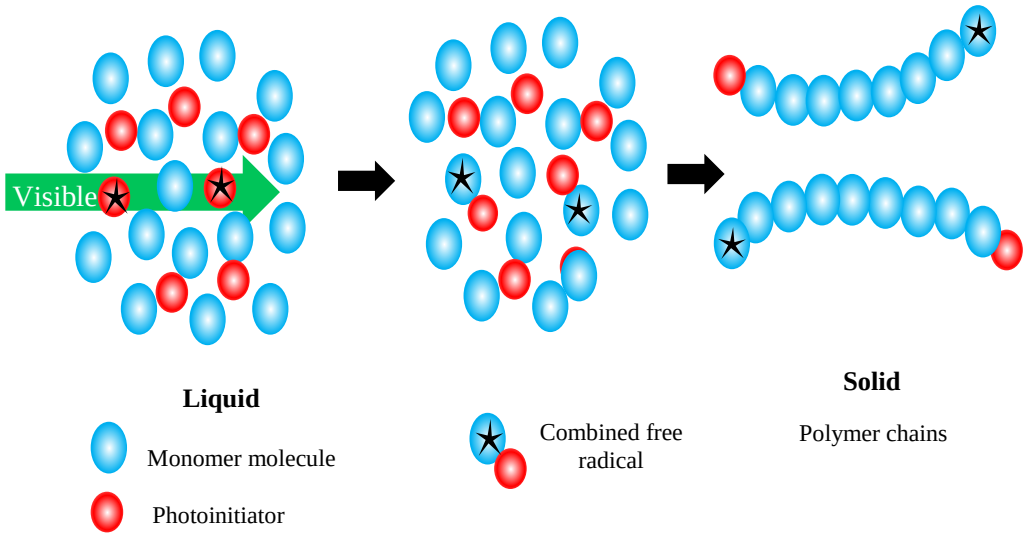

Fig. 2-2: Free radical polymerization by a visible beam in a two component photopolymerizable system (monomer and photoinitiator). Free radicals initially form at the illuminated part of the system, then polymer chains initiate.

The main characteristic of this technique is its higher curing rate and the availability of a variety of monomers that could easily be polymerized by this process. Two types of photo initiators are widely used in free radical polymerization. The first type induces a free radical chain process. The second type generates reactive species via an ionic mechanism (usually cationic) [29] or in few occasions anion centre or weak bases [16]. Even though free radical polymerization more highly influenced by oxygen inhibition than cationic polymerization it is still the most reliable and dominant because most monomers will undergo polymerization only by free radical initiator. Also, a wider range of photoinitiators are applicable for free radical polymerization compared with cationic polymerization. Furthermore, it has some advantages over cationic photo induced polymerization since it is not much affected by impurities and is a faster process [29].

The rate of a typical single photon photoinduced free radical polymerization is proportional to the exposure energy supplied by the curing light beam and the absorption efficiency of curable system. The photophysical and photochemical properties of the photocurable formulation are therefore extremely important in controlling the reactivity and it should possess the following properties. Firstly, high absorptivity in the region of activation, which will depend on the application and light source used. Secondly, high quantum yield for free radical formation [30]. Some important factors which have

fundamental impact on polymerization reaction will be considered in detail later in this chapter.

2.3 Photoinitiators

The first and foremost step in free radical polymerization is the absorption of an incident photon and hence the use of photons energy to cleave a bond or double bond at functional groups. The photon energy is described by the well-known equation

$$E_{Ph} = h\upsilon = h\frac{c}{\lambda} \ , \qquad (2\text{-}1)$$

where E_{Ph} is the photon energy, h is Planck's constant, υ is the optical frequency of the curing beam, c is the speed of light and λ is the wavelength. Most monomer materials have bond energies which overlap with UV spectral region as shown in Fig. 2- 3. But the commonly used monomers do not generate sufficient amounts of initiating species under UV exposure, which is due to low absorbance and poor cleavage efficiency. Therefore in order to improve the polymerization efficiency and shift to visible spectrum photo curing, special photoinitiators are usually added to the monomer [31].

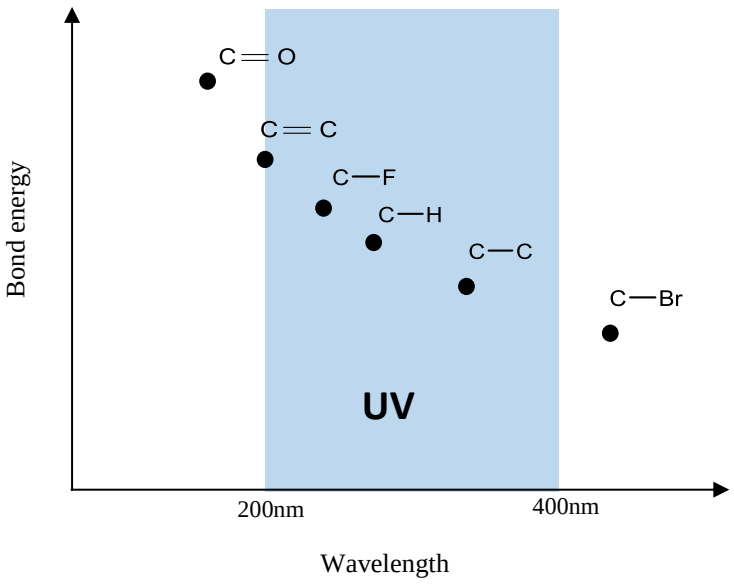

Fig. 2-3: Bond energies as a function of wavelength corresponding to different bonds in monomer function groups, the energy of the most of the bonds match with UV spectrum [12].

To achieve the desired polymer structure the chosen photoinitiator should possess the following properties; high absorptivity in the spectral region of curing light source; high quantum yield to produce maximum number of free radicals; adequate solubility in the monomer system; high storage stability and nontoxicity; non- yellowing after curing and cheap [29].

There are two initiator types for photoinitiated radical polymerization. The cleavage type I and the hydrogen abstraction type II. Type I photoinitiators are almost all spontaneously undergo "α-cleavage" after absorbing energy from light source, generating two free radicals by breaking C – C bond at one functional groups of the monomer. Type II photoinitiators will excite electronically to a higher energy state then react with hydrogen / electron donor coinitiator to drive free radical species [16]

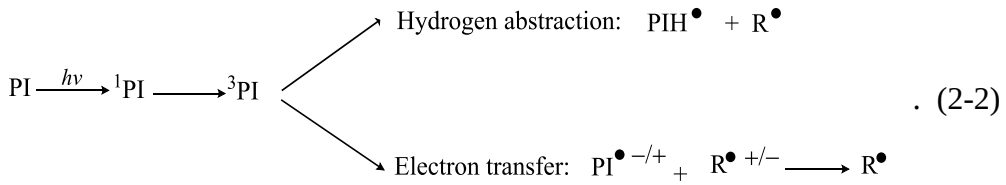

. (2-2)

Both of these photoinitiators have advantages and draw backs depending on the requirements of the particular application. For instance, most of the type I photoinitiators are only active under UV irradiation [32], whereas type II initiators are more sensitive to quenching either by monomer or by oxygen [16].

2.4 Photopolymerization stages

A typical photopolymerizable acrylate based system is a three component solution mainly consists of multifunctional acrylate monomer, photoinitiator and coinitiator (coI) [14]. Polymerization reaction of such system goes through three successive stages, which are photoinitiation, then propagation and finally termination.

2.4.1 Photoinitiation

Photoinitiation is commenced with light absorption, a molecule at the illuminated part of the solution exhibits UV, visible, or near- infrared spectrum absorption as a function of its skeleton [33, 34]. The molecular states as shown in the Fig. 2-4 are composed of electronic, vibrational and rotational energy levels due to the motions of the atoms in the molecule. Transitions among these energy levels are either radiative (photon emission) or non-radiative (no photon emission). Upon excitation by light, photoinitiator is promoted from its ground singlet state S_0 to its first excited singlet state S_1 and then converted into its triplet state T_1 via non radiative intersystem crossing. Transition from singlet to triplet state occurs because the vibrational energy levels of the two states are overlap, therefore the transition only needs one of paired electrons reverses its spin. Although fast transition from S_1 to S_0 is more dominant than S_1 to T_1 transition which slows down photobleaching and hence polymerization. Up to this stage all processes are photophysical as no chemical modification happens to the starting molecules.

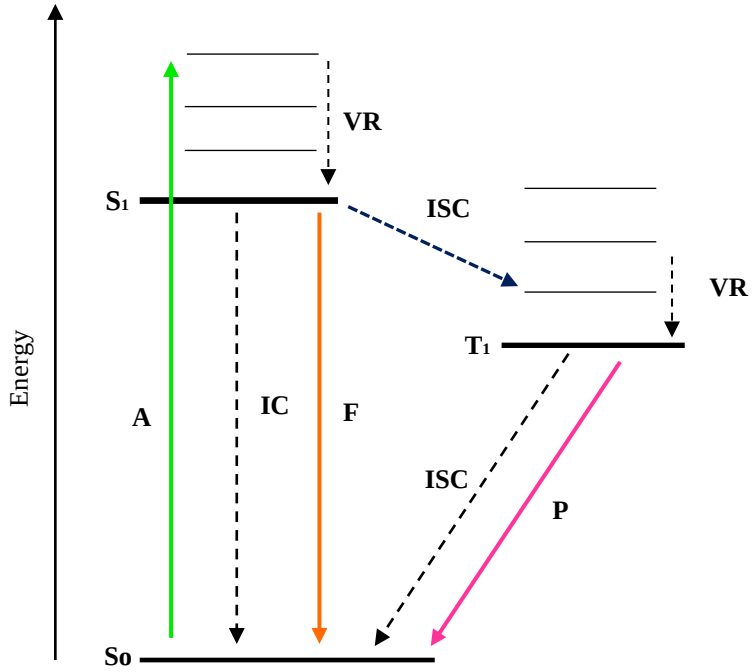

Fig. 2-4: Jablonski diagram shows the different stages of photoinitiation process. **A** absorption, **IC** internal conversion, **F** fluorescence, **VR** vibrational relaxation, **ISC** inter-system crossing and **P** phosphorescence [11].

The photochemical processes begins with photoinitiator bleaching through which transient state T_1 yields the reactive radicals $R^{\bullet}$ by reaction with a nearby monomer molecule M and initiates a chain polymerization. Sometimes a coinitiator is also added to the system which reacts easily with excited photoinitiators to generate more free radicals before polymer chain initiation. Along with polymerization initiation, many deactivation routes can take place during photoinitiation reactions, which can affect the free radical formation and slow down the reaction [30, 35]. The most common is fluorescence emission from singlet state to ground state which happens much faster than inter system crossing to triplet state.

2.4.2 Propagation

Propagation starts once excited photoinitiator molecules are converted to free radical species for type I initiators, or they react with electron or hydrogen donor coinitiator in the case of type II initiators. The following stages of the chemical process are similar for both cases [26]. The first step of propagation starts when the primary free radicals add to carbon–carbon double bonds of the monomer to produce live monomer radicals:

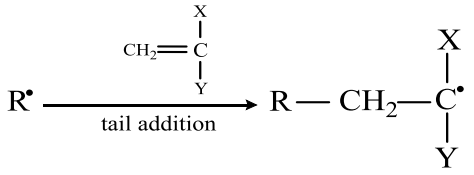

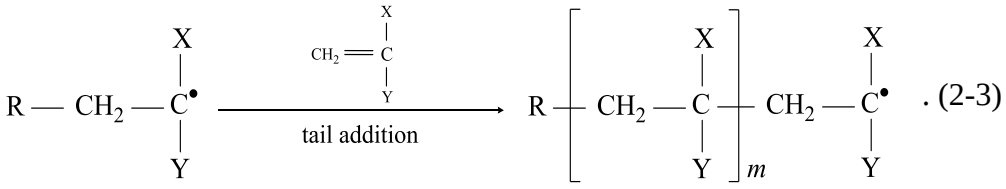

. (2-3)

These monomer radicals in turn propagate further and continue to add other monomer molecules by head-to-tail addition to form a chain-like structure [35].

For acrylate monomers which are widely used in photopolymerization X depends on the type of the monomer and Y is COOH [36]. The rate of the propagation reaction is controlled by the total energy supplied from the laser, since the amount of photoinitiator that produces free radicals is affected by the intensity of the laser beam as well as the time

of exposure. These two factors in turn influence the amount of photoinitiator converted or excited at various points of illuminated area. Hence, the amount of PI contributed in photopolymerization reaction depends on the radial direction from the centre of the laser beam that has been illuminated [37].

2.4.3 Termination

The final step of free radical polymerization is termination. Mono or bimolecular termination mechanisms occur either by attaching two heavy live radicals to each other:

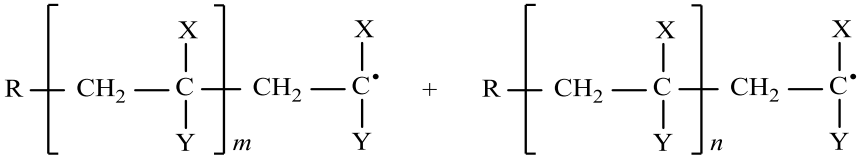
, (2-4)

which is bimolecular and called termination by radical combination:

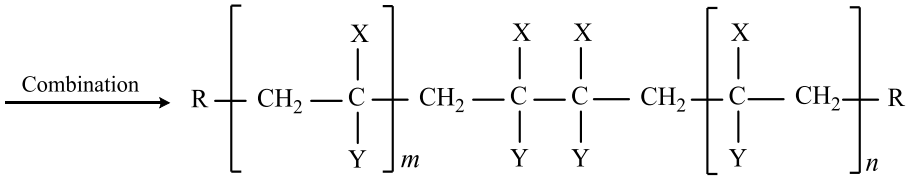
. (2-5)

Alternatively, when newly formed mobile radicals are captured by two heavy polymer chains shown in equ.(2-4), monomolecular termination occurs, which is known as termination by radical trapping disproportionation [37]:

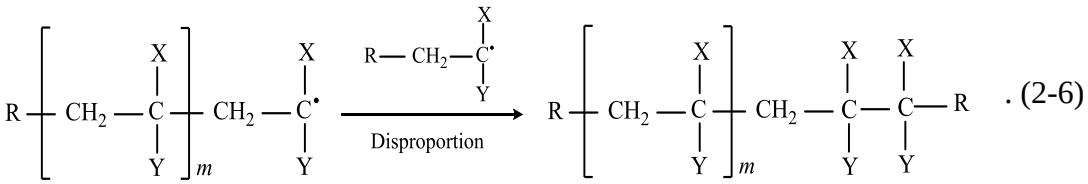
. (2-6)

In free radical polymerization, dark polymerization rarely takes place or it only continues for a very short time after blocking illumination. In contrary, it is a remarkable

characteristic in cation polymerization. Therefore, in the absence of the human intervention and other reactants, majority of polymerizations will terminate by the two aforementioned processes. In practice termination by combination is more dominant in the beginning and gives head-to-head linking leading to high conversion rate. On the other hand, termination by disproportionation only appears when the resin becomes so viscous that it is very difficult for monomer molecules to diffuse toward the reactive center and consequently it is easier for reactive chains to grab a highly diffusing recently formed free radical. Therefore, due to significant involvement of monomolecular termination the conversion rate of monomer is always lower than 100%. In general, there will be some unsaturated chain-ends as well as saturated polymer chains [11, 26].

2.4.4 Inhibition and retardation

Inhibition is an unavoidable incident in photopolymerization reaction, it has various forms and accompanies all stages of the reaction. It begins with photophysical inhibition processes that mainly occur at photoinitiation stage [38]. Singlet to triplet transition of photoinitiator is in competition with other fast deactivation transitions from S_1 to S_0, because the excited molecules of photoinitiator can be deactivated by fluorescence emission to ground state and the same transition also happens because of internal conversion through which the excess amount of energy is dissipated as heat. Also in T_1, deactivation to ground state occurs either by photon emission (phosphorescence) or by non-radiative inter system crossing. All these possible transitions are shown in Jablonski diagram Fig. 2- 4. Moreover, triplet–triplet annihilation and self-quenching ($T_1 + S_0$ reaction) are low probability processes which can happen.

The photochemical inhibition reactions are mainly involved with T_1 of the photoinitiator. The reaction development toward polymer chain initiation must compete with other side reactions, such as nonreactive quenching by monomer or oxygen (i.e., through energy transfer) [11]. To guarantee efficiency, adding a suitable co-initiator (electron-donor) is of great importance that reacts rapidly with the electronically excited photoinitiator to generate free radicals. The chain propagation can also encounter inhibition by oxygen, producing peroxides which then do not participate in the polymerization reaction.

Another type of photochemical inhibition is intentionally used to restrict, delay or in some cases to slowdown reaction. The addition of certain substances quench polymerization of monomers. The substances react with radical species and convert them to non-reactive species or reduce their reactivity and prevent them to propagate. These additive substances are known as inhibitors or retarders. Inhibitors are more effective since they completely suspend polymerization development until they are consumed. Retarders can impose less impact as they can stop some free radicals to initiate polymerization [28].

2.5 Effect of physicochemical parameters on photopolymerization

Many of the significant features observed in photopolymerization have been shown to have considerable impact on the reaction. Some parameters effect on the behaviour of electronically excited photoinitiator and efficiency of photoinitiation, some on the photochemical process and free radical generation or even on the post polymerization optical and mechanical properties of the tailored polymer structure. Here we consider those parameters that their influences involve mainly in the optical and mechanical properties of the polymer. In addition, the parameters that determine the shape, size and formation processes of the polymer.

2.5.1 Effect of oxygen quenching

The inhibition mainly happens by oxygen molecules, which are either dissolved in the compound or diffused from the surrounding. The mechanism of oxygen quenching by O_2 is clarified in Fig. 2-5.

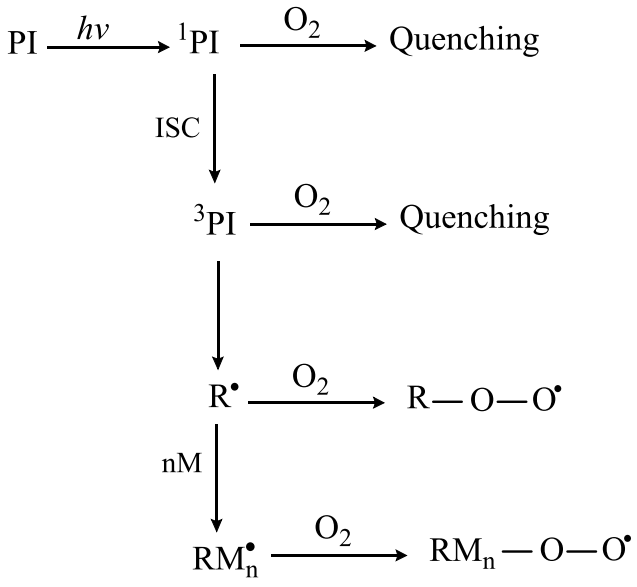

Fig. 2-5: Photopolymerization inhibition by oxygen [16].

Evidently, before chain initiation and propagation takes place, all pre dissolved O_2 molecules in the organic liquid monomer should be consumed by free radicals. They also bleach excited photoinitiator molecules and preventing them from free radical generation. Oxygen quench the excited photoinititors, the reaction takes place by transferring excitation energy to the oxygen molecules dissolved in the system. The quenching of singlet state is rare and complex whereas the quenching probability of triplet state is relatively higher. However, in the case of acrylate based systems oxygen molecules are mainly consumed by free radicals. The consumption of oxygen is usually fast process because O_2 is more mobile than heavy monomer molecules [39]. Oxygen molecules exert a detrimental effect on free radical polymerizations by quenching the reaction at all steps of polymerization from photoinitiation until chain propagation. It is more effective with type II photoinitiators by reducing the rate of initiation. Then it becomes more influential with growing polymer radicals to form peroxy radicals. The peroxy radicals are unable to reinitiate polymerization, and thus, oxygen essentially consumes free radicals. Therefore the polymerization cannot proceed until the propagation reaction dominates over inhibition reaction. For acrylate monomers, polymerization proceeds only when oxygen concentration drops from ~ 10^{-3} M to nearly ~ 4×10^{-6} M [40, 41]. The peroxy radicals are generally inefficient as initiators, but

they abstract hydrogen atoms from the monomer or polymer chain to re- drive free radicals into the system

$$R^{\bullet} + O_2 \longrightarrow ROO^{\bullet}$$
$$ROO^{\bullet} + RH \longrightarrow ROOH + R^{\bullet} \qquad (2\text{-}7)$$

In this aspect pre dissolved O_2 and those diffused can serve polymerization development [42].

Oxygen quenching is more influential at the surface of cured polymer because of oxygen diffusion from the surrounding atmosphere. In some photopolymerization reactions where the monomer is very viscous, oxygen hardly diffuses to the bulk thus the inhibition is limited to a thin surface layer because of the consistent diffusion of oxygen. The surface inhibition normally has a negative impact as it causes inhomogeneity at the surface morphology which is an undesired feature in some applications such as coating, and it can cause some optical losses in polymer waveguides [39]. To prevent surface inhomogeneity the curing can be carried out under an argon or nitrogen atmosphere. In some cases a thin sheet of polyester is used to cover the polymer film [36].

In some cases oxygen quenching can be utilized positively to fabricate a desired polymer structure for specific application. One can control the size of the structure by allowing oxygen diffuse into the reaction site. Also in the presence of oxygen growing polymer chains are terminated more frequently. Thus the chain consists of fewer monomer units and hence the crosslink density is lower which leads to lower shear modulus of the fabricated polymer. This can gives the polymer better characteristics to be used in sensing applications [39]. In some cases, oxygen inhibition has proved useful, while sometimes it is undesired. In either case, understanding its impact on the ultimate polymer structure is important to be optimized [25].

2.5.2 Effect of curing light intensity

The rate of photopolymerization is a strong function of light intensity such that the reaction and conversion rate is more dominant at the region where the intensity is maximum. Moreover, how deep the photopolymerization can be extended into the

monomer system is also determined by intensity of the light beam [37]. With increasing light intensity there will be a simultaneous increase in the rate of polymerization and conversion. This relationship is not linear such that beyond some certain point the depth of polymerization grows slowly with intensity [17]. Additionally, in the case of a Gaussian beam the polymerization at the edges of the beam should compete with inhibition processes especially with oxygen quenching by O_2 molecules diffusing from the boundary.

2.5.3 Effect of photoinitiator concentration

The proportion of light absorbed depends on how many molecules in the solution are involved with light interaction, the absorption of light by monomer molecules usually very weak and can be ignored since it is not sensitive to the curing beam. Therefore the absorption mainly occurs by photoinitiator molecules. The production of free radicals is highly linked to the absorptivity of photoinitiator in the spectral region associated with light source. The number of excited initiator molecules in a photopolymerization reaction is determined by the photoinitiator concentration. Therefore the number of reactive species increases with increasing photoinitiator concentration in the monomer. Consequently the curing speed increases remarkably [10]. The Beer - Lambert law is the empirical relation between intensity of curing light and photoinitiator concentration and response to the incident light:

$$I = I_{\circ} e^{-\delta d \mathcal{C}} \ , \qquad (2\text{-}8)$$

where δ is the molar extinction coefficient at the absorbed spectral region, d is the optical curing depth inside the formulation and $\mathcal{C}$ is the molar concentration. The absorbance of the illuminated medium at a given wavelength is defined by ($\delta d \mathcal{C}$). The law essentially describes the attenuation of light by the medium through which light travels. Presumably, here one can say molar concentration in the Beer - Lambert law is assumed to be initiator molar concentration exclusively. None the less, the absorptivity increases with photoinitiator concentration, it is a trade - off between absorbance and curing depth. An increase in concentration results in higher absorbance at the first illuminated part of the

system, but initial high absorbance also leads to high attenuation of light and in consequence the curing depth reduces [38]. The conversion rate of the monomer to polymer is another factor in photopolymerization which highly influenced by photoinitiator concentration. The conversion rate initially increases with initiator concentration then reaches to saturation point. Additionally, increasing photoinitiator concentration results in yellowing effects after polymerization. The yellowing effect is because of unbleached photoinitiator molecules or the molecules that neither quenched by oxygen nor reacted with the monomer molecules but relaxed to ground state. However this effect can be eliminated by further photobleaching after curing [33].

2.5.4 Effect of temperature

Photopolymerization is a chemical reaction that converts the state of illuminated material from liquid to solid and it is an exothermic process. A substantial amount of heat is released in a short time during the process and causes rapid increase in temperature. Temperature starts to increase as soon as photoinitiation begins. It reaches a maximum value just before the rate of termination becomes equivalent to the rate of initiation, then it decreases once termination becomes predominant over initiation. Heat production sharply falls due to photobleaching of initiator molecules and hence reduction of absorption and initiation [43]. The polymerization temperature significantly effects on the final properties of cured polymer [44, 45]. In addition, the nonradiative transition from the higher energy singlet state of photoinitiator to the ground state releases some heat into the solution which also increases temperature at the reaction site. The impact of temperature on the photopolymerization is complicated and depends on various conditions such as the molecular structure, molecular motion and kinetics of polymerization throughout the reaction [38]. Propagation is dominant at lower polymerization temperature before it reaches maximum value. Rising temperature increases the mobility of polymer chains and increases the probability of termination with polymer chains containing fewer monomer units. Consequently the rate of polymerization drops due to termination superiority over propagation. Elevated temperature also aids oxygen diffusion into the solution by reducing its viscosity. High temperature on the other hand, increases the mobility of unreacted monomer molecules and induce further tail propagation which also raises the possibility of further chain propagation. Also it reduces

the oxygen inhibition in early stages of polymerization due to decrease in the predissolved number of oxygen molecules in the polymerizing medium [42]. Heat transfer in the polymerizing sample and thermal boundary condition also need to be taken into consideration. Spatially controlled photopolymerization is usually happens at restricted sites allowing the system to be in the constant heat exchange with the boundary which helps the system to release some heat across the boundary rather than trapping it in the reaction site. The most concerning point in the temperature effect is the situation when temperature rises over the glass transition temperature Tg of the polymer. In this case the cured polymer might exhibit a change which tremendously effects the final properties of the polymer. Therefore a monomer with intermediate Tg could be a good candidate to be used in photopolymerization structural fabrication [26].

2.5.5 Effect of viscosity

Monomer viscosity plays an important role in the solution's homogeneity especial in the cases where photoinitiators are powders to be dissolved in the monomer. High viscosity is a serious obstacle in initiator dissolving in sticky monomers for instance epoxy acrylate matrices. The practical effect of viscosity of the polymerizable formulation strongly depends on the exposure and experimental conditions. Pre-polymerization shaping of the liquid monomer is crucial in manufacturing of integrated micro polymer structures such as micro lenses and optical waveguides, here viscosity has a decisive role in determining which shape and position a monomer can take. In highly viscous samples the oxygen diffusion is low, leading to high photopolymerization rate after a short period of oxygen quenching because of predissolved oxygen in the sample. Moreover, free radical scavenging by oxygen is reduced when viscosity becomes higher in the stage when the monomer reaches gelled and vitrified states [42]. Restricting oxygen diffusion gives a remarkable improvement in the surface curing of thin samples providing sufficient photoinitiator concentration and curing light intensity. High oxygenation causes substantial negative impact on the surface of polymer structures, the impact can be limited by viscous monomer samples. conversely, in low viscosity acrylate monomers oxygen flowing from the boundary is high and polymerization would be insufficient due to increasing of number of inhibition reactions by oxygen [11]. Upon polymerization viscosity dramatically increases, consequently the rate of polymerization sharply drops.

The reduction in the polymerization rate is because of limiting the mobility of reactive molecules in the viscous medium. Once viscosity reaches a certain point the rate of new chain initiation decreases such that reaction proceeds only because of propagation of existing active centers which formed earlier [46]. As mentioned earlier most of the effective parameters on polymerization reaction are interrelated. In the case of viscosity effect it is highly interrelated with oxygen quenching and temperature of the system.

2.5.6 Effect of molecular weight

Polymers produced by photopolymerization have a distribution of molecular weight. Polymer products which are prepared commercially and in a large volume are more subjected to a broad molecular distribution (polydispersity)[26]. Microstructure polymers which are fabricated by highly profile beams are more homogenous in terms of molecular weight distribution. However, full control of molecular weight distribution is complicated and needs special fabrication techniques. The previous parameters are only effective during reaction, their impact will vanish after polymerization. In contrary, the effect of molecular weight appears after polymerization especially on the optical transmission. But the interrelationship of molecular weight with the other parameters can give the manufacturer opportunity to control polymer's molecular weight via increasing or decreasing termination rate during reaction as termination determines how many monomer units exists in a polymer chain. Although it is still hard to obtain a polymer with specific molecular weight, fabrication of polymer with narrow molecular weight distribution is accessible.

Polydispersity or heterogeneous molecular weight is an intrinsic characteristic of polymers which makes them different from other materials. Even polymers which are prepared with very careful techniques are still mixtures of different molecular weight chains. Polydispersity in artificial polymers is mainly attributed to the polymerization process. Therefore the molecular weight is always average molecular weight $\bar{M}_n$ rather than exact number:

$$\bar{M}_n = \frac{\sum N_x M_x}{\sum N_x} \quad , \tag{2-9}$$

where M_x is molecular weight of a chain and N_x is the number of chains of that molecular weight. Polydispersity of polymer usually increases with reaction extension as it increases the probability of random polymer chains. The probability is proportional to the rate of polymerization of the specific chain with the nearby monomer units or another reactive species. High speed reaction is an advantage of free radical polymerization which gives the opportunity to obtain less polydispersity or narrow molecular weight distribution in polymer structure. The kinetics of photopolymerization has also a decisive role on the polymer molecular weight. The kinetic chain length is the most important parameter in the process. It is defined as the average number of monomer units attached to a free radical. In other words it is given by the ratio of how fast monomer molecules added to the chain to how fast a new chain initiated (rate of polymerization/ rate of initiation). In the stage, when rate of termination is equal to rate of initiation, the kinetic chain length would be constant, and providing the reaction is rapid the final polymer would be uniform in terms of molecular distribution. Also the mechanical properties of the polymer is highly related to the material's molecular weight. The average molecular weight above about a thousand is critical to provide significant mechanical strength. Increasing average molecular weight to tens of thousands gives more mechanical strength to the polymer. The trend is not linear from few tens of thousands up to hundreds of thousands the mechanical property changes slowly [26]. Regarding optical properties, the refractive index of polymer is generally considered to be independent of molecular weight. However in some polymer fibres a broad molecular weight distribution causes very high attenuation. The high loss is attributed to broad molecular weight distribution because huge polydispersity induces fluctuation in refractive index, leading to light scattering and hence high attenuation. A study showed that reducing average molecular weight to 1/6 of its initial value resulted in nearly doubling optical transmission [47].

Chapter Three

Polymer waveguides integrated with optical fibres

3.1 Optical waveguides

An optical waveguide is a dielectric structure to transfer electromagnetic signals efficiently from transmitter to receiver in optical communication and integrated optic systems. Some common optical guiding structures include optical fibres, semiconductor and polymer waveguides [48]. Typically, they are characterized by higher refractive index structure at the centre of channel n_{core} and relatively lower refractive index $n_{cladding}$ surrounding the core [49]. In practice the desired operating frequency, the distance to the destination and the amount of transmission losses that can be tolerated determine the type of guiding structure to be implemented.

Optical waveguides are at the heart of most optical communication systems. Their significant role results from their capacity to handle broad bandwidth with low loss and high data rate. Consequently optical fibre cables have displaced conventional metallic cables especially in long haul communication system, such that since 1990s fibre optics has initiated comprehensive revolution in information transmission [50]. Polymer waveguides also find a space in the modern systems due to their potential utility in local area networking as they are easy to install and splice. In addition, polymer waveguides are central to interconnects the various devices of an optical integrated circuit [51].

The vital role of global and local communication in the modern world resulted in a tremendous amount of research to increase the capacity and raise the efficiency of optical waveguides. In the same context, polymer waveguides have also drawn much attention to discover an alternative device for optical fibres when they are not the perfect candidate to use.

3.2 Total internal reflection

In any optical signal transmission system the waveguide is the main route through which light beams guide by mainly taking advantage of total internal reflection at the interface between the core and the cladding [52]. When light undergoes transmission between two dissimilar media, the rays change directions and their velocity varies slightly [53]. The phenomenon is governed by the incident angle and refractive indices of the dissimilar media through Snell's law resulting in light beam reflection and refraction

$$n \sin \theta_i = \acute{n} \sin \theta_t \ , \tag{3-1}$$

where n and $\acute{n}$ are refractive indices of incident and transmitted media respectively considering $n > \acute{n}$, and θ_i, θ_t are respectively the incident and transmitted angles with the normal to the interface between two media. Following beam incident on the boundary of the two optical media, it undergoes reflection and refraction depending on the incident angle θ_i as illustrated in the Fig. 3-1.

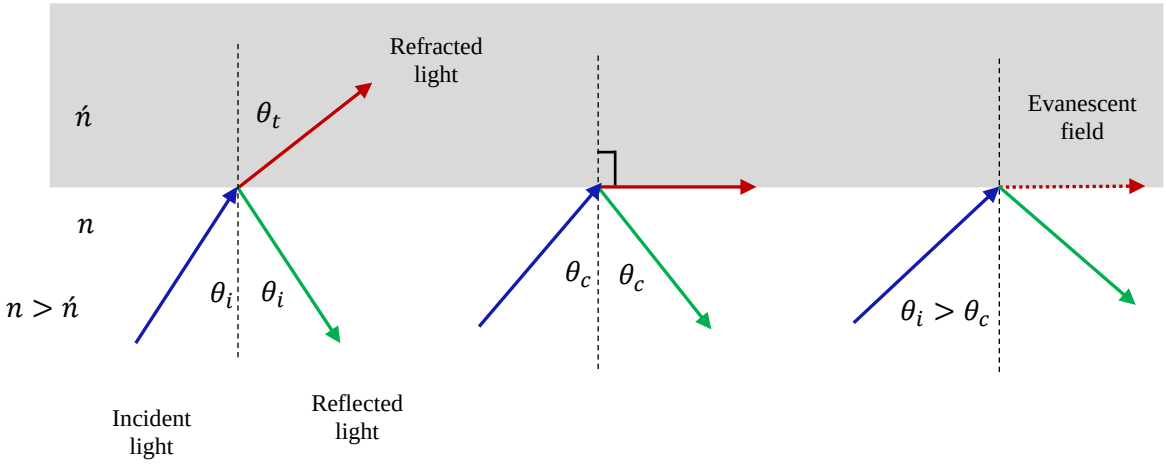

Fig. 3-1: Reflection and refraction of a parallel beam: (a) Incident light on an interface between two media; (b) Incident light on an interface at the critical angle; (c) Total reflection beyond the critical angle.

As a special case, total internal reflection happens when the incident beam makes an angle larger than the critical angle with respect to the normal to the interface as shown in Fig. 3-1. The critical angle θ_c is given by [52]:

$$\theta_c = \sin^{-1}\left(\frac{\acute{n}}{n}\right) \quad . \tag{3-2}$$

Equ. (3-2) determines the cone of incoming rays that allowed to be guided by the waveguide. Hence it plays essential role in coupling light in and out of the guiding structure. Light rays that impinge waveguide end at angles lower than the critical angle are mostly guided, whereas those outside the accepted cone are refracted into the structure, but do not reach the receiver because they are not totally reflected at the core-cladding interface [54].

3.3 Waveguide index profile

Optical waveguides are fabricated in two main types of index profile along the radial axis which are step index and graded index waveguides according to the application demands. The main difference between them is the refractive index variation between the core and the cladding and hence in the manner how beam rays confine and travel through the waveguide [54].

3.3.1 Step-index waveguide

In step index optical waveguides the core region is made of a homogenous material and the refractive index has a constant value and an abrupt change takes place at the interface of core and cladding in step index waveguide [55]. For the cladded waveguide refractive index of core is larger than that of the cladding depending on the guiding mechanism, whereas for uncladded ones the free space surrounding the waveguide plays the role of cladding which is significantly lower than that of the core. A step index profile is usually used for the waveguides with small core size (less than 10 μm) in order to support only fundamental mode or to not allow higher order modes propagate through the waveguide. Simple ray model can be used to understand the propagation characteristics of optical waveguides, but it does not provide a comprehensive understanding of the

phenomenon. For simplicity one can assume that the light rays propagate in zig-zag manner throughout large size multimode step index waveguide as in Fig 3-2.

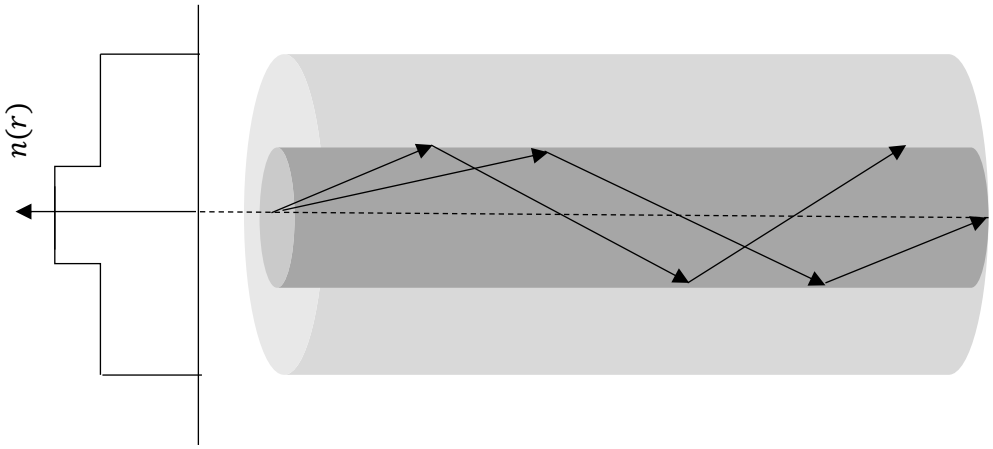

Fig. 3-2: Light guiding and rays path in step index optical waveguide, the inner part with larger refractive index is the core indicated by dark grey and cladding smaller refractive index is the outer part surrounded the core indicated by light grey.

3.3.2 Graded index waveguide

In a graded index waveguide, the refractive index of the core is non-uniform, it has maximum value at the axis of the waveguide and decreases gradually from the axis to its surface. Cladding is less influence in these types of structure as guiding light is completely confined in the core region. Contrary to a step index waveguide there is no sudden boundary change in the refractive index, therefore the light rays do not travel along straight lines but they tend to be bent in the form of sinusoidal waveform rather than sudden reflection at the boundary between the core and the cladding as shown in Fig. 3- 3 [56].

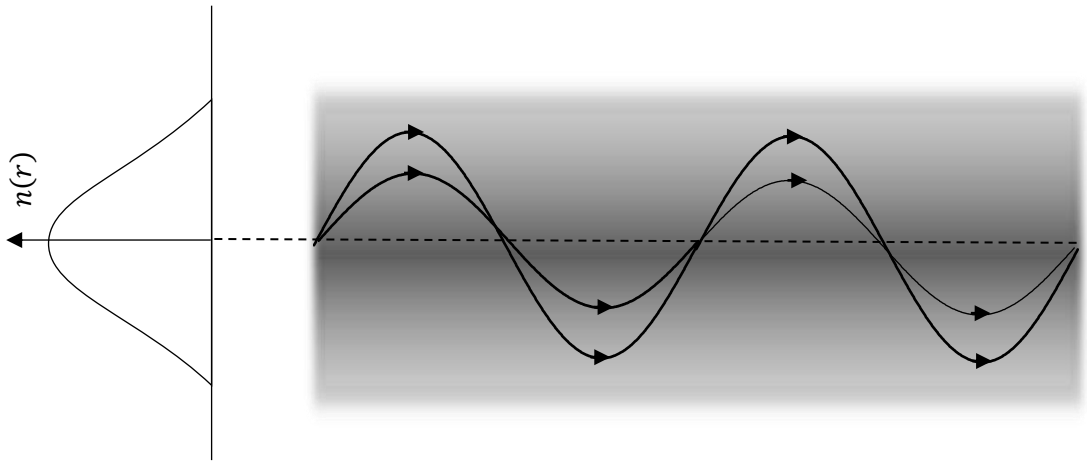

Fig. 3-3: Light guiding and bent rays in graded index optical waveguide. Refractive index monotonically decreases radially it has a maximum value on the waveguide axis.

Essentially the idea of graded index waveguide was introduced to reduce the intermodal dispersion in multimode optical fibres. This structure approximately equalizes group velocities of faster and slower modes. In the ray model point of view, higher order modes travel faster to compensate for further path lengths they travel. In the other words, rays which diverge further from the axis see lower refractive index and hence they travel faster to reach at same time as closer rays to the axis do [54, 57].

3.4 Light propagation in cylindrical waveguide

When an electromagnetic signal propagates through an optical waveguide the transverse field maintain their spatial distribution to form a discrete set of electromagnetic fields known as waveguide modes. A mode can be defined as a transverse profile of the light field which does not change with propagation, apart from a phase. Therefore each mode has a particular transverse field distribution, as well as particular phase velocity. As mentioned earlier, ray model to some extent describes propagation of both step index Fig. 3-2 and graded index Fig. 3-3 waveguides, but it does not provide a complete picture of guiding mechanism. The better method is wave optic approach which gives rigorous solution of wave equation and presents a solution of the electromagnetic field distribution and behaviour through optical waveguide [51].

3.4.1 Guided modes of step-index waveguide

The refractive index variation with radius r in the step index waveguide is characterized by:

$$n(r) = n_{core} \qquad 0 < r < a \qquad \text{core,} \tag{3-3}$$

and

$$n(r) = n_{clad} \qquad r > a \qquad \text{cladding.} \tag{3-4}$$

In a waveguide channel where the difference between refractive indices of core and cladding is very small such as optical fibre, the weakly guiding approximation can be used for solving wave equation [49]. In this approximation two polarization sets of modes can be assumed to have the same propagation constant. These are referred to as linearly polarized, LP modes. Although in the step index waveguide where the difference in refractive indices is large this assumption cannot be considered and the waveguide could support typical modes of conventional cylindrical waveguide such as TE and TM modes. From Maxwell's equations the scalar wave equation can be written as:

$$\nabla^2\Psi = \epsilon_o\mu_o n^2 \frac{\partial^2\Psi}{\partial t^2} \quad , \tag{3-5}$$

where Ψ is scalar field, ϵ_o is permittivity of free space and μ_o is permeability of free space. Assuming that the wave propagates through a cylindrical waveguide along z- axis. The solution of wave equation is written as:

$$\Psi(r, \phi, z, t) = \psi(r, \phi)e^{i(\omega t - \beta z)} \quad , \tag{3-6}$$

where ω is the angular frequency and β is the propagation constant. Substituting equ. (3- 6) into equ. (3-5) we obtain:

$$\left(\nabla^2 - \frac{\partial^2}{\partial z^2}\right)\psi + \left[\frac{\omega^2}{c^2}n^2(r, \phi) - \beta^2\right]\psi = 0 \, . \tag{3-7}$$

In cylindrical coordinates assuming that the waveguide is cylindrically symmetric, it is written as:

$$\frac{\partial^2\psi}{\partial r^2}+\frac{1}{r}\frac{\partial\psi}{\partial r}+\frac{1}{r^2}\frac{\partial^2\psi}{\partial\phi^2}+[k_o^2n^2(r)-\beta^2]\psi=0 \quad , \tag{3-8}$$

where $k_o = {}^{\omega}/_{c}$ is the free space wave number. Then using a separation of variables:

$$\psi(r,\phi)=R(r)\Phi(\phi) \ , \tag{3-9}$$

on substitution and dividing by $\psi(r,\phi)/r^2$ equ. (3-9) becomes:

$$\frac{r^2}{R}\left(\frac{d^2R}{dr^2}+\frac{1}{r}\frac{dR}{dr}\right)+\ r^2[k_\circ^2n^2(r)-\beta^2]=\ -\ \frac{1}{\Phi}\ \frac{d^2\Phi}{d\phi^2}=\ +l^2 \quad . \tag{3-10}$$

The variables have been separated. Each side of equ. (3-9) must therefore independently equal to a common constant l^2. Solving equation depending only on ϕ, the solution will be of the form $\cos l\phi$ or $\sin l\phi$, and for the function to be single-valued l must be an integer, i.e. $l = 0, \pm1, \pm2, \pm3$ ...etc . Thus, the transverse field is given by:

$$r^2\frac{d^2R}{dr^2}+r\frac{dR}{dr}+([k_\circ^2n^2(r)-\beta^2]r^2-\ l^2)R\ =\ 0 \quad . \tag{3-11}$$

This is an eigenvalue equation with β^2 representing the eigenvalues and it takes a set of discrete values corresponding to guided modes of an optical waveguide. For an arbitrary cylindrical waveguide with refractive index decreases monotonically from n_{core} on the axis to n_{clad} at core- cladding interface. The solutions of equ. (3-11) will be of the form of two distinct classes, the first class associated with:

$$k_\circ^2n_{core}^2\ >\ \beta^2\ >\ k_\circ^2n_{clad}^2 \quad . \tag{3-12}$$

For β^2 lying in this range, the fields $R(r)$ are oscillatory in the core and decay in the cladding and β^2 takes discrete values known as guided modes. The second class of solutions corresponds to $\beta^2\ <\ k_\circ^2n_{clad}^2$ representing radiation modes in the cladding. For step index optical waveguide refractive index variation is given by equ. (3-3) and equ. (3- 4). Therefore, using this case for $n^2(r)$ in equ. (3-11) we obtain:

$$r^2\frac{d^2R}{dr^2}+r\frac{dR}{dr}+\left(\ U^2\frac{r^2}{a^2}\ -\ l^2\right)R\ =0 \qquad ;\quad 0<r\ <a \tag{3-13}$$

and

$$r^2 \frac{d^2R}{dr^2} + r\frac{dR}{dr} + \left(W^2 \frac{r^2}{a^2} - l^2 \right) R = 0 \qquad ; \qquad r > a \,, \tag{3-14}$$

where

$$U = a\,(k_\circ^2 n_{core}^2 - \beta^2)^{1/2} \tag{3-15}$$

and

$$W = a\,(\beta^2 - k_\circ^2 n_{clad}^2)^{1/2} \quad . \tag{3-16}$$

For guided modes both U and W are real. The normalized waveguide parameter V is the important quantity characterizing an optical waveguide which is given by:

$$V = (U^2 - W^2)^{1/2} = k_\circ a\,(n_{core}^2 - n_{clad}^2)^{1/2} \quad . \tag{3-17}$$

It is convenient to define the normalized propagation constant:

$$b = \frac{\beta^2/k_o^2 - n_{clad}^2}{n_{core}^2 - n_{clad}^2} = \frac{W^2}{V^2} \quad . \tag{3-18}$$

Hence,

$$W = V\sqrt{b} \qquad \text{and} \qquad U = V\sqrt{1-b} \quad . \tag{3-19}$$

For guided modes the condition $0 < b < 1$ has to be satisfied. The two independent solutions of equ. (3-13) are Bessel functions $J_l\left(Ur/a\right)$ and $Y_l\left(Ur/a\right)$, although the latter one has to be dismissed as it diverges as $r \to 0$. Also the solutions of equ. (3-14) are modified Bessel functions $K_l\left(Wr/a\right)$ and $I_l\left(Wr/a\right)$, as in previous case, the latter one has to be dismissed as it diverges as $r \to \infty$. Accordingly for guided modes, the transverse dependence of the modal field is given by:

$$\psi(r,\phi) = \begin{cases} \dfrac{A}{J_l(U)}\, J_l\left(\dfrac{Ur}{a}\right) \begin{bmatrix} cos\, l\phi \\ sin\, l\phi \end{bmatrix}; & r < a \\ \dfrac{A}{K_l(W)}\, K_l\left(\dfrac{Wr}{a}\right) \begin{bmatrix} cos\, l\phi \\ sin\, l\phi \end{bmatrix}; & r > a \end{cases} \quad (3\text{-}20)$$

Assuming that ψ and $\partial\psi/\partial r$ are continuous at core-cladding interface where ($r = a$), the solution of equ. (3-20) gives universal curves describing how b varies with V. For a certain value of l there will be a finite number of solutions such that mth ($m = 0,1,2 \ldots$) solution indicates LP_{lm} mode [52, 58]. The first few modes which excited by a step index waveguide is shown in Fig. 3-4. These are particular intensity distribution associated with each linearly polymerized mode which has significant role in the mechanism of polymer waveguide writing later in this thesis.

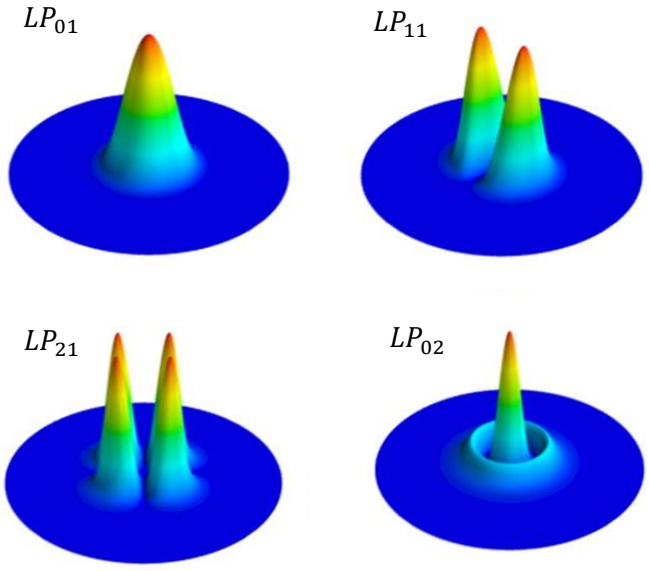

Fig. 3-4: Three dimensional profiles and intensity distribution of linearly polarized modes ($LP_{01}, LP_{11}, LP_{21}$ and LP_{02}) for a step index SMF 28e fibre at 600 nm [59].

3.4.2 Guided modes of graded-index waveguide

In a graded index profile waveguide the refractive index decreases gradually from a maximum value on the axis of the core to the core–cladding interface, then in the cladding it is constant. For simplicity we assume infinitely extended parabolic index waveguide then refractive index in cylindrical coordinate system is described by:

$$n^2(r) = n_{axis}^2\left[1 - 2\Delta\left(\frac{r}{a}\right)^2\right] \tag{3-21}$$

and

$$\Delta = \frac{n_{axis}^2 - n_{clad}^2}{2n_{axis}^2} \approx \frac{n_{axis} - n_{cald}}{n_{axis}}, \tag{3-22}$$

where a is constant and n_{axis} is a refractive index on the axis. Substituting equ. (3-21) in the wave equation for equ.(3-5) yields:

$$\nabla^2\Psi = \frac{n_{axis}^2}{c^2}\left[1 - 2\Delta\left(\frac{r}{a}\right)^2\right]\frac{\partial^2\Psi}{\partial t^2} \tag{3-23}$$

Again we look for solutions of the form of modes:

$$\Psi(r, \phi, z, t) = \psi(r, \phi)e^{i(\omega t - \beta z)} \quad . \tag{3-24}$$

Then the wave equation becomes:

$$\frac{\partial^2\psi}{\partial r^2} + \frac{1}{r}\frac{\partial\psi}{\partial r} + \frac{1}{r^2}\frac{\partial^2\psi}{\partial\phi^2} + \left\{k_\circ^2 n_{axis}^2\left[1 - 2\Delta\left(\frac{r}{a}\right)^2\right] - \beta^2\right\}\psi = 0 \quad . \tag{3-25}$$

The solutions of equ. (3-25) are Hermite- Gauss functions. Hence, the mode profile and associated propagation constant are given by:

$$\psi_{mn}(r, \phi) = \left[N_m H_m(\xi)\, e^{-\frac{1}{2}\xi^2}\right]\left[N_n H_n(\eta) e^{-\frac{1}{2}\eta^2}\right] \ , \tag{3-26}$$

and

$$\beta_{mn} = k_o n_1 \left[1 - \frac{2(m+n)+1}{k_o n_{axis}} \sqrt{\frac{2\Delta}{a^2}}\right]^{1/2} \tag{3-27}$$

with

$$N_m = \left[\frac{\Upsilon}{2^m m! \sqrt{\pi}}\right]^{1/2} = \left[\frac{\sqrt{V}/a}{2^m m! \sqrt{\pi}}\right]^{1/2} \quad . \tag{3-28}$$

Where m and n are integers and Hermitian polynomials are defined as a function of new variables of transverse coordinates as follow:

$$\xi = \Upsilon r \, , \qquad \eta = \Upsilon \phi \, ,$$

such that,

$$\Upsilon = \left(k_\circ n_{axis} \frac{\sqrt{2\Delta}}{a}\right)^{1/2} = \frac{\sqrt{V}}{a} \tag{3-29}$$

$$V = k_\circ n_{axis} a (2\Delta)^{1/2} \quad , \tag{3-30}$$

where V is the waveguide number. N_m and N_m are referred to as the normalization constants.

Waveguide modes are represented by different values of m and n. Thus equ. (3-27) is an analytic solution of propagation constant of (m, n) th mode in the waveguide [60, 61]. The solutions given by equs. (3-26 and 3-27) consider the waveguide that its refractive index is given by equ. (3-21) which is realistic assumption for polymer waveguides later we fabricate by self-writing photopolymerization method. For polymer waveguides it is crucial whether the waveguide is step index or graded index, as it determines the application that the waveguide can be used for, for instance sensing or interconnection applications. Later in the chapter 4, we show both step and graded index polymer structures can be fabricated by the same photopolymerization procedure using different monomer solutions. Polymer waveguide with step index profile surrounded by lower refractive index air atmosphere shows significant evanescent field regardless of how many modes are excited through the waveguide as shown in Fig. 3- 5(a). Conversely, the

waveguide with larger cross sectional size show graded index profile with no evanescent field leaking from the waveguide and the propagating light is well confined in the guiding structure Fig. 3- 5(b).

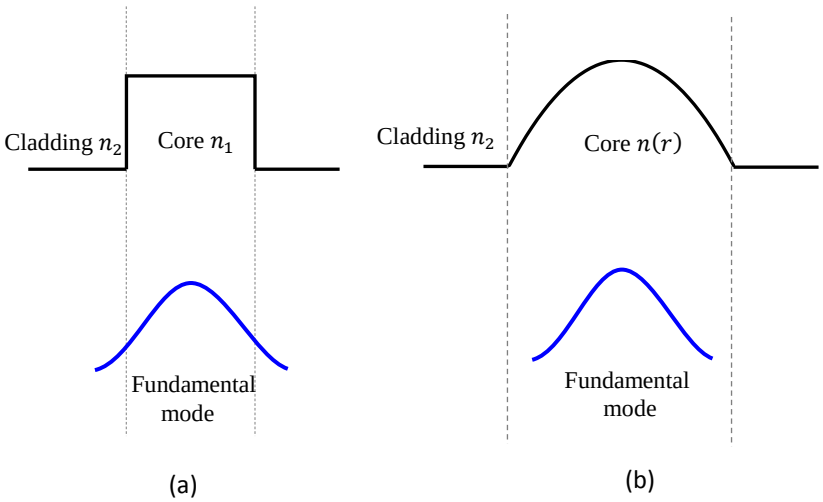

Fig. 3-5: Propagation of fundamental mode through: (a) A step index optical waveguide, some of the guiding beam leaks into the cladding known as evanescent field. (b) A graded index waveguide, the light beam is totally confined in the core region.

3.5 Polymer waveguides

Transparent polymers such as PMMA (poly methyl methacrylate) (n = 1.49), polystyrene (n = 1.59), polycarbonates (n = 1.5 – 1.57), and some other acrylate based polymers hold properties that make them useful for polymer optical fibre (POF), microstructured polymer optical fibre (mPOF) and short range waveguides integrated with optical systems. Due to their large numerical aperture and hence their ability to gather more light, coupling to polymer waveguides and polymer fibre is much easier than silica fibre [1, 47, 62]. Furthermore their fundamental optical coefficients such as refractive index, loss, and electro-optic property can be tailored to intended application. This gives the manufacturer an ability to fabricate various optical waveguide for various applications [63]. On the other hand, high attenuation is the major disadvantage of polymers that limits their application in communication systems and makes silica fibre the dominant element in fibre technology. Never the less recent investigations have significantly reduced resonance loss in PMMA by replacing the hydrogen atom in C-H bond by heavier atom such as fluorine. Great improvement has been achieved in

minimizing attenuation of doped PMMA, such that insertion loss of the fibre has been reduced to few dBs per kilometre [62, 64].

3.6 Light-induced polymer structures integrated with optical fibres

The small core of an optical fibre presents challenges at the fibre interfaces. Once light emerges from fibre, it diffracts which results in intensity reduction. Consider a Gaussian beam propagating through a very narrow waveguide as shown in Fig. 3-6. The beam intensity is highest on the axis, and drops by a factor $1/e^2$ at the radial distance $r = w(z)$, this distance is defined as beam radius. Since the beam diffracts the beam width is a function of z and governed by [65]:

$$w(z) = w_o \left[1 + \left(\frac{z}{z_R}\right)^2\right]^{1/2}, \tag{3-31}$$

where

$$z_R = \frac{\pi w_o^2}{\lambda}, \tag{3-32}$$

z_R is known as the Rayleigh range and λ is the wavelength.

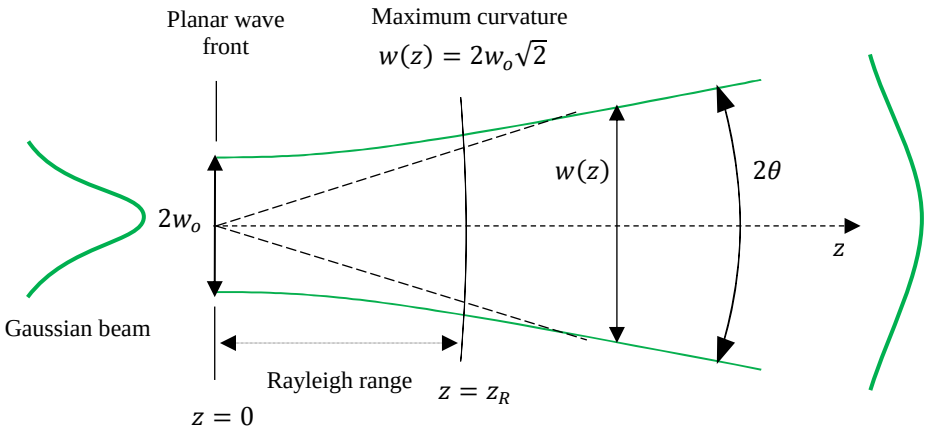

Fig. 3-6: At the waveguide end, the light diffracts and spreads with a radius $w(z)$ given by $w(z) = 2w_o\sqrt{2}$.

At a point from waveguide where $z \gg z_R$, the first term in equ. (3-31) can be neglected, accordingly the beam radius increases linearly with z. The divergence angle of the beam is then given by:

$$\theta = \frac{\lambda}{\pi w_o} \quad , \tag{3-33}$$

and mainly depends on the core size and wavelength of the guided wave. Consider the waveguide is an optical fibre as shown in Fig 3-7(a). To maintain intensity and manipulate light outside the fibre many different approaches have been introduced to direct light or couple it to a source or detector or even another waveguide. These techniques include fabrication of microlenses on the optical fibre by various methods such as electric arc-melting [66], laser micromachining [67], and chemical etching [68]. These methods need high energy, long process and precise control over experimental parameters [69]. One reasonable and cost effective technique is to integrate a self-aligned photoinduced polymer microstructure with the fibre. The structure is fabricated by guided light itself through the process of photopolymerization and there is no need to align an external source [69-71]. In the presence of a deposited photopolymerizable droplet on the end of the fibre, the liquid experiences rapid conversion from liquid monomer into a solid polymer as indicated by fluorescence region where the reaction happens Fig. 3-7(b). The reaction site will be determined through a competition between diffraction against spatial polymerization. The initially diffracted beam develops a region of polymerized material with a higher refractive index which leads to confine the guided beam into a polymerized channel which has been made by the light beam itself along the propagation axis [72, 73]. Consequently, the refractive index evolution provides a condition of total internal reflection at the interface of converted solid polymer and surrounded unreacted monomer. Thus modification of the initial monomer is restricted to illuminated part of the photopolymerizable system whilst the unexposed part remains unchanged and can be removed by a solvent [74]. This means that by shining light down a fibre core into a photopolymerizable material, the polymerization is automatically aligned with the fibre core, greatly simplifying the alignment [73, 75]. The change in refractive index is permanent as the illuminated part of the droplet solidifies in response to the light beam at specific wavelengths. This photosensitivity produces the largest changes in refractive index where the intensity is highest, and so the largest changes also occur on the

propagation axis. Even with the monomer formulation the beam initially diffracts, but with time it forms a region of higher refractive index along the propagation axis [72].

Photopolymerization is a spatially consecutive process, firstly begins at the vicinity of the fibre then develops very quickly through the entire droplet as long as the power of light emerging from cured part is sufficient to accomplish polymerization. The process will continue until it reaches the end of the deposited droplet. After rinsing a polymer tip appears as the extension of fibre core Fig. 3- 7(c). Fig. 3- 7(d) is a scanning electron microscope image of the polymer tip fabricated at the end of a single mode fibre SMF 28e.

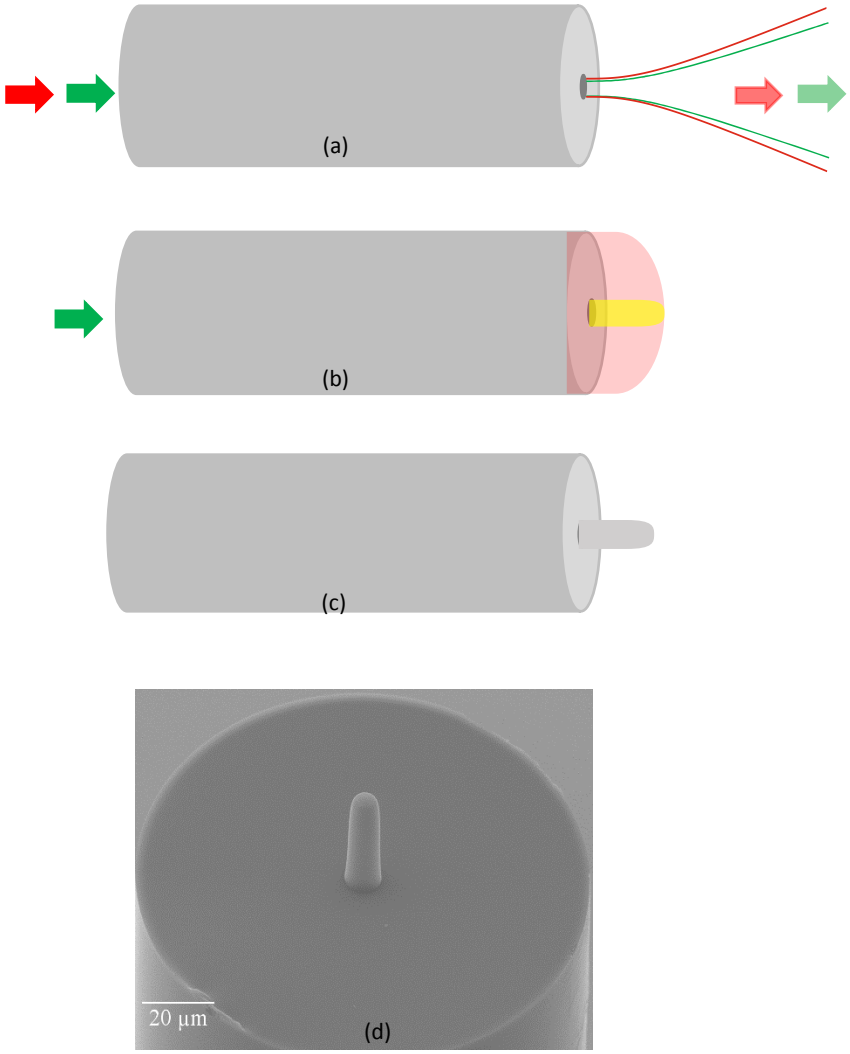

Fig. 3-7: (a) Light emerging from an optical fibre. (b) Illumination of photopolymerizable droplet deposited on the end of fibre. (c) Polymer tip formed by photopolymerization. (d) SEM image of a polymer tip fabricated during work for this thesis.

The lensing effect of its end gives polymer tip to be used as integrated lens for coupling applications, for example to couple light into a silicon on insulator waveguide [76]. Coupling efficiency as high as 70% was achieved by coupling a polymer tipped optical fibre to a semiconductor NIR edge emitting laser diode [3]. Additionally, carbon nano-probes were grown on to polymer tips for a high resolution image application [4].

The size and shape of the polymer tip is determined by the drop size, the laser power, exposure time and laser beam profile or guided mode. Varying laser power and mode gives a chance to manufacturer to create polymer tips with different radius of curvature. High beam power and long exposure produces flatter tip end and vice versa. The polymer tip pattern is also a direct replica of the guided mode by the fibre [77]. Typical fibres are single moded at conventional communication wavelength (1550nm), therefore higher order modes can be excited when they guide curing laser beams, usually in the spectral range of UV and near UV visible. Fig. 3-8 shows a polymer tip fabricated by linearly polarized mode (LP_{21}) guiding mode through a photopolymerizable droplet deposited on the end optical fibre [78].

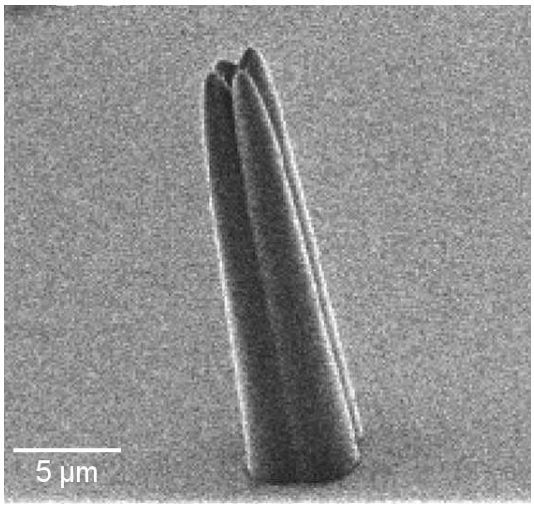

Fig. 3-8: Electron micrograph of polymer tip fabricated over the multimode fibre core, the writing beam has a field distribution corresponds with LP_{21} mode [78].

The self-writing technique can also be used to fabricate a polymer waveguide between two similar sizes or even between two dissimilar waveguides. Free space coupling can cause significant loss because of diffraction, Fig. 3-9(a) or as a result of lateral misalignment and different fibre sizes. Therefore to transmit light from one waveguide to another efficiently a polymer bridge can be implemented. Similar to polymer tip

fabrication, if a droplet of monomer is put between two aligned fibres the propagation of a beam through the photopolymerizable liquid creates a self-written polymer channel as indicated by fluorescence region where the reaction happens, Fig. 3-9(b). After illumination for few seconds and then rinsing away the liquid part a straight polymer waveguide appears between two fibres Fig. 3-9(c). The phenomenon of self-focusing and self-writing photopolymerization can be theoretically modelled through an iterative technique which give the value of electric field at successive points in the direction of light propagation regarding the alteration that has happened to photopolymer refractive index [79].

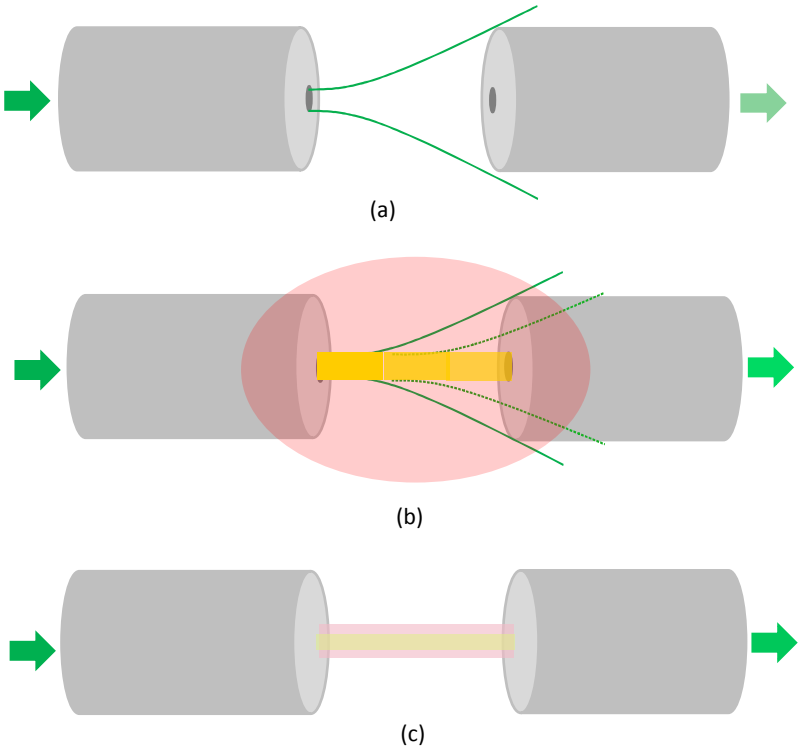

Fig. 3-9: Schematic explanation of self-written polymer waveguide formation. (a) Free space coupling, some light will diffract and coupling loss increases with air gap between two fibres. (b) Light induces polymerization of monomer droplet deposited between two fibres, yellow strip is a fluorescence emission results from excited photoinitiator molecules transition from higher energy state to ground sate and indicates the boundary where the polymerization happens. (c) Polymer waveguide appears between two fibres after washing off unaffected part of the droplet, light is confined in the polymer bridge.

3.7 Photopolymerizable systems

Two different types of photopolymerizable systems were used in this investigation. Firstly and mainly, a three compound system based on an acrylate multifunctional

monomer with the aid of photoinitiator and coinitiator which is sensitive to visible light. Secondly, commercial transparent UV curable Norland optical adhesives.

3.7.1 Three compound acrylate based system

The system was introduced in several research papers, it was firstly proposed for fabrication of polymer thin films by exploiting the evanescent field from an optical fibre [80]. It has also been used to fabricate polymer tips on the end of optical fibres [70, 71, 78, 81]. The system as shown in Fig. 3-10 mainly consists of a trifunctional acrylate monomer Pentaerythritol Triacrylate (PETA) which forms a backbone of photopolymer compound. To extend sensitivity of the system into visible region also to improve reaction efficiency via producing large number of free radicals a photoinitiator or a sensitizer dye 2X, 4X, 5X, 7X-tetrabromo-fluorescein disodium salt (Eosin Y) and a coinitiator amine Methyldiethanolamine (MDEA) were added to the monomer.

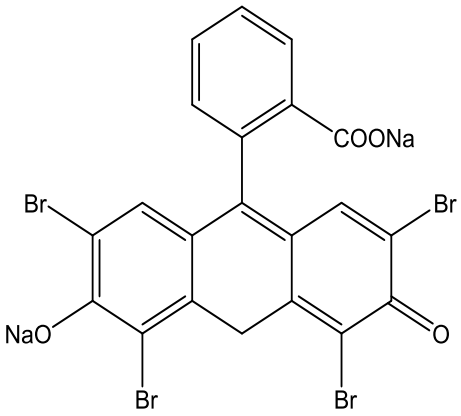

Eosin Y

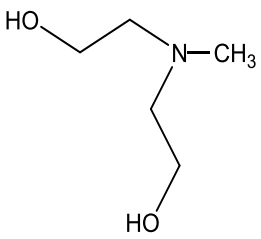

Methyldiethanolamine

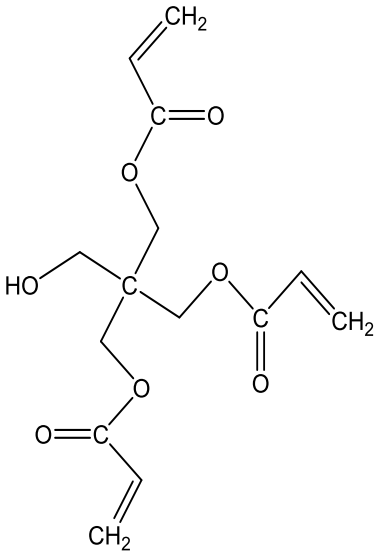

Monomer
Pentaerythritol Triacrylate

Fig. 3-10: Three components of photopolymerizable PETA system.

The amine is added to the system to raise curing efficiency, because the Eosin is type II initiator and it is strongly quenched by oxygen the amine can reduce the oxygen quenching especially at the surface of polymer where oxygenation is relatively higher. Although it has some drawbacks as it cause some yellowing in the cured polymer films. Also, dark reactions often happen in a system includes dye/ coinitiator which lead to short shelf life of the system [28, 33].

This formulation was developed originally because it can be polymerized by abundant visible laser sources such as frequency doubled Nd-YAG laser (532 nm), since it is highly sensitive to the spectral region from 450 nm to 550 nm with a peak absorption at 532 nm. Additionally, this liquid system is very flexible as it is possible to modify the physical and chemical properties of the formulation, namely viscosity, spectral sensitivity, polymerization threshold energy. Adjusting the properties could be done by changing the proportion of each components, supplying heat energy, and substituting the photoinitiator with different one to shift the spectral sensitivity.

3.7.1.1 Sample preparation

The three component photopolymer system was prepared by dissolving 0.02 g of Eosin Y in pre warmed 3 g of MDEA and the mixture was stirred vigorously at 50 °C for 20 min in order to allow the larger amount of the powder dye to dissolve in the liquid amine. The liquid was left for 10 min for cooling down then the top half was poured into a 10 ml cuvette. Then the mixture was left for another 30 min to allow the undissolved Eosin to precipitate at the base of the cuvette. Meanwhile 9.2 g of PETA was heated for 15 min at 50 °C and stirred in order to reduce its viscosity and encourage it to mix easily with the Eosin and MDEA mixture. Finally 0.805 g of solution which contained sensitizer dye and coinitiator amine was added to the monomer to obtain the final compound which consisted of 92 wt. % of PETA , 0.05 wt. % of Eosin Y and 8 wt. % of MDEA. The sample was stirred and maintained at constant temperature on a hot plate during preparation to guarantee a uniform solution with a minimum amount of residuals. Then the compound was left for 30 min and top half of it was poured into a new cuvette. This is a sample with minimum photoinitiator concentration. Using same procedure, some other samples with different Eosin concentrations of 0.1, 0.2, 0.5, 1, and 5 wt. % were prepared by the same procedure and order, using larger quantities of Eosin. Although the

liquid monomer proportion is much larger than MDEA, it is difficult to dissolve Eosin powder in it because when Eosin was added to PETA immediately it accumulated and stuck together in lumps which could not be dissolved even by over heating or stirring the compound. Therefore to avoid undissolved Eosin precipitation Eosin was dissolved in MDEA first then added to PETA.

3.7.1.2 Reaction mechanism

The general outline of free radical polymerization was presented in chapter two, here some specific features of the reaction associated with PETA system will be considered. Upon the absorption of green photons by Eosin Y molecule as it contains four C-Br bonds and the bond energy matches with incident photon's energy around 500 nm as in Fig. 2- 3, Eosin is excited to its singlet state then to its triplet state as in Fig. 2-4. The triplet state then undergoes photo-reduction by reaction with the electron donor amine as in equ. (2- 2). The corresponding amine in turn generates free radicals which are capable of initiating polymerization of acrylate monomers by chain formation. Polymer chains extend diversely through the solution and add up nearby monomer molecules until peer chains meet and propagation terminates by two radical interactions. The successive stages of reaction are shown in Fig. 3-11. Throughout polymerization, because of acrylate monomer multi-functionality, it is highly probable that some chains interact with more than one chain to form a crosslinked structure, which increases conversion rate remarkably [78]. The main advantages of free radical polymerization are the high speed curing rate and it is not highly influenced by impurities. Accordingly, materials were used as purchased from supplier without purification [29]. On the other hand the reaction path from eosin excitation up to polymer chain formation undergoes several relaxation radiation, internal conversion, and deactivation mechanisms. Also photopolymerizations involving free radicals are extremely sensitive to oxygen quenching such that all initial free radicals are quenched by oxygen molecules [40, 82].

After consuming most of the dissolved oxygen molecules, the polymerization reaction can begin. The amount of energy absorbed by the solution at the early inhibition stage is known as the threshold energy [78]. Beyond this energy, the most generated free radicals can contribute in the polymerization reaction. Regarding polymer microstructures integrated with optical fibres, the quenching effect by oxygen diffusion is more dominant

at the sample air interface. Therefore the final shape of a written polymer structure is highly affected by the curing position relative to the surrounding atmosphere.

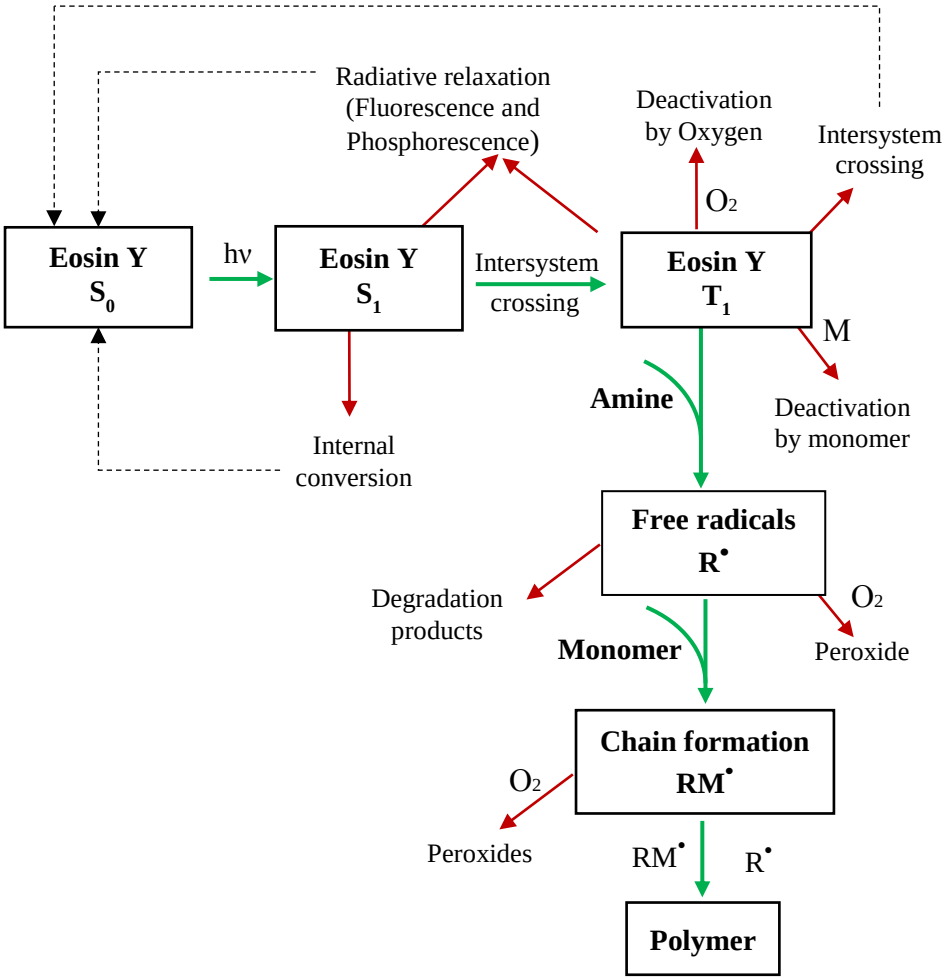

Fig. 3-11: Photopolymerization reaction stages of three compound PETA system [14].

3.7.2 UV curing optical adhesives

Norland optical adhesives, NOAs are commercially available transparent adhesives. They are viscous solutions mainly consisting of thiol-ester with an acrylate monomer. Thiol is a compound that forms a functional group of the monomer which contains a sulphur atom and a hydrogen atom (-SH) [83]. NOAs are sensitive to UV spectral ranges between 320- 400nm. Different products are fundamentally the same in structure and appearance but their viscosities, refractive indices and adhesion characteristics to different materials such as glass are different. Higher viscosity adhesives are hard to rinse and lower viscosity ones are hard to deposit to form a proper shape liquid bridge pre

polymerization, therefore we mainly used medium viscosity product NOA61. NOA adhesives were used as they received from supplier without adding any photoinitiator to them or warming and stirring. Free radical polymerization in NOAs occurs directly from UV absorption which derives free radicals from monomer molecules directly, therefore there is no need of adding photoinitiator unless one wants to improve polymerization efficiency and extend curing beam to visible spectrum.

Chapter Four

Freestanding photopolymer waveguides between two fibres

The work described in sections 4.2, 4.4, 4.6, and 4.10 of this chapter is published as: Long, free-standing polymer waveguides fabricated between single mode optical fibre cores [84]. All polymer waveguides are fabricated between SMF 28e fibres.

4.1 Introduction

Optical fibres are an enabling technology in many applications including routing light from remote sources to remote sensors and detectors, bringing light inside the body in diagnostic endoscopes and giving a light path immune to outside interference and misalignment. However the small core of an optical fibre presents challenges at interfaces; bringing light from a source into the fibre, building a sensor where the light must interact with its environment so cannot remain buried in the core of a fibre, bringing light from a fibre core to a detector, or joining similar or dissimilar fibres. Many different solutions are available to these challenges, one of which is to use photopolymers to construct self-aligned structures on the core of a fibre [70, 71, 78] . Photopolymerization enables modification of the initial liquid monomer at the illuminated part of the photopolymerizable system to form a permanent solid polymer waveguide at the end of fibre. If a second optical fibre is aligned to the growing self-guided polymer waveguide, then light can be coupled from one fibre to another. This is often referred to as light induced self-written waveguides, the phenomenon was described in section 3-6. They were first fabricated in 1993 by Frisken through an experimental work to fabricate a polymer waveguide from UV cured epoxy at the end of an optical fibre [2]. Then in 1995, it was theoretically described by Monro *et al.*[85]. A few months later Kewitsch *et al.* [73, 86] demonstrated experimental fabrication and a theoretical model of refractive index

change under the influence of electromagnetic field in the photocurable acrylate monomer. Since that time, different experimental procedures have been used to construct polymer waveguides between two fibres, mostly two multimode fibres of same and different dimeters, and few between two single mode fibres. Multimode fibre has a larger core size which eases holding fragile polymer structures integrated with fibre. Mensov *et al.* in 2007 reported high optical transmission 2.8 mm long polymer waveguides fabricated between two multimode fibres [87]. The transmission during very early stages of polymerization was reported from the initiation of polymerization and only for up to 4 seconds after, and only for single wavelength 850 nm. The optical performance was not reported after rinsing, because the two fibres and photopolymerizable monomer were sandwiched between two glass plates separated by 200 μm, so the excess monomer could not be removed. Yamshita *et al.* demonstrated 1.17 mm long polymer waveguides fabricated between two graded index fibres with core diameter of 62.5 μm reported an insertion loss of about 2 dB [8]. More recently, Gunther *et al.* reported 300-800 μm long polymer waveguide between 50 μm and 105 μm core diameter multimode fibres with attenuation of 0.9 $dB.cm^{-1}$ at single wavelength of 638 nm [9]. Regarding single mode fibres, up to now only short polymer waveguides have been reported. In 2002 Dorkenoo *et al.* proposed bridges as long as 1 mm but with little optical characterization because of mode confinement difficulties in the written channel. The difficulty arises because telecommunication single mode fibre allows propagation of higher order modes at the curing beam wavelength (450 nm - 550 nm) [88]. Jradi *et al.* reported an average coupling efficiency of about 65% (1.8 dB loss) for a polymer waveguide bridge of length 90 μm between two single mode fibres [6]. Using a similar approach, Eccoffet and Lougnot investigated the influence of light power density on the dynamic development of coupling between two fibres via a polymer channel during the first few seconds of photopolymerization [89]. Missinne *et al.* fabricated cladded 50 μm and 100 μm long self-written waveguides with minimum insertion loss of 0.3 dB [7].

This chapter describes fabrication of low loss free-standing polymer waveguides up to 600 μm long between two standard single mode optical fibres. We also show that the optical power required for photo-polymerization is sufficiently low that it is possible to use a xenon discharge lamp rather than a laser, which allows investigation of the optical transmission over a wide range of wavelengths from visible to near IR. This broad area incoherent source ensures even illumination for writing the waveguide at wavelengths

where the fibre is multimode. The aim of switching from multimode fibres to single mode fibres is to miniaturize integrated polymer structures to reach higher spatial resolution, as the size of a written waveguides highly depend on the core size where the beam emerges [90]. Polymer micro- and nano-wires integrated with optical fibres are products of these miniaturization attempts. They offer some advantages in sensing applications. For instance, polymer nano wires allow gas molecules to diffuse into the structure or to form a chemical bond at the surface of polymer, this interaction with semiconductor nanowires and glass nano fibres is difficult. Furthermore, the chemical and physical properties of photopolymers and easy processing give a chance for a variety of materials to be doped into polymer nanowires to aid sensing applications based on their optical and electrical properties. Polymer nanowires have been applied in various sensing applications to detect metal ions, toxic gases and biotin-DNA [91-93]. New communication systems include many different devices which need to be optically interconnected efficiently. Self-written waveguide provides auto alignment between guiding devices which offers a substantial aid in this field as the major challenge in these all interconnections is accurate alignment of optical devices [9, 94, 95]. Photopolymer waveguides doped with specific elements and dyes were used for optical signal amplification [96, 97], also for converting a random optical signal to a Gaussian distributed like beam [98].

4.2 Photorefractive solitons

Photopolymerization is a nonlinear process where during the reaction an incident light beam produces a permanent refractive index change at the illuminated area. The change in refractive index depends on the absorbed total light energy rather than the instantaneous light intensity as in Kerr index change. The main feature of light propagation through a Kerr medium is that light can guide without diffraction in the phenomenon known as spatial soliton propagation. The self-trapping and self-focusing process of photopolymerization is similar to the spatial soliton propagation during photo curing reaction [99]. The reaction induces a refractive index change larger than that of Kerr nonlinearity effect by orders of magnitude even though the process requires intensity only few microwatts per square centimeter whilst Kerr effect needs intensity of megawatts per square centimeter. Moreover the response time of Kerr nonlinearity is of order of femtosecond whereas it is increases to milliseconds and minutes as photopolymerization

proceeds [72]. Kewitsch and Yariv demonstrated a new form of nonlinear wave equation associated with light propagation within a photopolymerizable acrylate material during the reaction with an irreversible refractive index change to be about 0.15. The nonlinear index change in conventional Kerr and photorefractive mediums is less than 10^{-3} and it vanishes after illumination [73]. Experimentally a narrowing feature was systematically observed during photopolymerization at given places along the illumination axis via fluorescence as shown in Fig. 4-1.

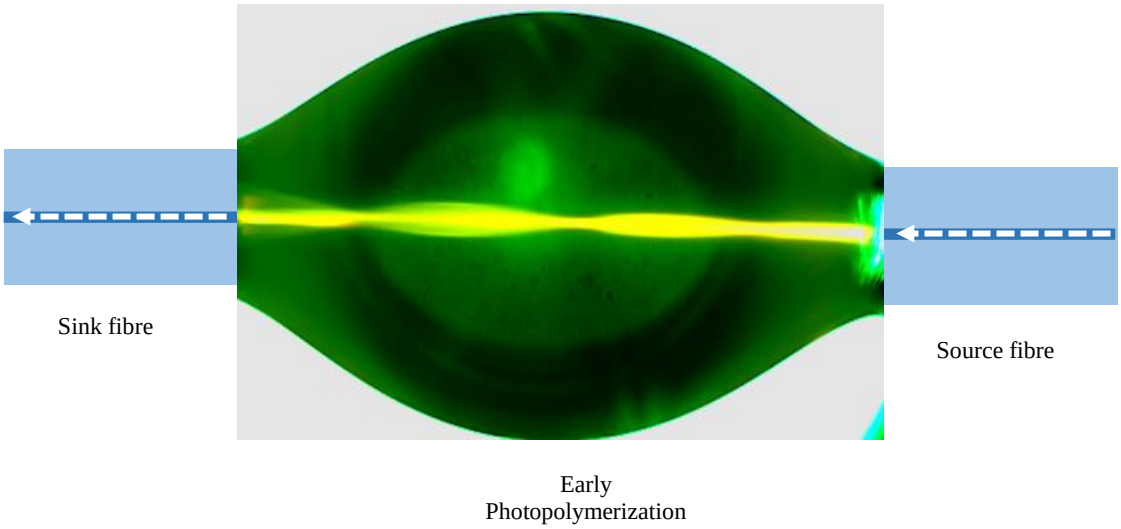

Fig. 4-1: Optical micrograph of early stage of photopolymerization by light emerging from the fibre on the right on a drop of PETA with length of 600 µm, writing beam power of 12.8 µW and sample containing Eosin of 0.5wt. % . The guided beam produces nodes in the written waveguide immediately after photopolymerization, the nodes only last for a few seconds.

The effect has been referred to as a quasi-solitonic behaviour and at the initial stages of writing the guided beam produces nodes in the written waveguide [70, 88]. However, the effect is not long lasting because of the rapid conversion of the irradiated monomer refractive index under the action of photopolymerization [70]. The node formation has been numerically predicted by Hocine *et al.* using beam propagation method modelling through a medium where the refractive index increases with illumination and time [79].

4.3 Photocuring light sources

Usually the light required for photopolymerization is provided by a coherent laser beam, as this is easy to couple into an optical fibre core and provides high power density. All research associated with self-written waveguide have used monochromatic laser sources to cure polymer waveguides. However we show that the process is also possible for broadband incoherent light sources such as laser driven xenon source. The broad spectral range of absorption of the photoinitiator is able to gather sufficient energy from this low intensity source to be able to reach the threshold for initiating polymerization.

4.3.1 Curing by laser

The three compound photopolymerizable system contains Eosin Y which absorbs visible light in the range 450 - 550 nm [71]. This formulation exhibits peak absorption at 532 nm and is transparent at 633 nm. Two laser sources at these wavelengths were used for curing and prepolymerization alignment respectively. Initially low power of the range of 5 µW was sufficient to cure short bridges in the range 100 µm. The outcome was a uniform single channel waveguide as shown in Fig. 4-2.

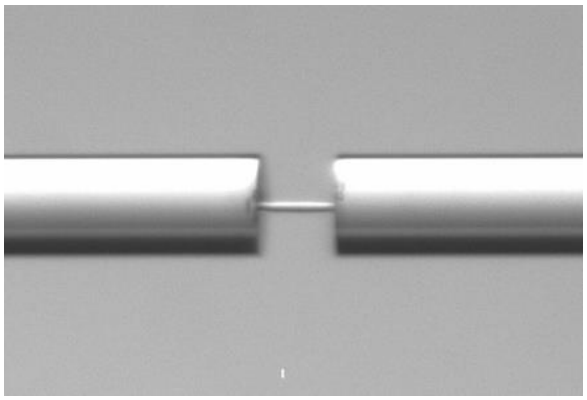

Fig. 4-2: 100 µm polymer bridge fabricated by 532 nm CW laser diode. The fabrication parameters were power of 5 µW, Exposure time 20 s and PETA with Eosin concentration of 0.5 wt. %. The loss of waveguide was 1.2 dB at 532 nm.

Increasing the gap between the two fibres stopped the progression of photopolymerization toward the output fibre end because Eosin molecules at the initially illuminated part near the input fibre absorbed a substantial amount of the curing

beam [100]. The situation led to oxygen quenching being dominant at some point beyond middle point of the bridge, such that the excited photoinitiator molecules instantaneously deactivated by predissolved or diffused oxygen molecules. Increasing beam power is one solution to prevent polymerization deterioration and to allow the reaction to proceed until whole waveguide forms. When the power was increased the single channel guide remained confined for a certain length. Then at some point the guided channel broke up into multiple fluorescence filaments as shown in Fig. 4-3(a). As the reaction developed the channel maintained its chaotic behaviour toward output fibre, see Fig. 4-3(b) [88].

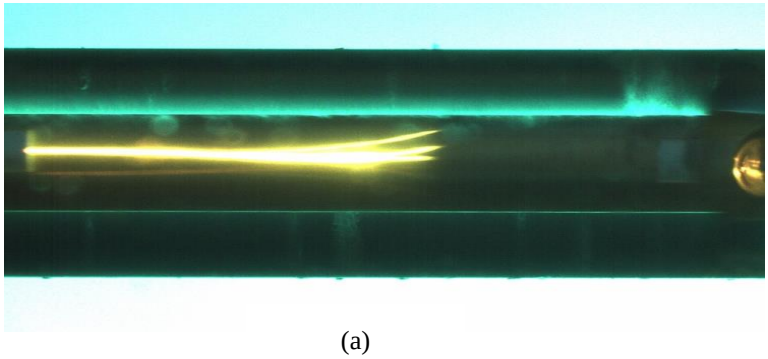

(a)

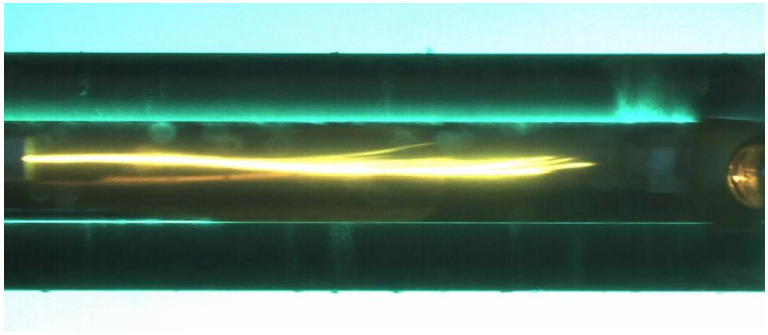

(b)

Fig. 4-3: Written single channel breaks up into separate guided channels upon increasing beam power of 532 nm CW diode laser. (a) Multiple channels appeared at the beginning of the chaotic processes after 2 s of illumination and when beam power was increased to 45 µW to form 2 mm polymer waveguide. (b) Development of chaotic channel toward sink fibre, same curing power and at 5 s from polymerization initiation.

The problem can be attributed to the fact that used optical fibre (*Corning*, SMF 28e) is single mode at conventional telecommunication wavelengths which allows higher order modes when green laser propagtes through it. The used fibre has V - number about 6.8 which is multimode at 532 nm and therefore the beam profile has not intensity distribution

as fundamental mode and may cause some non - uniformity in the written waveguide. To overcome the problem mode filters have been introduced to both input and output fibres. Fibres were tapered down from 125 µm to 40 µm such that the V- number (equ. (3- 17) filters higher order modes and only allow fundamental mode to be guided through the fibre [101-103]. The tapering was done for this experiment by Dr. S. Yerolatsitis. The schematic diagram of polymer bridge fabrication using monochromatic laser sources is illustrated in Fig. 4-4.

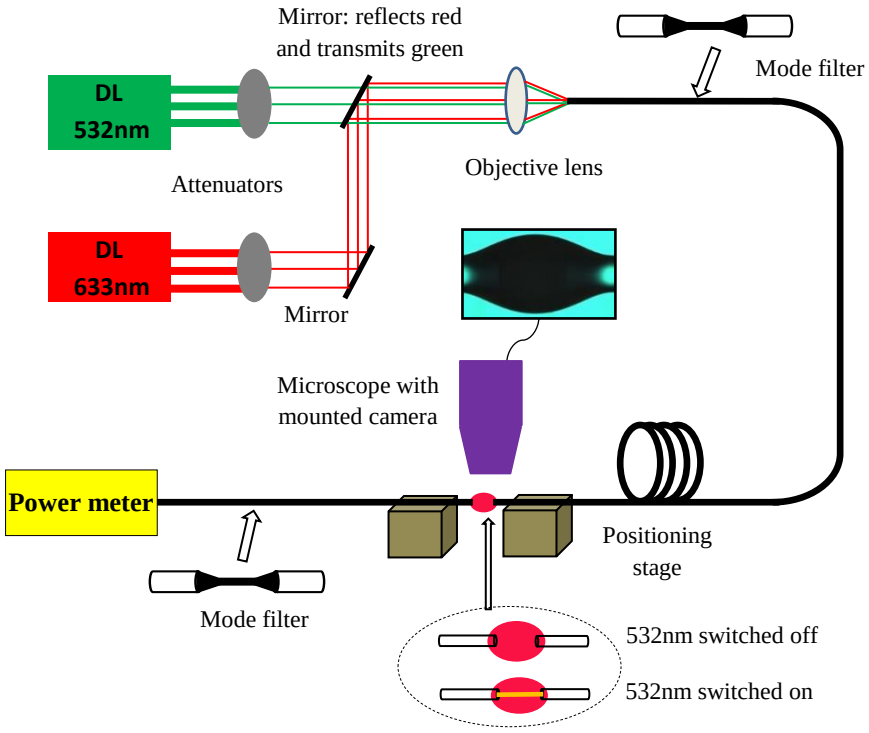

Fig. 4-4: Experimental setup of self-written waveguide fabrication by 532 nm CW diode laser. The waveguide fabricated between two aligned fibres which were aligned by 633 nm laser after drop deposition. Two mode filters in the source and sink fibres for allowing them to let fundamental mode propagation. Loss was measured by logarithmic relationship between the output power through the polymer bridge and input power emerges from source power.

This experimental set up enabled us to fabricate waveguides with high reproducibility and satisfactory optical transmisson but loss measurement was only possible at two wavelengths. Also loss varied with different mode filters for the same bridge length depending on the quality of tapering. The loss variation because of mode filters resulted in large uncertainities in loss mesurement associated with polymer waveguide. Moreover

the tapered parts were very fragile and often broke during cleaving and preparing fibres for new bridge fabrication. Single mode photocuring has a unique advantage of spatial resolution allows fabrication of very small size structures to be applied in optoelectronic interconnections and fibre interconnections. Although the spatial resolution improves by using short wavelength curing light, most fibres support higher order modes as wavelength decreases which raises the problem of light confinement in the written polymer waveguide.

4.3.2 Curing by incoherent lamp

Experience with laser curing shows that the required power for photopolymerization of the tiny cross-section of a polymer waveguide is 2 to 20 µW, but there are reports using powers as low as 0.1 µW [71, 104]. An incoherent beam is a great advantage as the writing wavelength may be much shorter than the operating wavelength, meaning that the fibre is likely to be multimode at the writing wavelength. On the other hand, as mentioned previously a narrow band laser source with high beam quality will excite a combination of modes which will potentially provide a varying beam pattern at the output of the fibre where the waveguide is to be written. This can be mitigated by careful coupling or by building a mode filter into the fibre, but it is much more simply eliminated using a spatially and spectrally incoherent source. The broad area source ensures stable equal excitation of all the fibre modes, whilst a broad wavelength band washes out the intensity fluctuations caused by changing interference between modes as the fibre is moved. Therefore, using a broadband light source provides a Gaussian like beam profile at the end of source fibre by superposition of all excited modes, and hence a uniform polymer bridge all along the written channel can be guaranteed. Accordingly a laser-driven xenon discharge lamp (*Energetiq* EQ-99) was used, providing a bright broadband source of light from <300 nm to >2000 nm. An ordinary xenon discharge lamp would also provide the required power density, but the laser driven lamp provides high spatial stability of the small discharge which is important for good coupling into the fibre. Moreover this light source can serve a double purpose of photopolymerization and optical transmission investigation, allowing reliable loss measurements for the waveguides [84]. When quoting a single loss figure for a waveguide the measured loss was averaged between 1500 – 1600 nm, in the single mode region of the SMF 28e fibre.

4.4 Method for waveguide fabrication by incoherent light

The fabrication procedure is significantly similar to what explained in previous section, except the lasers replaced by a xenon lamp and power meter by optical spectrum analyzer (OSA, *Ando* AQ-6315E). The new method also allowed more accurate optical measurement and wider vision of polymer device characterization. The polymer waveguide bridge fabrication commenced with a single piece of fibre. Light from the xenon discharge lamp was coupled into the fibre and a baseline transmission spectrum was recorded by OSA. The input and output alignment was then fixed to allow all spectra during and after fabrication to be referenced to this baseline, allowing accurate measurement of the optical performance. This initial spectrum also showed that the total curing power of 12.8 μW was available for photoinitiation over the absorption bandwidth of Eosin. The fibre was then cleaved in the middle and the two new ends were aligned with a set distance between them (40 to 600 μm) as shown in Fig. 4-5.

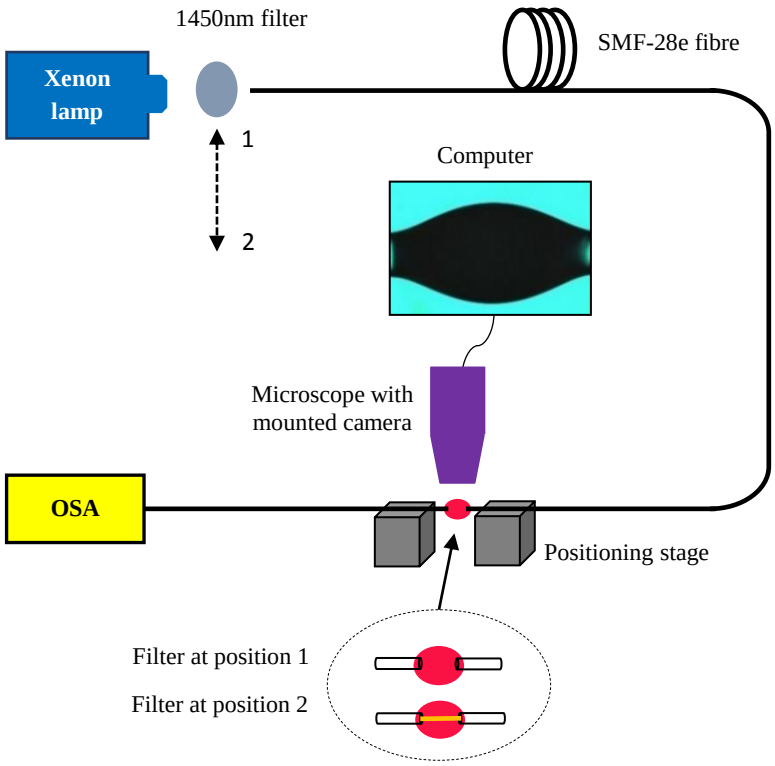

Fig. 4-5: Experimental system for self-written polymer waveguide fabrication by broadband incoherent light source and optical characterization, the magnified diagram of the fibre ends.

The transverse position was optimized by observing the transmitted power at 1550 nm (where the fibre is single mode) received by the OSA. Once transmission at 1550 nm was maximized, the spectrum was recorded as the air gap transmission between fibres. Next a long pass, 1450 nm, filter (*Thorlabs,* FEL 1450) was placed between the xenon lamp and the input fibre to prevent premature photopolymerization. A small drop of the monomer mixture was put between two fibres to make a liquid bridge between them. The positioning of the fibres was adjusted again to get maximum transmitted power at 1550 nm since deposition causes some misalignment. By removing the optical filter photopolymerization started, Fig. 4-6(a). The fluorescence results from radiative deactivation of singlet excited state of Eosin and is bright initially then it becomes dimmer as reaction proceeds consuming Eosin molecules. The emission is an indication of where the reaction takes place and gives idea about the cross sectional size of the waveguide [6].

The progress was monitored by taking repeated transmission spectra and optical micrographs. An initial waveguide bridge formed very rapidly between the two fibres but full formation took about 2- 5 minutes of consistent illumination depending on the bridge length. The remaining uncured monomer was rinsed off using ethanol, leaving an exposed polymer waveguide bridge rigidly attached between the fibre ends as an extension of the fibre core, as shown in Fig. 4-6(b). The rinsing step is critical in the bridge fabrication because the adhesion bond between polymer and fibre is weak so that imposing tiny extra pressure may break the bridge at the fibre/polymer interface.

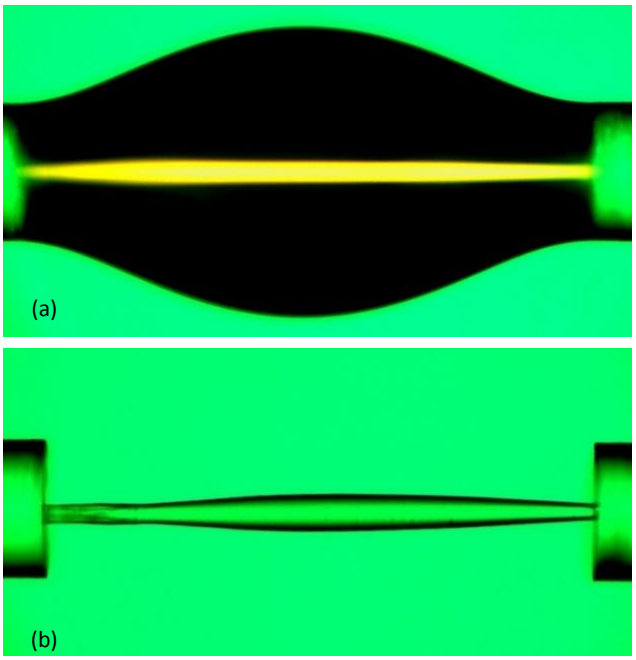

Fig. 4-6: Optical microscope images of formation of a polymer waveguide bridge, the green background is from illumination by a cluster of green LEDs which has given the best resolution of polymer waveguides. The fabrication parameters were; beam power 12.8 µW, PETA drop with 0.5wt.% Eosin concentration, and 5 min illumination before rinsing. a) Fluorescence shows the region where photopolymerization is in progress. Light is incident from the right-hand fibre. b) 600 µm long polymer bridge between two fibres, 1.26 dB loss at 1550 nm.

The fabrication process of all waveguide lengths went through the same procedure regarding photocuring. The main challenge was deposition of droplet to form a relatively symmetrical liquid bridge before polymerization. In the beginning, a gap of 100 µm was set between cleaved fibres then a small drop was deposited. The desired distance was established by tuning the position stages. Acquiring a liquid bridge up to 300 µm long was feasible with clean fibre ends beyond that the drop slid toward one of fibres and liquid bridge vanished. To allow droplet stays between two fibres for bridge lengths from 400 µm – 600 µm, the fibre ends were gently lubricated with a very thin layer of hydrocarbon grease such that the grease only cover the surface of the fibre. To do so fibres were greased and then cleaved. Lubricated fibres could hold drop up to 750 µm long.

4.5 Absorption at the photosensitive spectral range

The absorption is high in the spectral range where Eosin is sensitive, particularly at the early stages of polymer bridge formation, as in Fig. 4-7. Then it deteriorates with reaction development because substantial amount of Eosin molecules are bleached to contribute in free radical generation. In photopolymerization initiation, the loss is highest because the bridge has not formed entirely and light is lost to diffraction as well as absorption. There is a 10% decreasing in absorption between first and second trace as light strongly confined in the channel and Eosin is consumed to quench oxygen and to initiate polymerization. There is a 90 s time gap between two successive traces during the photocuring. As the reaction continuous, the cured channel becomes more transparent and absorption decreases. The change becomes significant once more after rinsing because all monomer washed off. Then it slows down again after bleaching large proportion of residual Eosin molecules.

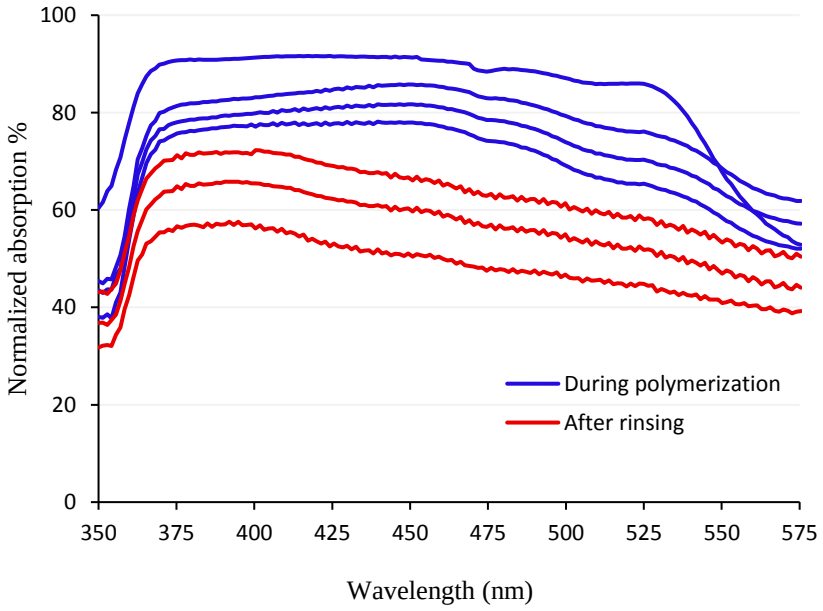

Fig. 4-7: Absorption development during polymerization associated with 500 µm PETA bridge, 0.5wt. % Eosin concentration. The time between every two successive traces is 90 s except the last one which was taken after 3 min from previous one. Absorption decreases with polymerization over the spectral range of photoinitiator sensitivity. Blue curves during polymerization and red curves after rinsing.

Fig. 4-8 demonstrates absorption percentage of the waveguide at 450 nm for exposure time of about 10 min from the polymerization initiation. There is a sudden decrease in the absorption from 76% to about 66% after rinsing because all monomer liquid has been washed out and no more photopolymerization reaction occurs at the boundary of the polymer bridge, although absorption is still significant as there will be some Eosin molecules remaining in the bulk of the channel which will absorb some of guiding light.

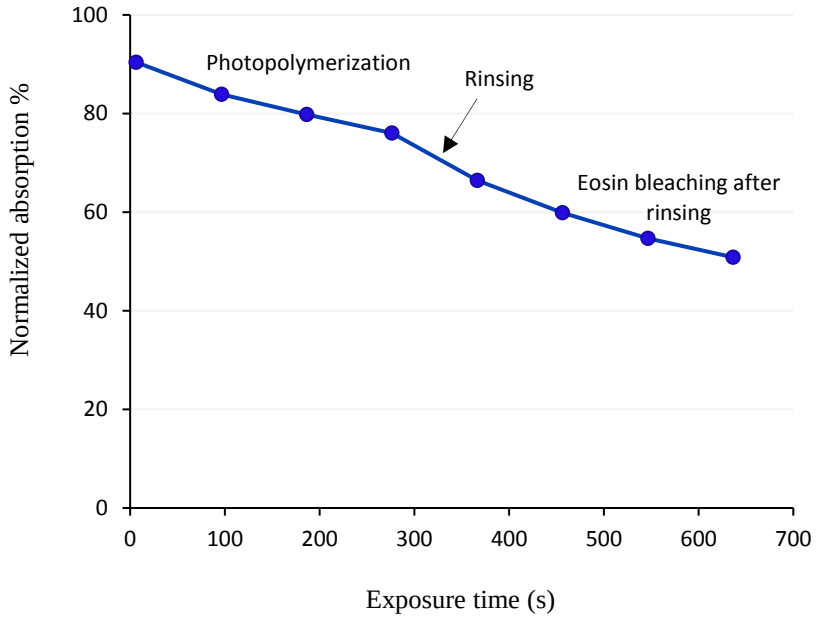

Fig. 4-8 : Absorption at 450 nm (average from 400 – 500 nm) for 500 µm long waveguide during photopolymerization and after rinsing. The fabrication parameters are the same as for Fig. 4-7.

With extending the monomer drop between two fibres the amount of photopolymerizable sample and hence the number of Eosin molecules also increase, which in turn enhances the absorption as indicated in Fig. 4-9. The relation between absorption and bridge length is linear in the beginning then its growth declines between 300 µm to 500 µm. A rapid increase happens again when the gap extended to 600 µm, the rapid change is not entirely absorption by photoinitiator but is partly because of intensity deterioration at the final 100 µm. The incidence also leaves its impact on the waveguide after rinsing as discussed in section 4.10.1.

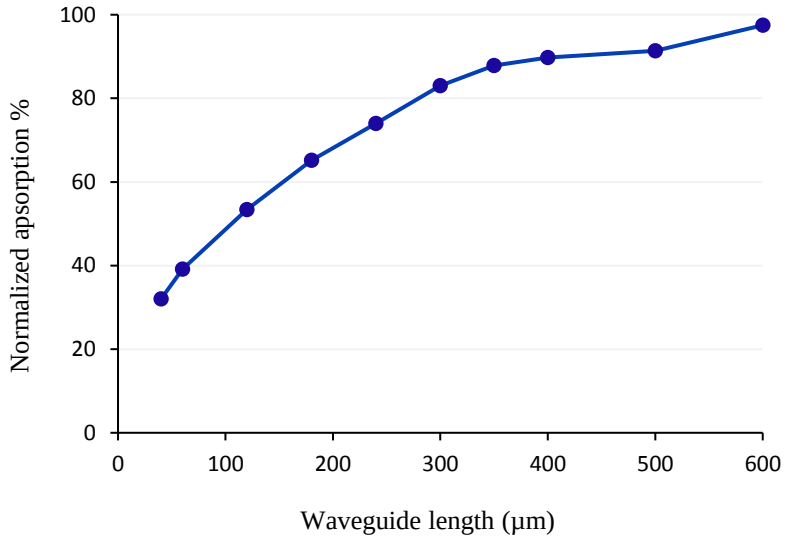

Fig. 4-9: Maximum absorption as function of waveguide length at 450 nm (average from 400 - 500 nm), for PETA system with Eosin concentration of 0.5wt. %.

4.6 Optical transmission of polymer waveguides

The Optical transmission spectrum was recorded for the waveguide bridges throughout the fabrication stages. Fig. 4-10 shows loss spectrum of a 400 µm air gap, the waveguide bridge during formation and the final rinsed polymer bridge, all referenced to the transmission of the initial single fibre before cleaving. There are abrupt features associated with high order mode cut-offs at 900 - 1100 nm and 600 - 800 nm indicated by dashed circles in Fig. 4-10. The absorption of the Eosin between 400 nm and 550 nm is clearly visible in the initial spectrum during polymerization, but decreases as the dye is bleached over 5 minute exposure. The final polymer waveguide bridge shows little residual absorption by unbleached Eosin molecules and a low loss where the germanium doped step-index fibre starts to have high transmission to the upper limit of the OSA at 1750 nm. Insertion loss is higher in UV from residual absorption, then ~ 0.5 dB all across visible to IR. The general shape of the transmission spectrum is the same for all bridge lengths. The only difference is the absorption and attenuation values for each channel such that for longer bridges the absorption is higher during polymerization and loss value generally higher at corespondent points.

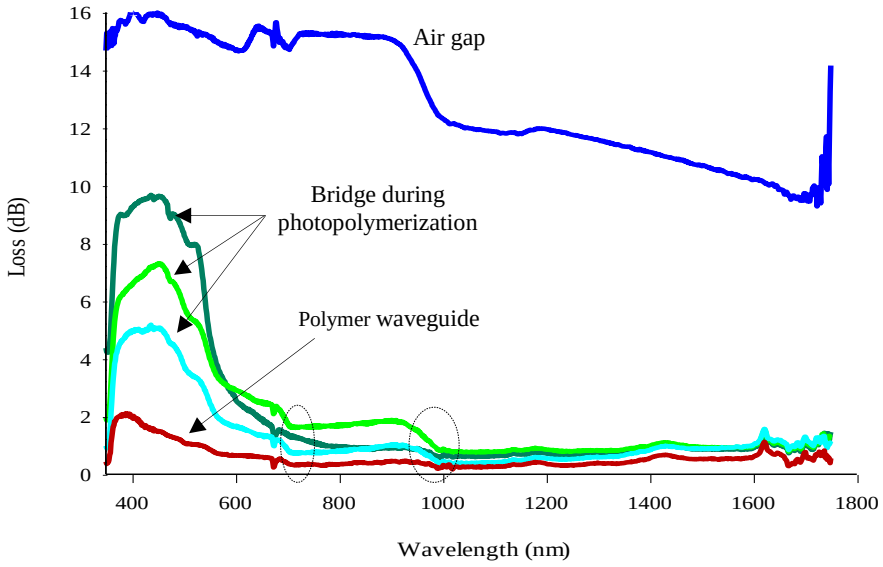

Fig. 4-10: Loss as a function of wavelength associated with 400 µm air gap and polymer waveguide bridges at different stages of formation. The waveguide fabricated from PETA drop with 0.5wt. % Eosin concentration illuminated with beam power of 12.8 µW of for 5 min.

Nearly all polymer waveguides fabricated showed similar broad band, low loss transmission, and there was no significant increase of loss as the waveguide length increased. The polymer channels guide light very efficiently, especially when compared with an air gap between two fibres. This comparison is illustrated in Fig. 4-11, showing a loss between 0.5 dB and 1.26 dB for bridges 40 to 600 µm long in the spectral region where the fibre is single moded. At other wavelengths the attenuation was similar, even at shorter wavelengths where the fibre is multimode. For each length there was a target of 0.5 dB transmission loss, and one or two low-loss waveguides were fabricated, with the better loss presented in Fig. 4-11. Insertion loss remains around 0.5 dB for all bridge lengths up to 400 µm, then deviated from low loss line at 500 µm and 600 µm to cross 1 dB value, as a result of fabrication difficulties. The rapid change is possibly a consequence of the poor surface morphology of the ends of these longer bridges, as discussed in section 4.10.1. Other factors may also have contributed in this efficiency falling. Transverse shifts of the fabricated bridge are more likely to happen for long bridges during rinsing. Also for such a large gap the initial alignment by maximization of measured at 1500 nm is very difficult because even with moving one of the fibres by a few microns the transmitted power does not change, so the waveguide growing from one core may be misaligned from the receiving fibre.

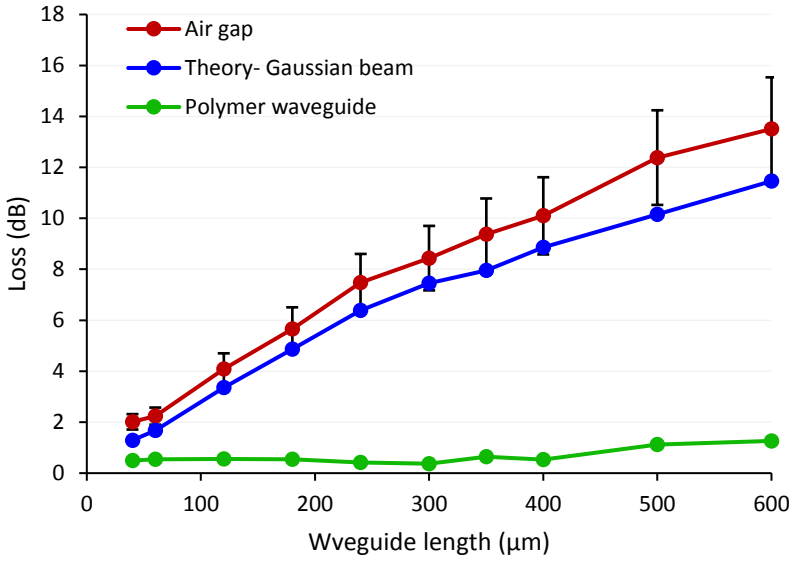

Fig. 4-11: Loss recorded between two aligned fibres with air between (red line) and theory line (blue line) associated with Gaussian beam emerges from SMF 28e fibre at 1550nm compared with loss in a polymer waveguide bridge (green line). Data taken from spectra as in Fig. 4-10 averaged from 1500 -1600 nm, in the single moded region of the fibre.

In all of the bridges there are several possible mechanisms for attenuation after polymerization is completed. Firstly, there are bulk effects in the material itself; residual, unbleached, absorption from the initiator (particularly at short wavelengths) or scattering from bulk impurities. Secondly, with insufficient exposure waveguides may not be sufficiently well attached to the ends of the fibres. Finally, the shape of the waveguide affects the propagation of waveguide modes. For single mode transmission, the mode of the input fibre must match the mode of the waveguide bridge at the input and output. Cross sectional variation along with the waveguide's length must be slow to allow the waveguide mode to adapt adiabatically. Additionally, rinsing may cause some unseen damages at the fibre/polymer interfaces which reduces transmission efficiency. Occasionally bridges were formed which appeared to be appropriately constructed but because of unseen mismatching at the interfaces the losses were much higher than the targeted or expected value.

4.7 Photobleaching

The electronically excited Eosin molecules in singlet and then triplet states either are deactivated through radiative and non-radiative transitions or they react with coinitiator MDEA to form primary free radicals and in this case they are bleached. Photobleaching depends on exposure time, some Eosin molecules might be excited several times until they grabbed by MDEA molecules. Deactivation via fluorescence is visible and allows us to monitor the process of photobleaching and conversion rate. With consistent irradiation and sufficient beam intensity the number of unbleached eosin molecules become fewer which is indicated by dimmer fluorescence. Fig. 4-12 shows that the fluorescence becomes weaker and weaker as the bridge is irradiated for two hours after rinsing.

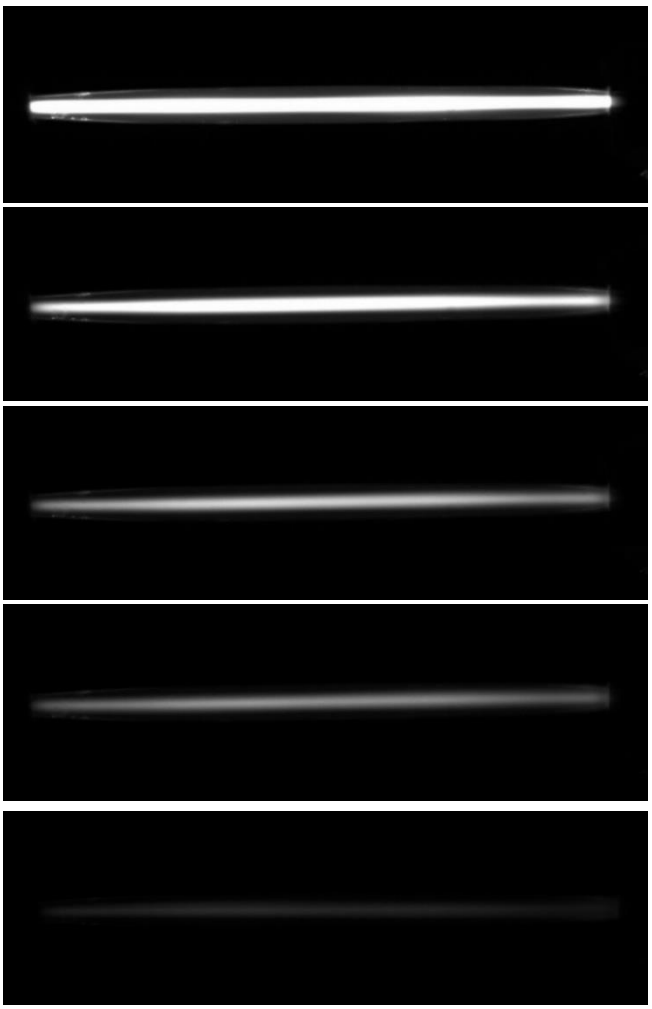

Fig. 4-12: Photobleaching in 500 μm waveguide at fabricated from PETA with Eosin 0.5 wt. % and illuminated with beam power of 12.8 μW for 5 min. The pictures were taken; immediately after rinsing, then at 2 min, 10 min, 1 hour, and 2 hours from the top to the bottom.

Complete bleaching takes a long exposure time and even with very long exposure the conversion rate never reaches 100% indicating some residual Eosin molecules remaining in polymer structure [105]. However the absorption peak in the blue region in Fig. 4-10 might be related to yellowing effect caused by coinitiator which prevents reaching 100% conversion rate. Therefore polymer waveguides after rinsing are not fully transparent, in the other words they are not showing maximum transmission. The bright fluorescence immediately after rinsing indicates that there is still a substantial number of unbleached Eosin molecules in the polymerized structure.

Fig. 4-13 (a and b) show variation of insertion loss at 1550 nm during two hours of continuous illumination. In the first 10 min there is a notable decrease in loss from 1.1 dB to 0.8 dB as continuous irradiation increases polymerization rate which improves the polymer waveguides transparency. Then the trend becomes semi plateau from 10 min until the whole two hours, although there is still some improvement in transmission efficiency associated with fluorescence weakening under extended exposure, but the slope of variation is very small as it is clear from the logarithemic scaled Fig. 4-13(b).

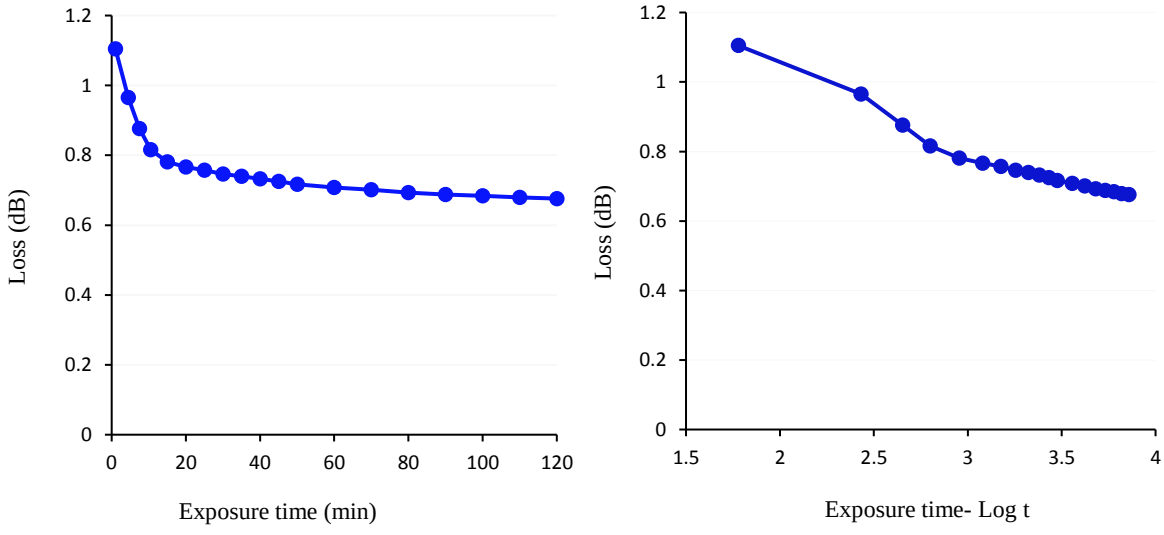

Fig. 4-13: Loss variation associated with polymer bridge in Fig. 4-12 at 1550 nm under photobleaching. (a) Exposure time on linear scale. (b) Exposure time on logarithmic scale.

4.8 Polymer bridges using UV curing Norland adhesives

The experimental set up shown in Fig. 4-5 with a broadband light source gives opportunity to polymerize different monomer solutions which are sensitive to UV, visible and NIR without changing apparatus or replacing the light source. Some research has been published using Norland optical adhesives (NOA) to fabricate polymer waveguides [7, 106]. We used NOA61, NOA63, and NOA 85 to fabricate UV cured waveguides. These different adhesives are all transparent liquids and sensitive to UV, with maximum absorption lies in wavelength range of (350 – 370 nm). The main difference between them is their viscosities which are (300 cP, 2500 cP and 200 cP) for NOA61, NOA63, and NOA 85 respectively. Viscosity is an important parameter in self-written waveguide fabrication. Firstly, higher viscosity allows us to construct a longer liquid bridge between two fibres without lubrication. Secondly, high viscosity prevents oxygen to diffuse easily into the droplet, which in turn leads to a bridge size which is independent of the drop shape. However too high viscosity causes rinsing process difficult as the uncured liquid was not removed easily even with stronger solvent such as acetone, therefore fabrication process with NOA63 was ruled out. NOAs possess excellent adhesion quality to glass after curing which reduced the risk of the polymer detaching at fibre/polymer interfaces. Never the less, there were some obstacles in waveguide fabrication. The main challenge is that SMF- 28e fibre is doped with Germanium which strongly absorbs UV $<$ 380 nm and weakens the curing beam intensity which made us also to rule NOA85 out as it has narrow spectral sensitivity limited between 325-365 nm. Fig. 4-14 shows the fabrication steps of a 150 µm NOA61 waveguide. No fluorescence emission is associated with NOA curing because the liquid does not contain any photoinitiator dye. The reaction here is directly caused by free radicals generated from monomer molecules following UV absorption. However the polymer channel formation can be monitored through refractive index change in the liquid at the illuminated area, which is visible in Fig. 4-14 (a).

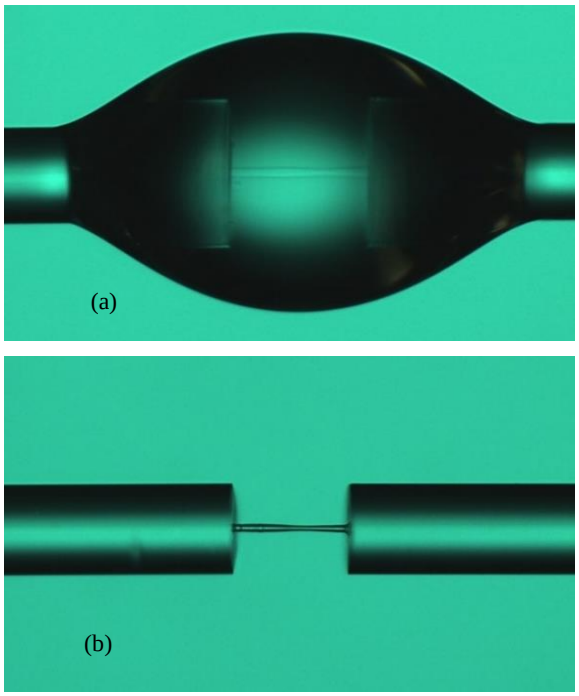

Fig. 4-14: 150 µm NOA61 waveguide; (a) during polymerization and (b) after rinsing. Polymerization happens only in small cross sectional area (of the order of fibre core size) where the beam intensity is higher, unlike PETA system the reaction has not extended to the wings of the written waveguide indicating high threshold energy of polymerization corresponding to NOA adhesives.

NOA61 was the best sample to deal with experimentally as well as optically. The sample has moderate viscosity and provided the best optical transmission. Fig 4-15(a) and (b) show optical transmission of 100 µm and 200 µm NOA61 waveguides respectively. As it is clear transmission efficiency of the waveguide is not as good as that of PETA bridges.

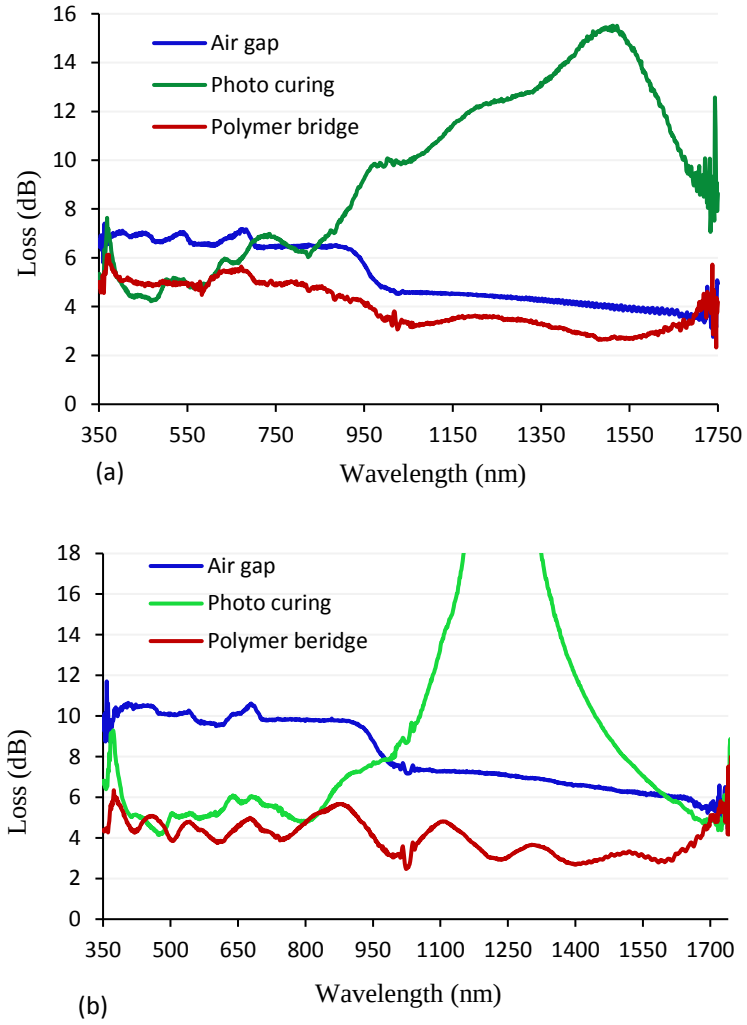

Fig. 4-15: Loss as a function of wavelength associated with (a) 100 µm and (b) 200 µm air gaps and NOA61 polymer bridges at different stages of formation. The optical transmission of the two waveguides have different characteristics, unlike the case in PETA bridges where various waveguide lengths showed the same behavior at different stages of polymerization.

The enormous inflation in loss is due to the waveguide bending during photo curing rather than actual absorption by the monomer. It could be a result of temperature rising during photopolymerization that reveals thermo-plastic property of NOA as the waveguide does not retain its straight form after rinsing. Loss reduces during bridge formation between (1300-1700nm) as can be seen from green line of Fig. 4-15. The reduction is not due to intrinsic properties of the waveguide material but because the bridge was straightened by adjusting translation stages to prevent the bridge from breaking at interfaces. The transmission of rinsed polymer waveguide also shows there is no substantial absorption due to O-H vibration. Although the waveguides were completely straightened after rinsing but still losses are high. The poor optical

transmission can be attributed to the thin bridge size, deformation after rinsing due to lack of crosslinking, and mode mismatching at the polymer/fibre interfaces [15]. Some of these negative factors can be eliminated by adding photoinitiators which own high absorption in UV or even visible spectral region and improve polymerization efficiency also better mechanical and optical properties or using high intensity UV source [7]. Generally, unlike PETA waveguides, plain NOA samples lead to bridges with unstable transmission and poor reproducibility.

4.9 Index profile of polymer waveguides

Consider the curing beam emerges from incident fibre is approximately Gaussian. The intensity is highest on the propagation axis, hence it produces the highest refractive index change at the center of waveguide. Depending on whether the polymerization is an on/off process or a gradual process this will result in a step index or graded index polymer waveguide. The three compound PETA system leads to quasi graded index waveguide upon photocuring depending on the waveguide cross sectional size and total exposure energy. The index profile was investigated by putting a drop of higher index liquid (*Cargille* n =1.57) with refractive index larger than the polymer to form a liquid cladding surrounding a 300 μm long channel, Fig. 4-16(a), also by pouring some fine dust on a 250 μm long waveguide, Fig. 4-16 (b). The result shows very small change in optical transmission both with liquid cladding and dust deposition as illustrated in Fig. 4-17, which indicates that the index profile of the PETA waveguide is graded.

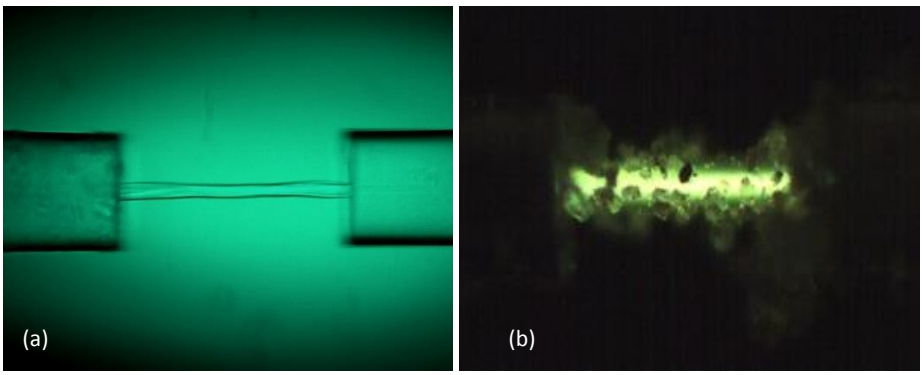

Fig. 4-16: Investigating index profile of (a) 300 μm long PETA waveguide surrounded by liquid cladding with refractive index 1.57 and (b) 250 μm long PETA waveguide with fine dust poured on the surface of the waveguide to scatter evanescent field. Both waveguides fabricated under the condition physical and chemical conditions.

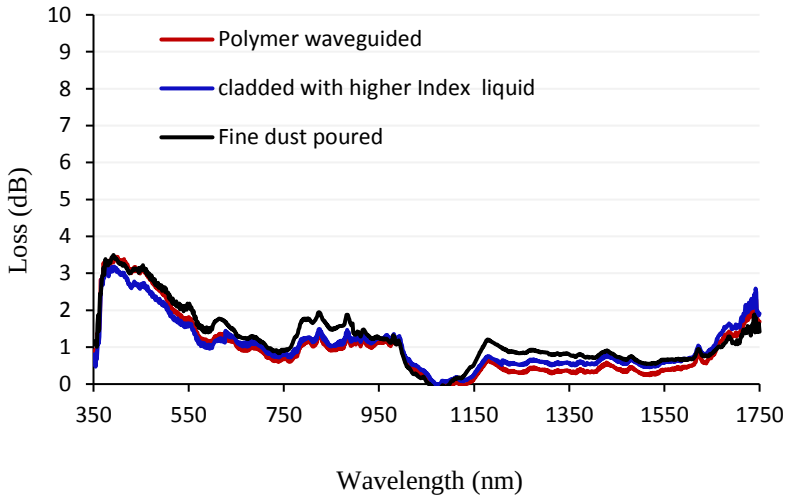

Fig. 4-17: Optical transmission of a plain 300 µm long PETA waveguide, cladded with higher index liquid, and fine dust. No significant change can be noticed in loss over the whole spectral range, suggesting very weak evanescent field guided along the waveguide.

Under maximum power irradiation and an exposure time about 60 s polymer bridges associated with PETA system are fabricated with cross-sectional diameter of order of 30 µm. This range of waist size is much larger than the beam waist because polymerization rate is high and some free radicals diffuse to the boundaries of the curing beam and form some polymer chains with lower conversion rate and hence lower refractive index [107]. The refractive index gradually decreases and leads to graded index profile structure. Fig. 4-18 shows a guided beam in polymer bridge, the beam size is clearly smaller than the diameter of the waveguide indicating the beam is totally confined with in the bridge and no evanescent field at the surface of the waveguide.

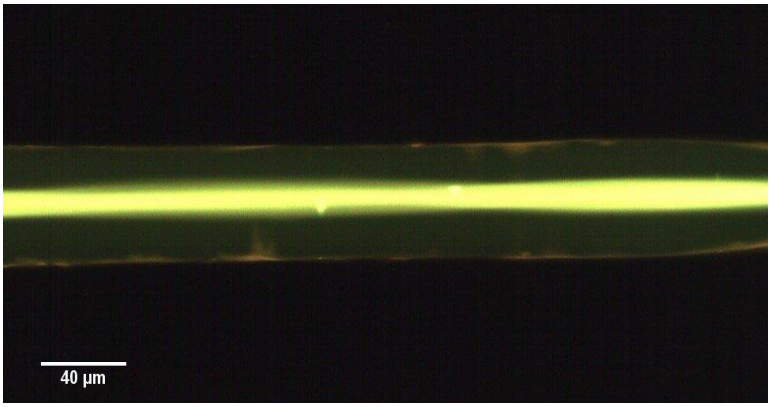

Fig. 4-18: A section of PETA waveguide average diameter of 55 µm, a pencil of light of diameter about 15 µm propagates in the centre part of the waveguide. No light on the edge of the waveguide.

On the other hand, polymer waveguides associated with UV cured NOA61 are always step index. In this case light beam emerges from fibre is very weak in the UV region, the curing power is about (0.5 µW), consequently polymerization only occurs at small cross sectional area associated with the beam spot size which leads to a small size polymer bridge, in the other word free radicals are formed and remain active only at the centre of the beam where beam intensity is very high, therefore the channel remains small regardless of exposure time. Although curing NOAs with high intensity UV laser could result in larger bridge diameter and hence graded index polymer waveguide. Missinne *et al*. reported graded index NOA68 polymer bridge between single mode fibres [7]. This supports the hypothesis that the index profile of self-written polymer waveguides to a certain extent are determined by the waveguide diameter. To examine the index profile experimentally, similar to the PETA waveguides, a 150 µm NOA61 waveguide was cladded with higher index liquid with refractive index larger than that of the polymer as shown in Fig. 4-19(a), also the same bridge was covered by fine dust poured on its surface of the waveguide as shown in Fig. 4-19(b).

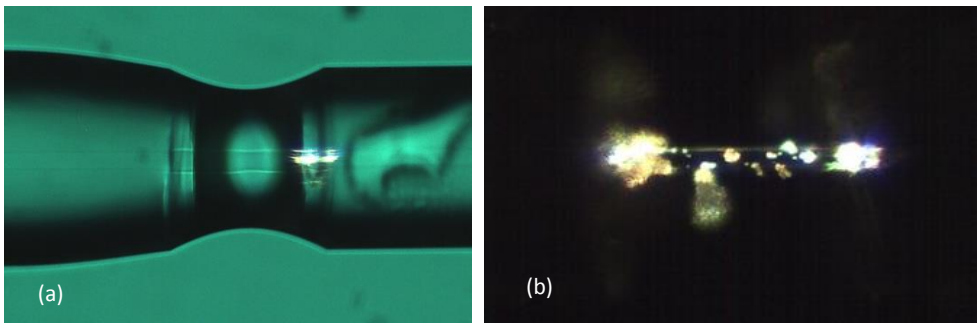

Fig. 4-19: Investigating index profile of (a) 150 µm long NOA61 waveguide surrounded by liquid cladding with refractive index 1.57 and (b) 150 µm long waveguide with fine dust poured on the surface of the waveguide to scatter evanescent field.

Contrary to the PETA waveguide, loss increased after bridge was surrounded by a high index cladding and also by scattering centres on its surface as illustrated in Fig. 4-20. The bright dust grains on the surface of the waveguide indicate strong scattering of propagating light at the surface of the polymer.

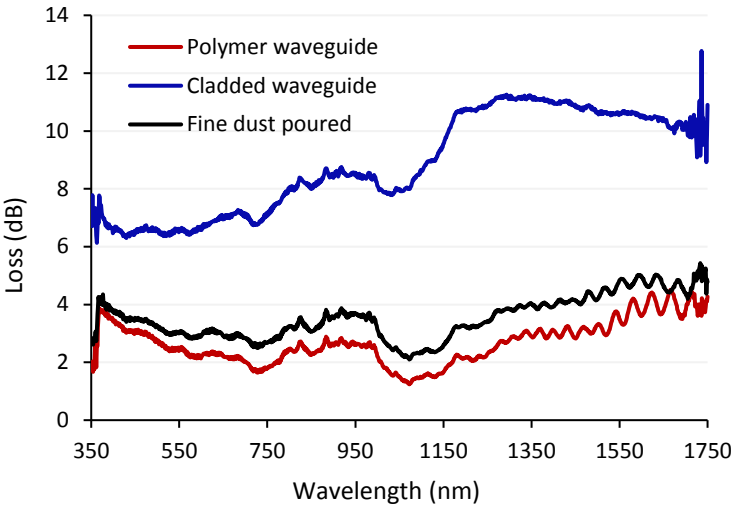

Fig. 4-20: Optical transmission of a plain 150 µm long NOA61 waveguide, cladded with higher index liquid, and fine dust. Loss increased significantly when the waveguide was cladded since the liquid coated with all surface of the NOA, whereas for the dust case the evanescent field was only scattered at the points where grains exist.

To further investigate step index profile of NOA bridges, a drop of PETA was deposited on a 150µm long NOA61 bridge and irradiated along the fibre with the xenon lamp. The fluorescence emission during and after polymerization Fig. 4-21 implies that Eosin in PETA drop absorbs evanescent field associated with light propagation through the NOA61 waveguide.

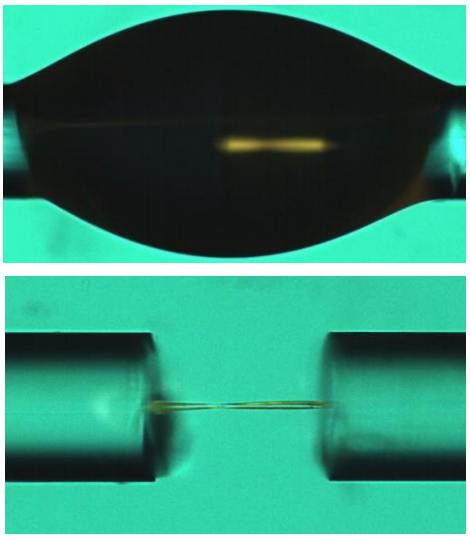

Fig. 4-21: 150 µm long NOA61 polymer waveguide, cladded with PETA solution then illuminated, fluorescence indicates evanescence field in the waveguide, after rinsing there is still fluorescence emission.

4.10 Geometrical features of photopolymer bridges

Some chemical and physical factors have a decisive impact on the self-written waveguides. Therefore we investigate some factors which have the largest effect on the geometrical features and optical transmission of polymer bridges. These factors include exposure energy, drop shape which highly related to oxygen diffusion and Eosin concentration in the PETA system.

4.10.1 Effect of exposure energy

Photoinduced polymer waveguides imprint the profile of the guided mode through the photopolymerizable liquid system. Accordingly the shape and size of the polymer bridge is determined by the writing beam emerging from the fibre core, its shape and exposure energy which is given by:

$$E_{exp} = P_{curing} \times \mathcal{T}_{exp}, \tag{4-1}$$

where total exposure energy E_{exp} is a product of curing beam power P_{curing} and exposure time $\mathcal{T}_{exp}$. To fabricate polymer bridges using a high power (5-10 µW) collimated beam from a laser source the curing time is in the range of a few seconds in our experience and previous reports [6, 108]. On the other hand, the curing time needed to form waveguides with high transmission using a xenon discharge lamp was few minutes. This exposure time is much greater than the time necessary for building up the polymer bridge itself, however the polymer waveguide needs to be over exposed in order to enhance its mechanical properties through crosslinking degree of the polymer structure to resist the pressure of rinsing and shrinking caused by ethanol so as to optimize its optical transmission performance. A short exposure leads to narrow bridges, since the oxygen inhibition is dominant in the beginning of the reaction and photopolymerization happens only at the brightest region of the guided mode while at the edge of the beam the energy cannot reach the polymerization threshold [70]. The effect is more prominent with beam intensity variation, although threshold exposure time still needed to form a robust polymer bridge. During polymerization the intensity reduces along the propagation axis

because of high absorption of the writing beam by Eosin. For long bridges fluorescence emission weakens gradually along the illuminated path as seen in Fig. 4-22(a). The faint fluorescence indicates strong absorption happened earlier, therefore the beam intensity is no longer sufficient to polymerize the end part of the bridge properly. The phenomenon results in beam diffraction as shown in Fig. 4-22(b). After a few seconds the diffraction disappears and the beam returns back to the straight path, Fig. 4-22(c), but the diffraction leaves a permanent effect on the polymer waveguide surface, Fig. 4-22(d). The uneven surface was only observed at the final 20 µm and 120 µm of 500 µm and 600 µm bridges respectively, at the point where the writing beam was not confined properly at early stages of polymerization. Modal effects may have a role in the surface deterioration as the fibre has several modes at the excitation wavelength. However, this phenomenon has not been noticed with waveguides written at the end of multimode waveguides using high power lasers [87, 109, 110], which suggests that intensity reduction caused the occurrence.

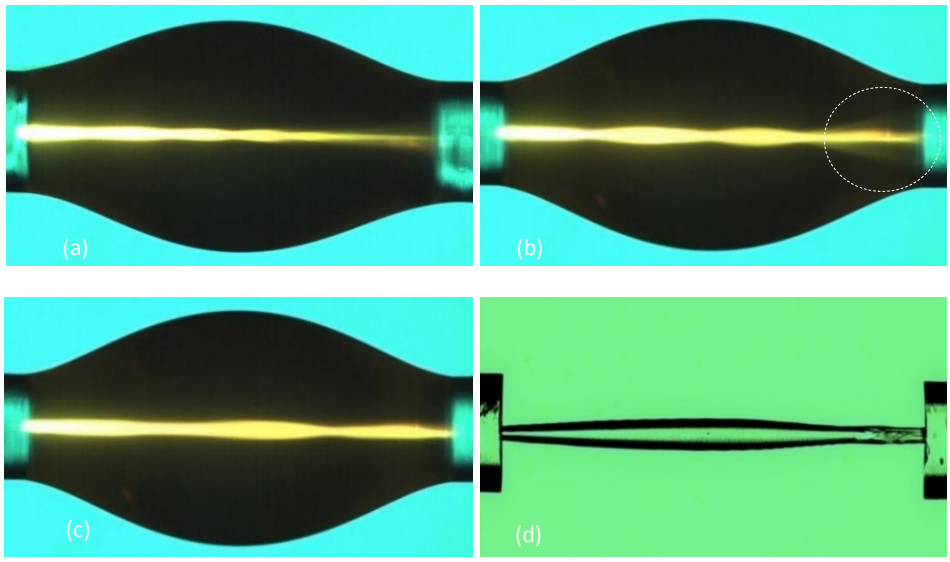

Fig. 4-22: Photopolymerization evolvement in 500 µm long waveguide made from PETA with 0.5 wt. % Eosin concentration, illumination was done from left hand side fibre. (a) Polymerization initiation, intensity of writing beam declines as beam approaches sink fibre or the end of the bridge. (b) Few seconds later, written beam diverges at the final quarter, diffraction beats polymerization or beam confinement. (c) Two minutes later, writing beam eventually confined into the written waveguide. (d) 500 µm polymer bridge, rough surface at the output (right hand) end as a consequence of intensity declining and poor beam confinement during polymerization.

The poor surface morphology of the ends of longer bridges has a negative impact on the optical transmission, which is the main reason that loss suddenly increases with 500 µm and 600 µm as seen in Fig. 4-11.

Further investigation was made regarding the exposure energy effect on the waveguide size and its optical properties. Two 300 µm long thin bridge and wide bridge were fabricated. Fig. 4-23(a) shows a thin waveguide was fabricated by reducing the curing beam power to about half (6.4 µW) and shortening exposure time from 5 to 1.5 min which is the time needed to take the whole spectrum by the OSA. Fig. 4-23(b) is a waveguide fabricated by illuminating the droplet with maximum power (12.8 µW) from light source and 5 min exposure time. The optical transmission performance of these bridges during formation and after rinsing is shown in Fig. 4-23(c).

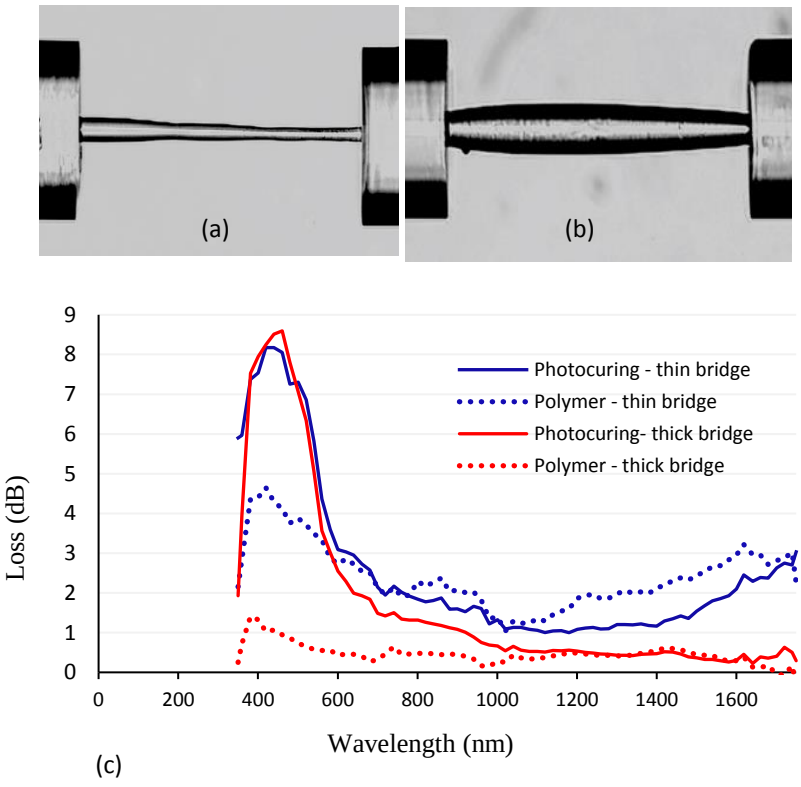

Fig. 4-23: For a straight liquid drop and 300 µm length, a narrow bridge results from low exposure (a) and a wide bridge results from high exposure (b). In both (a) and (b) the light is incident from the left hand fibre. (c) Optical transmission associated with the bridges shown in (a) blue lines and (b) red lines. Solid lines are spectra taken during the first 90 s of polymerization, dotted lines are the waveguide bridges after rinsing.

The optical performance of the wider bridge is much better than that of the thinner one. The difference is smaller during photopolymerization when the bridges are still surrounded by uncured monomer liquid and so have a smaller refractive index contrast. The wide bridge has a transmission loss of 0.4 dB (90 % transmission) so all of the loss mechanisms are small. The narrow waveguide will have a relatively large mode field mismatch for coupling from and to the fibre mode, and is also likely to have a larger overlap of the guided mode with the waveguide surface, leading to increased surface scattering. The combination of these effects gives the high loss shown in Fig. 4-23(c).

High intensity illumination generates a polymer bridge with larger cross sectional diameter and vice versa. Further reduction in intensity causes the written beam to be diffracted radially as the beam propagates through the monomer system. This happened when two SMF fibres were coupled to the xenon lamp simultaneously to fabricate two parallel bridges nearby each other. The spot size at the output of incoherent light source is relatively large, therefore the two input fibres will collect some proportion of the incident light. The light coupling will be very small, as the best coupling occurs when the beam is focused between two fibres, in which case only the edge of the spot will overlap with fibre cores which results in very weak beam guiding through each fibres. As a result, the curing beams were not confined well in the polymerized channels as the beams advanced toward the output fibres shown in Fig. 4-24, since the refractive index change response is slow and conversion rate is low the curing beams diffract.

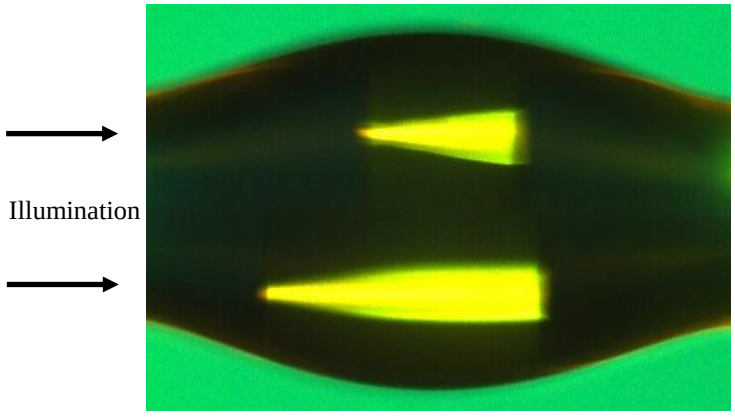

Fig. 4-24: Polymerization of the droplet deposited on the between two paired fibres of 150 µm and 250 µm gaps between top and bottom fibres respectively, illumination from left hand side fibres. The writing beams diverge radially as diffraction overcomes polymerization toward sink fibres.

The phenomenon was reported elsewhere through light intensity distribution of the writing beam propagation through a photosensitive solution [72]. From the fluorescence, it is clear that the polymer bridges will be non-uniform. Also, because of a low degree of crosslinking [111] and lack of high polymerization rate the polymer bridges did not survive rinsing. In the case of long bridges if the intensity is low the reaction stops at some point and the polymerized channel does not evolve further. This limitation is attributed to the writing beam intensity and absorptivity of monomer system [112, 113]. The maximum intensity level was the main reason that we could not fabricate waveguides longer than 600 µm.

4.10.2 Effect of drop shape

The final shape of polymer channel substantially depends on the deposited liquid drop shape connecting the two fibres before polymerization. The impact of drop shape mainly arises from the possibility of oxygen diffusion from the surrounding atmosphere. Photopolymerization will overcome oxygen inhibition more easily in reaction sites where the diffusion length of oxygen is longer. Therefore polymerization extends easily to the beam edge in a larger drop which leads to a larger waist. The influence of pre-polymerization drop shape on the final waveguide shape is illustrated in Fig. 4-25. Three different liquid drop shapes were tested under photocuring with all other physico-chemical parameters unchanged. The right column shows the associated polymer bridges cured with maximum light intensity and two min exposure time. A small hour-glass shape drop (Fig. 4-25(a)) results in a narrow waveguide bridge with a central narrower waist, a straight drop (Fig. 4-25(b)) results in a uniform waveguide bridge, and a large bubble shaped drop (Fig. 4-25(c)) results in a wide bridge with a central bulge. The lowest loss (~0.5 dB) was achieved with the uniform waveguide formed in a straight drop, Fig. 4- 25(b). Because of this, a straight drop was used wherever possible in fabrication, although for 400 µm length and longer the drop shape was harder to control and a more bubble shaped drop was formed after deposition. The other shapes showed higher loss of 0.5-1 dB for a waveguide like one in Fig. 4-25(c) and 1-1.5 dB for waveguide like one in Fig. 4-25(a). This means that with some loss penalty one can adapt the waveguide shape for different applications; for example using a waveguide with a narrower waist to enhance evanescent interactions with the guided mode in a sensor application.

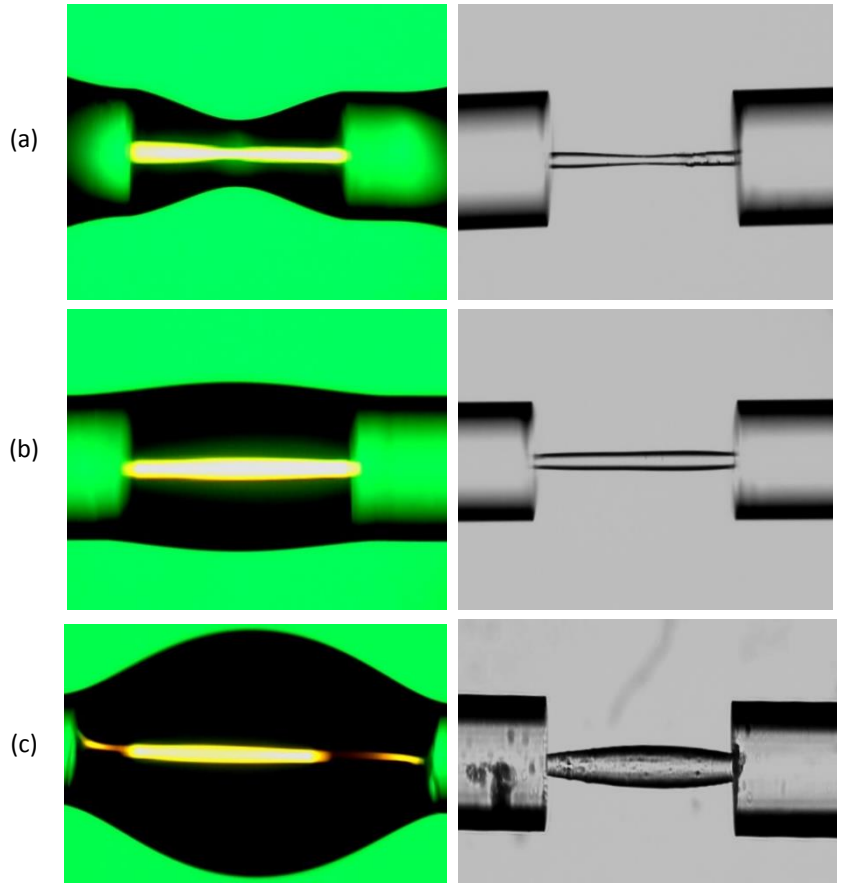

Fig. 4-25: The effect of oxygen diffusion and deposited drop shape on the final polymer bridge shape. Length 240 µm all bridges made of PETA with 0.5wt. % Eosin concentration and they were illuminated with beam power of 12.8 µW for 2 min. Left column; optical micrographs during polymerization (light is incident from the right-hand fibre). Right column; optical micrographs of the waveguide bridges after rinsing.

4.10.3 Effect of Eosin concentration

Mixtures with different photoinitiator concentrations were used for polymer waveguide fabrication, to investigate the effect on mechanical strength and optical transmission. In the photoinitiation stage, absorption strongly depends on the Eosin concentration. It causes a considerable effect on the self-written waveguide evolution. Fig. 4-26 shows absorption at the start of polymerization as a function of Eosin concentration for 120 µm long bridge. Absorption increases as photoinitiator concentration increases [114]. For short bridges the impact was limited to change in the

size of the bridge such that the waveguide diameter associated with high Eosin concentration was slightly larger than that of low Eosin concentration samples.

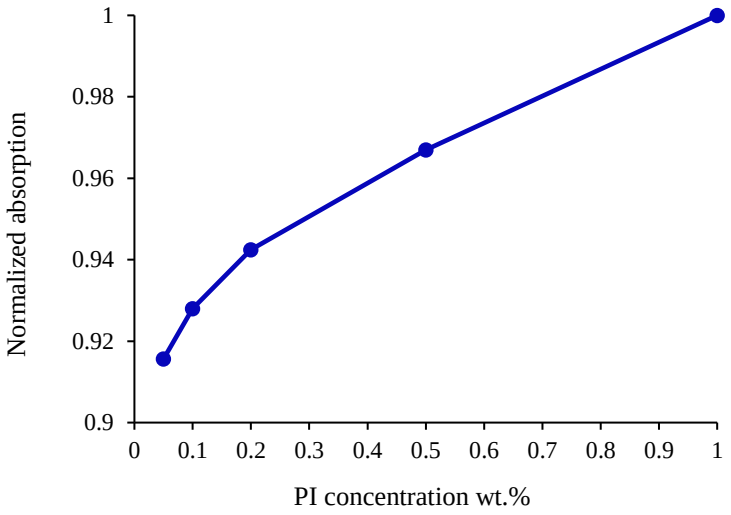

Fig. 4-26: Absorption as a function of Eosin concentration associated with 120 µm liquid bridge between (450 nm-550 nm).

On the other hand for long waveguides, particularly 500 µm and 600 µm, there was a degradation of the waveguide quality towards the output end. The effect was related to the photopolymerization quality at the end of bridges. To examine the effect of Eosin concentration on the surface roughness and optical loss, three different Eosin concentration samples were investigated. Fig. 4-27 shows the spectrum immediately after illuminating the liquid drop. It shows that the absorption depends on the Eosin concentration, for 1wt. % concentration sample, the absorption is very high and loss remained high over all spectral range because a small proportion of light emerged from the output fibre. For 0.5wt. % and 0.2wt. % concentration samples, from green and red traces, there is a considerable difference in absorption in the beginning prior waveguide formation. This large difference soon vanishes as polymer channel forms.

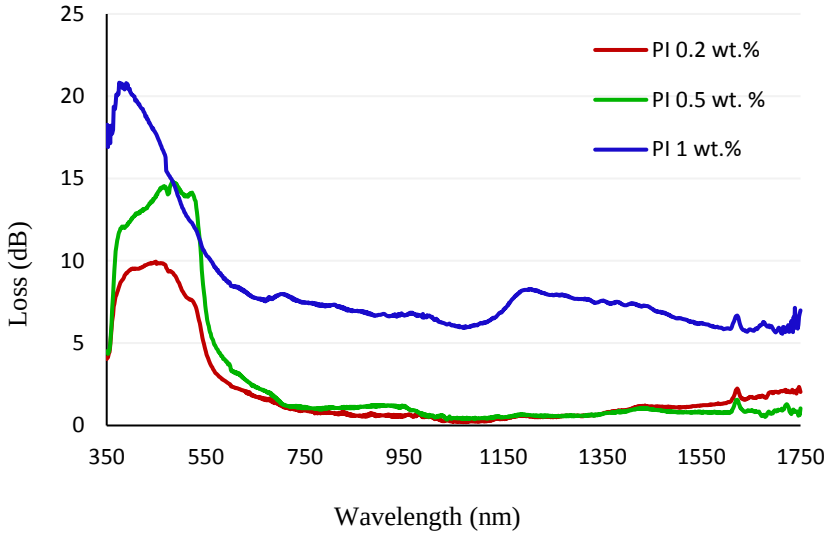

Fig. 4-27: Absorption of three different photoinitiator concentration samples immediately after polymerization initiation. The gap between fibres is 600 µm.

In all samples longer than 400 µm surface structure appears at the end of the waveguide. This effect mainly attributed to decreasing intensity of the curing beam, so Eosin concentration also has a role in the surface deterioration. Fig. 4-28 shows 600 µm waveguides associated with the samples under polymerization in Fig. 4-27. There is a difference in the point at which the surface structure appears, the waveguide associated with 0.5wt. % Eosin concentration sample is showing the longest clean waveguide, whereas the one associated with 1wt. % has longer deteriorated surface.

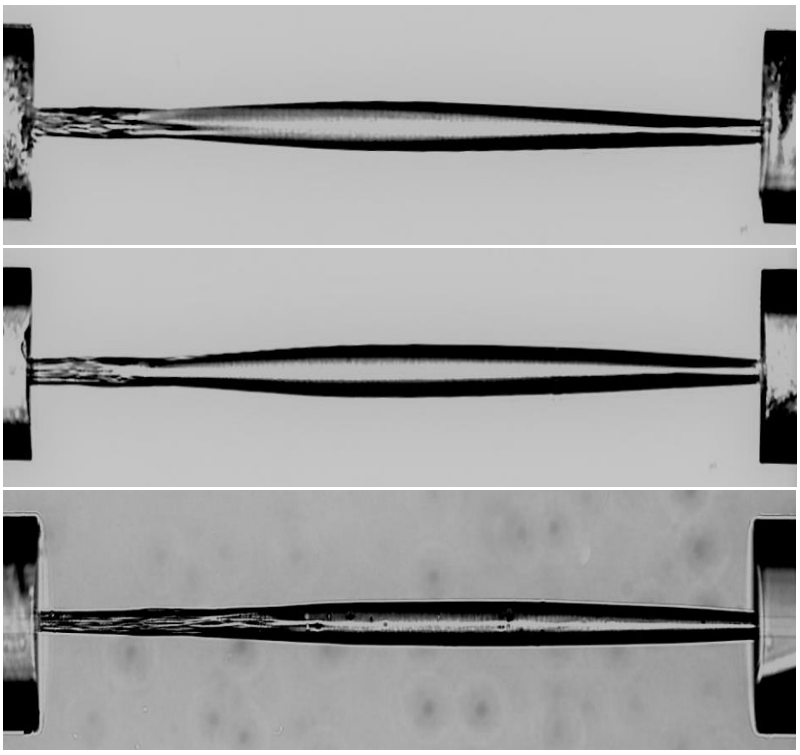

Fig. 4-28. 600 µm bridges associated with three different Eosin concentration samples showed in Fig. 4-27. For photopolymerization, light was incident from the right-hand fibre. (a) 0.2 wt. %, (b) 0.5 wt. %. (c) 1 wt. %

This difference is also seen in the optical performance as shown in Fig. 4-29. A high Eosin concentration has two conflicting effects. It causes generation of a higher number of free radicals at the illuminated area and decreasing diffusion length of reactive species to grab a monomer molecule nearby, hence it raises the polymerization rate. In contrast, high Eosin concentration causes strong absorption at the vicinity of the source fibre which results in an extreme reduction of light intensity near the sink fibre [107] . The disturbance is a sufficient reason to make a polymer bridge have the longest deteriorated surface, Fig. 4-28(c) also high loss, Fig. 4-29. Generally the best optical and mechanical performance was obtained for 0.5 wt. % eosin, and this concentration was the choice for all bridge lengths.

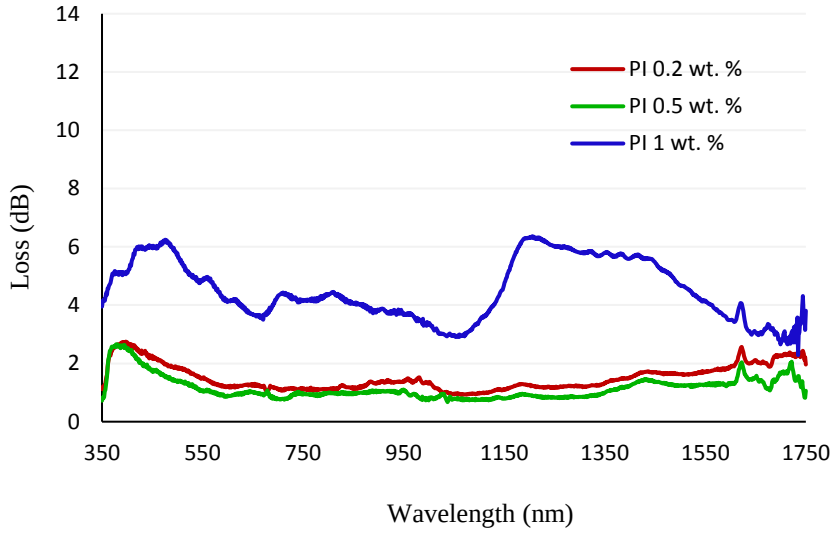

Fig. 4-29: Optical transmission of three 600 µm PETA bridges fabricated from three samples with different Eosin concentrations and the same beam power and exposure time. Loss is highly influenced by the severity of surface deterioration as in Fig. 4-28.

4.11 Summary

This chapter has described the technique of self-written waveguide fabrication considering both monochromatic coherent laser source and incoherent broadband light source. Then the optical characteristic such as loss and index profile of the polymer waveguides were investigated. Finally, the physico-chemical parameters on the polymer waveguide geometrical feature as well as optical performance were investigated. The experimental limitations regarding extending the polymer bridge length beyond 600 µm were discussed to be dealt with in the next chapter. Also the formed bridges showed poor mechanical strength particularly weak adhesion quality at polymer/fibre interfaces, which led to some waveguides breakage under rinsing. Therefore in the next chapter we investigate an approach to improve mechanical properties of the polymer waveguides.

Chapter Five

Mechanical properties of self-written polymer waveguides

5.1 Introduction

Optical fibre based systems play a crucial rule in transition from electronics to integrated photonic devices mainly because of their advantage in the optical wave guiding, it also presents substantial challenges [115]. Particularly a typical optical system includes many optical interconnections which requires tolerance in positioning between the optical elements. In real application optical interconnections demand positional accuracy in the range of few microns. Several factors could cause physical drift of the optical interconnections. These inevitable factors include physical stress which may cause some mismatching and temperature fluctuation which results in contraction and expansion of optical waveguides especially in polymer structures [116]. Freestanding polymer waveguides connecting two optical fibres are low loss efficient channels to interconnect optical fibres of various sizes, although it is always subjected to transversal misalignment which can cause large reduction of the optical transmission efficiency. More significantly the drift could cause damage at polymer/fibre interfaces. Hence it is essential to improve the adhesion joint strength in these hybrid systems. The adhesion quality between two dissimilar materials is as important as the waveguide tailoring itself as it is a decisive factor of optical efficiency of polymer channel. Therefore here we consider the mechanical and optical performance of freestanding polymer waveguides connecting the cores of two fibres with ends separated by several hundred microns. Although normal arc splicing can connect two identical fibres efficiently, but polymer bridges play more generalized role as they can interconnect two waveguides of different materials and sizes.

Much research has been conducted using different techniques and different photopolymerizable systems to construct self-written waveguide integrated with optical fibres. The vast majority of these reports have mainly considered the optical characteristics of the polymer waveguide. There are few reports concerning the mechanical properties of polymer bridges fabricated between two optical fibres. Huang *et al*. investigated strain in a hybrid silica/polymer optical fibre sensor in the form of a 180 μm long polymer waveguide made of UV curing Norland adhesive (NOA61) between two multi-mode fibres (MMFs). The polymer channel showed maximum tensile strain of 56% [117]. Photopolymer waveguides have mostly been fabricated either on a fixed substrate [9] or in a liquid container [109] or even integrated with large size MMF which is less fragile [8, 118], only a few of them considered freestanding waveguides integrated with SMF which is thin and fragile at interfaces. Furthermore, they all considered mechanical and optical misalignment pre-polymerization rather than post waveguide formation. The published studies have contemplated the possibility of waveguide formation while the two fibres were laterally misaligned and investigated the maximum misalignment that allows the polymer bridge formation, and the optical performance associated with misalignment [119]. Regarding small size fibres and small waveguide length, only a small offset is possible. Yoshimura and Seki 2013 used a finite difference time domain method and then fabricated polymer channels between two 600 nm diameter waveguides 4 μm apart. A coupling efficiency of 90% and 80% was obtained with 0.6 μm and 0.9 μm misalignments respectively [120]. On the other hand, with large core size MMFs, a large offset with a long gap is possible, Matsui *et al*. 2006 reported 6 mm polymer waveguide between two 700 μm diameter MMFs with maximum lateral shift of 700 μm that allows waveguide formation, which induces insertion loss of 7 dB [118]. In the same context, Yoshimura *et al*. presented 65% optical efficiency associated with 300 μm polymer waveguide between two 50 μm core size fibres one of them transversely shifted by 30 μm [119]. Regarding SMF, Mensov and Polushtaytsev reported 20 μm as a maximum misalignment that allows formation of single polymer channel between two fibres with 1.6 mm distance between them, the fibres were sandwiched between two parallel glass plates to prevent external mechanical forces [121]. Also Cheng *et al*. 2010 investigated optical alignment tolerance of 100 μm self-written waveguide connected two SMF fibres, 4 μm misalignment lead to insertion loss of 1 dB [116].

5.2 Polymer / fibre interfaces bonding failure

In chapter 4 the optical characteristics of three compound PETA system and a UV curing optical adhesive were investigated. Polymer bridges fabricated from NOA61 and NOA63 demonstrated satisfactory mechanical properties despite small cross sectional interface with fibre, but their optical transmission efficiency was not as good as that for the PETA system. Therefore here we only study the optical and mechanical performance of PETA waveguides that contains Eosin concentration of 0.5wt. % . We have already showed excellent optical transmission of these waveguides but the concerns were fragility of the polymer/silica interface and waveguide structural uniformity. The final rinsing with solvent was always found to be challenging in such integrated polymer structures as any tiny extra pressure during rinsing could detach the polymer from the fibre and this was made worse by the fact that solvents cause polymer swelling and bending. The failure of proper bonding is more probable for long waveguides in the range of 400 μm and becomes more significant with longer bridges. The rinsing pressure was more damaging at the output fibre/polymer interface where photo curing was done from one direction only. Statistically nearly one out of four bridges did not survive rinsing, and another one did not perform efficiently because of unseen faults at the interfaces.

Although physical bonding always occurs through Van der Walls forces at interfaces, this is rather weak to hold polymer bridge firmly. These weak forces are sometimes supplemented by stronger bonds such as hydrogen bonds, but such bonding does not form in polymers which lack H-bonding partner in silica. Never the less, there are some solutions to improve adhesion strength joint between dissimilar surfaces such as polymer-silica fibre. Possible interventions involve the adhesion (polymer) penetrating into the adherent (fibre facet) or inducing chemical bonding [122].

5.3 Adhesion promoter

An adhesion promoter is a liquid monomer applied to the fibre ends to improve joint strength between two different materials through covalent bond to the surfaces of polymer and silica. It was employed here as an intermediate element to overcome the bonding failure at the polymer/fibre interface, also to yield polymer bridge mechanical stability which can endure rinsing pressure and other mechanical effects. The fibre ends were

treated with adhesion promoter 3-(tri-methoxysilyl) propyl methacrylate (3TPM) to improve their ability to hold polymer waveguides more firmly. The treatment involves a molecular interaction of adhesion promoter with adherend (fibre facet) that modifies fibre ends to hold polymer bridge [123]. The reaction occurs through methoxsylil groups. The methoxysilyl groups allow the molecule to covalently bind to –Si-O-H groups on the silica surface by a condensation reaction, whilst the methacrylate tail of 3-TPM is available to polymerize with the PETA system. The 3-TPM molecule has three methoxysilyl groups, but only one acrylate group so is not able to polymerize itself, forming a single layer bound to the silica surface. Selection of the adhesion promoter requires it to meet some conditions in order to improve polymer bridge optical and mechanical properties. Primarily, it must stick well to both polymer and silica. Then the refractive index should match the system and the material needs to be transparent over the spectral wavelength used for curing also optical transmission measurement. High transparency can provide higher coupling efficiency after waveguide fabrication. In contrary, if adhesion promoter forms a reflection surface the mechanical improvement becomes associated with high loss. Secondly, the liquid must possess low viscosity to aid quick spread and adapt to the details of the fibre facet [122]. Furthermore low viscosity liquid can easily be removed from fibre end after treatment.

5.4 Pre-polymerization fibres treatment

As mentioned earlier, one mechanical drawback of hybrid polymer/silica fibre structures is lack of adhesion at the interface of the organic/inorganic materials. The active functional group of an acrylate monomer does not make a robust bond with silica. Therefore 3-TPM was used to overcome the bonding failure. Before commencing waveguide fabrication the fibre ends were cleaved and cleaned with acetone, then they were immersed in a plastic bottle filled of adhesion promoter in a refrigerator for different time durations (5 s. 20 s, 5 min, 20 min, and 1 hour) as shown in Fig. 5-1.

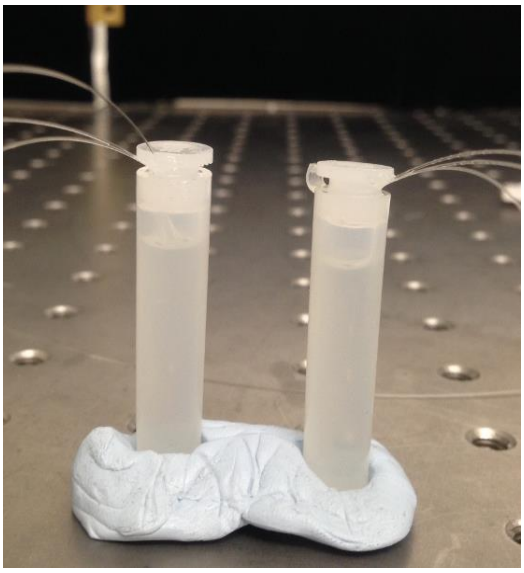

Fig. 5-1: Fibre ends are treated with 3-TPM by immersing the cleaved ends into the liquid for different time durations before waveguide fabrication.

Then the fibres were shaken well and dried by manual air duster. The ultimate goal of the treatment and a better adhesive joint is to produce an interface that is strong and durable. An excellent interface after treatment should acquire minimal imperfection to support a high quality polymer bridge.

5.5 Effect of treatment duration

Polymer bridges were fabricated using the experimental set up shown in chapter 4, as shown in Fig. 4-5. The optical characterization was also done with same procedure. The experimental results show the substantial impact of the adhesion promoter, where uncured liquid surrounding the bridges after polymerization was aggressively rinsed by pouring successive drops of ethanol. In contrast to the fabrication using untreated fibre ends the bridges formed after the pre-treatment showed no fragility as a result of rinsing. Moreover, waveguides were laterally misaligned to test the polymer/silica adherence. For each of the pre-treatment durations a set of three bridges with 200 μm length was fabricated and deflected transversely in 5 μm steps and the maximum deflection before breakage was recorded for each bridge. From Fig. 5-2, one can notice that for untreated fibres the bridge can be deflected to about 10 μm on average and on one occasion it did not survive rinsing. The maximum lateral deflection increases with increasing treatment

duration, although the trend is not linear but there is a plateau region from 5min to an hour. A saturation like this is expected as the available reaction sites on the silica surface become filled. In general, 3-TPM was very effective, such that the treated fibres held polymer bridges for about 90 µm lateral shift.

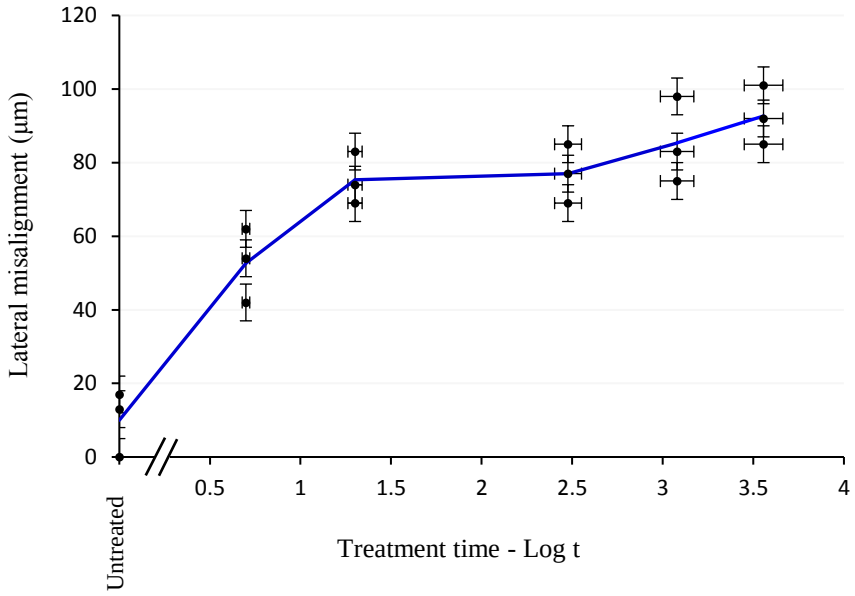

Fig. 5-2: Maximum misalignment before polymer detaches from fibre as a function of treatment time with 3-TPM. Points show three different repeats for each treatment, line shows the mean.

Figs. 5-3 (a-e) show micrographs of 200 µm bridges associated with fibres which were untreated, treated for 5 s, 20 s, 5 min, and 20 min respectively with straight waveguide, maximum off set, and at fracture point. The comparison was done for polymer bridges that were made under the same physical and chemical circumstances for instance; curing power, exposure time and bridge length. Also the fibre ends were fixed firmly in the v- grooves by a pair of strong magnets in order to prevent the fibres moving freely. Some bending of the fibres was still observed and so deflection was measured from the micrographs, not from the translation stages.

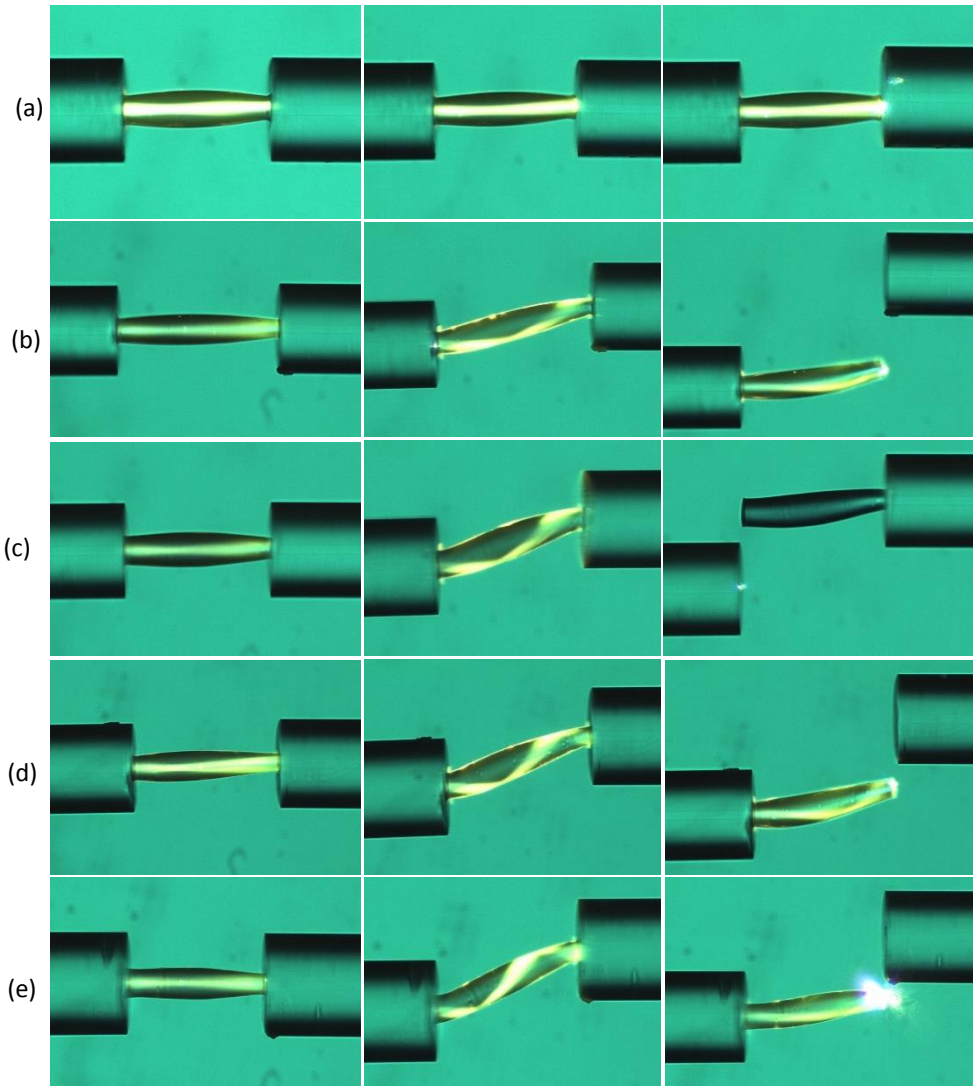

Fig. 5-3: Straight waveguide (left), then maximum lateral deflection (centre) and detaching (right) corresponding with a) Untreated fibres. b) Fibres were treated for 5 s, c) 20 s, d) 5 min and e) 20 min. Maximum deflection was measured from micrographs of the centre column. Bend in the fibres is evident from the fibres springing further apart when the bridge breaks (right).

Misalignment was performed by shifting the output fibre by 5 µm steps and for each step the bridge was pictured and the loss was measured at 1550 nm. Fig. 5-4 shows the effect of treatment time on loss evolution against lateral misalignment. Generally the loss increases with deflecting polymer bridges laterally. The impact of treatment is clear from the optical transmission of the bridges in the first three steps up to 10 µm displacement. One can see that loss significantly decreases with increasing treatment time. The loss associated with the polymer waveguide fabricated between untreated fibres is about

14 dB when we deflect the output fibre 10 µm, while for the same misalignment the waveguide loss associated with modified fibres dropped to about 6 dB. The optical improvement can be attributed to the stronger adhesion between the polymer bridge and fibre end at interfaces. No further optical improvement was observed corresponding to the fibres treated for longer time durations.

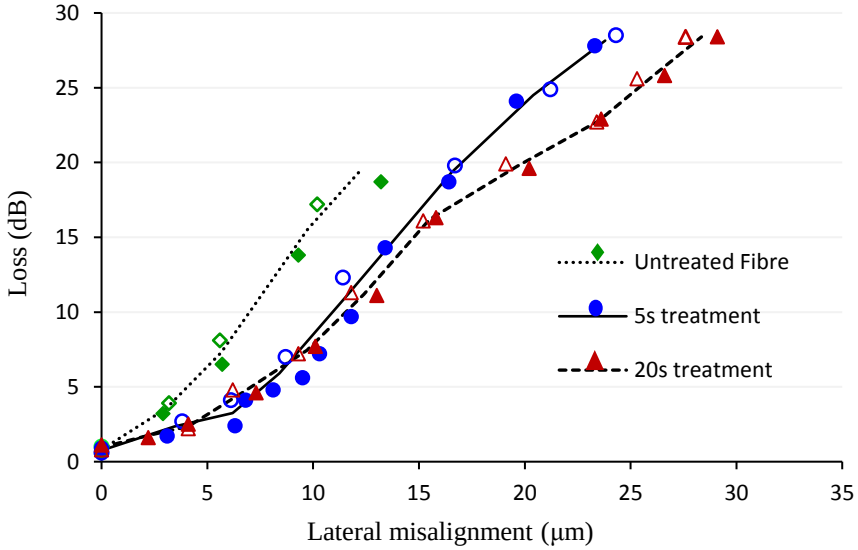

Fig. 5-4: Optical loss development against measured lateral misalignment associated with 200 µm polymer waveguide fabricated between fibres which have been treated for different time durations. Points show two different repeats for each treatment, lines are the mean.

5.6 Polymer bridges under shear stress

Polymer bridges with various lengths were fabricated between fibres which had been treated in the 3-TPM for 20 min. According to the results presented in previous section, this treatment time seems to be a reasonable duration to make fibres to bind polymer waveguides firmly and provide satisfactory optical performance. Lateral misalignment was investigated to provide the self-written waveguide reliability to be used as an optical interconnection. It is noteworthy that the lateral misalignment is not purely shear stress, but a combination of primarily shear stress with a small contribution of tensile stress as the waveguide does not retain its original length when the misaligned fibre is returned to its horizontal position. This phenomenon indicates that the polymer is not a perfect elastic material. The average stress increases with increasing misalignment, and the tensile stress

contribution increases as well. The higher the combined conditions, the higher the average detaching force on the waveguide at the interfaces to detach it from the fibre [123].

5.6.1 Misalignment tolerance

The mechanical assessment was conducted by laterally displacing one of the fibres from original aligned position at 5 µm steps on the micrometre knob of the translation stages. Although the 5 µm on the knob does not exactly mean 5 µm deflection of the waveguide, since fibres show some bending flexibility despite of they were fixed firmly on the translation stages. Therefore for accurate misalignment measurement Image J program was used for precisely measuring fibre deflection from micrographs. Figs. 5- 5 (a- d) show the maximum lateral deflection of polymer bridges with different lengths (100 µm, 200 µm, 300 µm, and 400 µm).

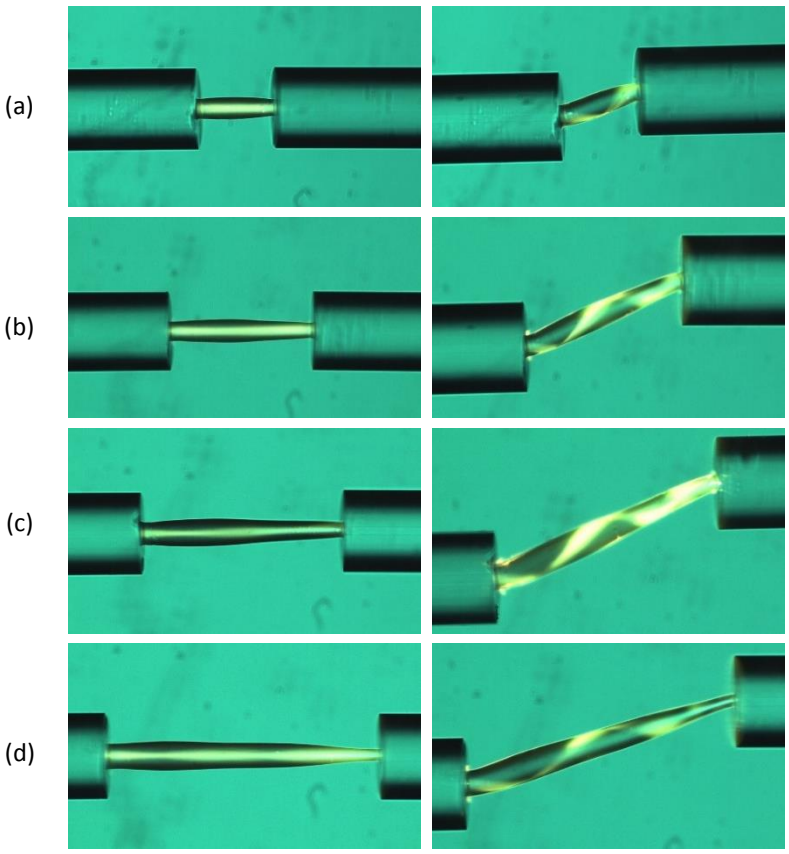

Fig. 5-5: Various polymer waveguides constructed between pretreated fibres for 20 min. A single-sided curing beam emerges from the left hand fibre. The row starts with the straight channel and at the maximum lateral deflection. a) 100µm, b) 200 µm, c) 300 µm and d) 400 µm.

The maximum offset increases with increasing bridge lengths. But interestingly the trend slightly declined as the bridge length increased from 300 µm to 400 µm as shown in Fig. 5- 6.

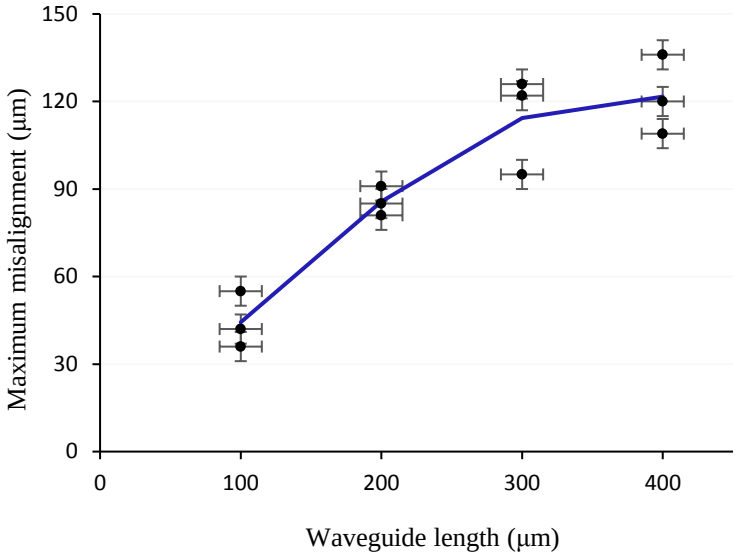

Fig. 5-6: Maximum lateral deflection of various length waveguides before detaching at polymer/ fibre interface. Points correspond to different repeats for each bridge length and the line is the mean.

The decline can be attributed to the fabrication factors that cause the active joint area at the output polymer/fibre interface to reduce from 23 µm to 16 µm corresponding to 400 µm and 300 µm bridge respectively. This change can be seen through micrograph pictures shown in Fig. 5-5 (c) and (d) and quantitatively from Fig. 5-7. This reduction mainly originates from the fact that for a longer bridge the drop shape becomes thinner at the ends, which results in the photopolymerization to be more subjected to oxygen quenching since the diffusion length of oxygen from the surrounding atmosphere is reduced. It also may be attributed to curing power weakening towards the end of the waveguide. The two factors together lead to a smaller polymerized waveguide cross section which in turn reduces the interaction area at the output polymer/fibre interface.

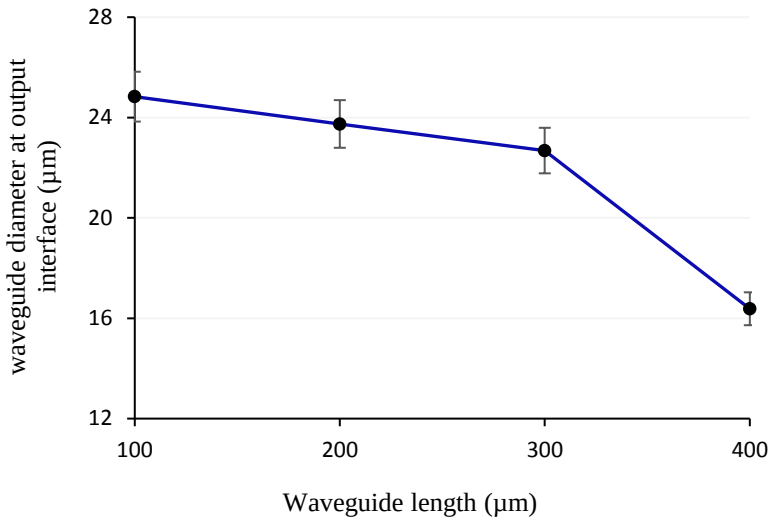

Fig. 5-7: Polymer waveguide diameter at the polymer/fibre output interface.

Displacement rates of about 30 µm/min were applied during experimental test. This is relatively high rate, a low displacement rate may allow the polymer channel enough time to deform and redistribute the applied stress which allows more uniform stress distribution and consequently a higher joint strength at polymer/fibre interfaces. Conversely high displacement rate causes limitation of molecular rearrangement and hence lower adhesion bonding [123].

5.6.2 Loss development with lateral misalignment

Fig. 5-8 shows optical loss development as a function of transverse deflection for different bridge lengths. The experiment showed that for all waveguide lengths the transmission efficiency decreases with lateral displacement. The trend is slow at the beginning but it rapidly grows monotonically, because the waveguides are graded-index and the variation of refractive index is not steep enough to bend the light beam properly toward the propagation axis. Subsequently some light leak out from the bridge as it is clear from the beam paths in Fig. 5-5 and causes rapid increase in insertion loss. The result also shows the shorter the polymer bridges the higher the sensitivity to lateral misalignment. Hence short polymer waveguides show misalignment tolerance of about 5 µm, in longer ones it extends to about 10 µm, this tolerance is in the acceptable range as insertion loss remained around 1 dB. As waveguide length increases the loss evolution

against lateral misalignment is less rapid because the shear stress decreases with increasing bridge length. Therefore insertion loss reaches 5 dB loss limit at different displacement values, it extends to nearly 20 µm from 8 µm as waveguide length increased from 100 µm to 400 µm.

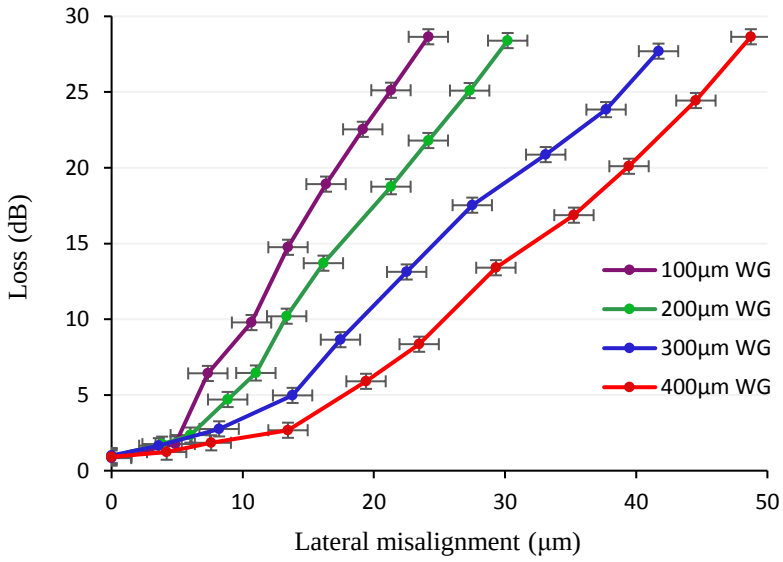

Fig. 5-8: Insertion loss of (100 - 400 µm) self-written polymer waveguide as a function of lateral misalignment.

Up to here, all polymer bridges have been constructed by uni-directional illumination. The mechanical and optical efficiency of single-side illumination may not show their optimum value due to asymmetric size of polymer bridges especially at both ends. The asymmetricity was more obvious in the longer bridges and because of deterioration mechanisms at the output end in spite of fibre treatment the joint bonds were weak in 500 µm and 600 µm long waveguides.

5.7 Waveguide fabrication by bi-directional illumination

To overcome the mechanical deterioration and to equalize the interaction joint area at both polymer/fibre interfaces photo curing was accomplished from both fibres. A fibre photonic lantern [124, 125] was fabricated for this experiment by Dr. S. Yerolatsitis in order to couple light equally into two single mode fibres from a light source as shown in

Fig 5-9. Two SMF 28e fibres were inserted into a fluorine doped silica capillary (NA= 0.22, ID/OD 260/375µm). The structure was then fused and tapered down to 114 µm diameter, forming a single input port coupled to two output ports.

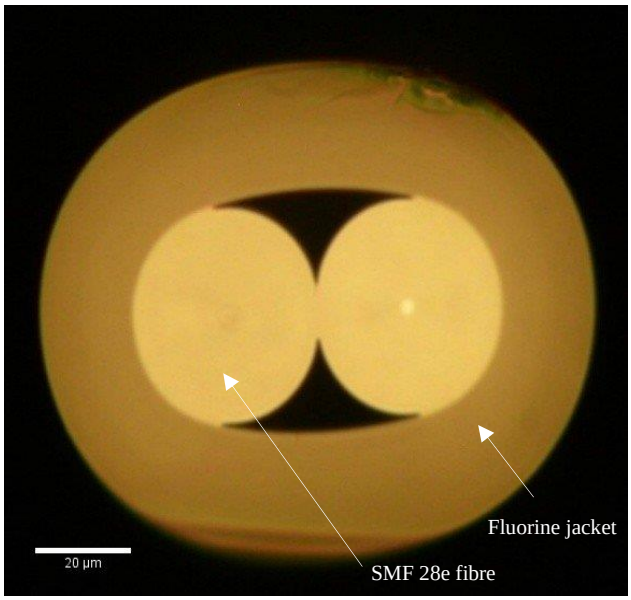

Fig. 5-9: Optical micrograph of the input facet of the photonic lantern fabricated from two fused SMF 28e fibres in the fluorine jacket. The two inner circles are the input facet of the two fibres (the core) and the surrounding dimmer ring is the fluorine jacket (the cladding) with lower refractive index which helps the confinement of the light. The two fibres are stuck together and they approximately collect the same amount of light from relatively big beam spot from a xenon lamp.

Fig. 5-10 illustrates experimental setup for fabricating bi-directional illuminated polymer bridges. The maximum curing power emerging from each port of the photonic lantern was about 10 µW which is about 3 µW less than that from single fibre. The two fibres which hold polymer bridge were connected to the output of the photonic lantern via FC/PC connectors. The other ends were treated with 3-TPM and aligned with the desired distance between them. For bridge lengths up to 300 µm the fibre ends were used as cleaved, whereas from 400 µm to 600 µm the sides of the fibres close to the end were lightly lubricated, as in chapter 4, to aid holding extended liquid drops by improving the surface condition.

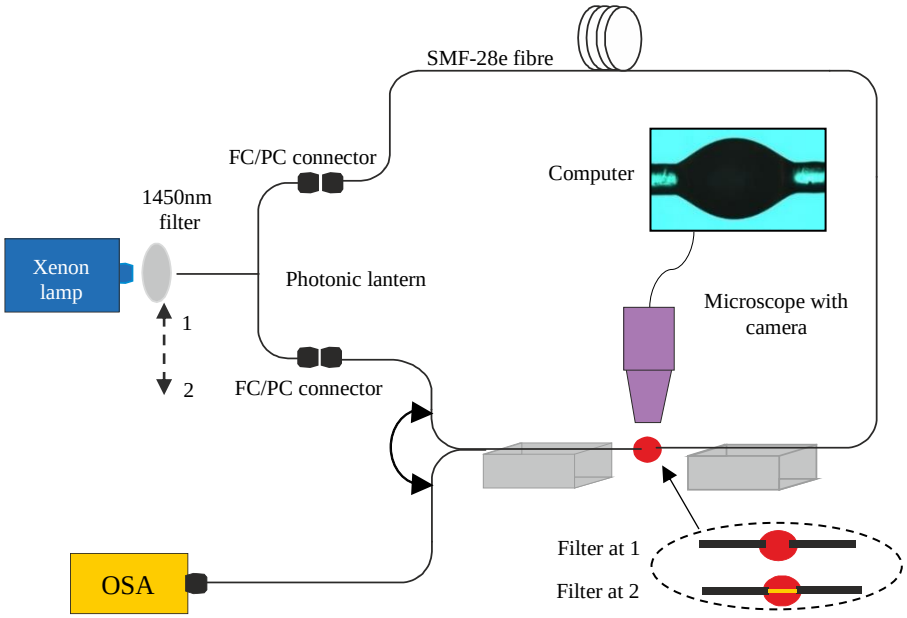

Fig. 5-10: Experimental system for bidirectional photopolymerization and optical characterization. The magnified diagram of the fibre ends and photopolymerizable droplet deposition.

Fibre alignment optimization and the different transmission spectra for baseline and airgap were recorded using a modification of the procedure of unidirectional photocuring explained in chapter 4. Two pre-treated fibres which were connected to the upper FC/PC connector and the OSA were aligned on the translation stages. After optimizing alignment, the fibre end which was coupled to the OSA was then connected to the lower FC/PC connector to allow photocuring from both fibre ends. Polymerization was started by removing the long pass optical filter. The progress was observed and pictured by taking consecutive images of polymerization growing from each fibre until the curing beams met at the middle, Fig. 5-11. Eventually a polymer bridge formed between the two fibres in 5 s to 2 min of illumination depending on the bridge length and size. Shorter and thinner bridges require shorter exposure time and vice versa. The remaining uncured monomer was rinsed off using ethanol, leaving an exposed polymer bridge rigidly attached between the fibre ends as an extension of the fibre core, as shown in Fig. 5-11(j).

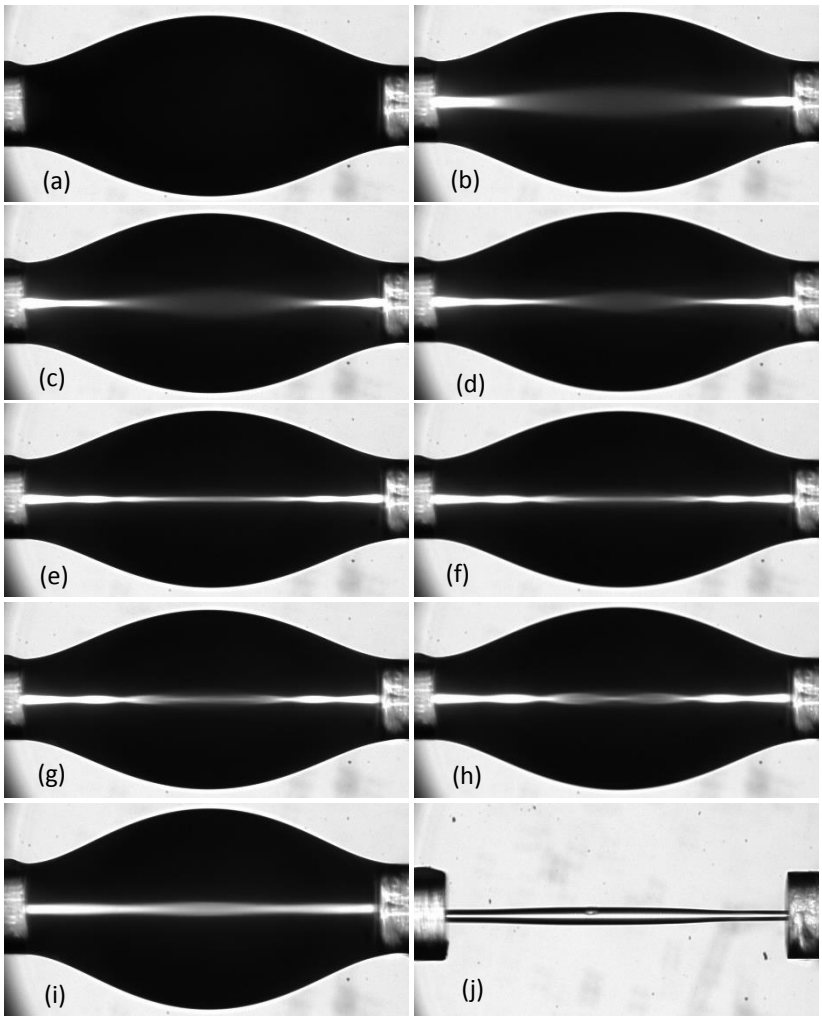

Fig. 5-11: Consecutive stages of waveguide formation by illumination from both fibres, polymerization development follows Zig-Zag pattern from left top. (a) The liquid bridge when filter inserted then at 1 ms, 40 ms, 80 ms, 120 ms, 200 ms, 300 ms, 400 ms, 500 ms, after 2 min of photocuring and last one is a 600 µm long polymer waveguide rinsed after 2 min of photocuring.

Adhesion joint strength was significantly improved by treating the fibre ends with adhesion promoter and with the assistance of bidirectional photocuring. The new approach significantly reduced the risk of polymer fracture at the interfaces. It also improved optical performance of polymer waveguides, as investigated in sections 5.8 and 5.9.1.

5.8 Characteristics of bidirectionaly cured waveguides

With bi-directional illumination polymer bridges become more uniform and cross sectional dimeters at the two ends are almost identical providing that there is similar beam intensity from both fibres. Although with the new procedure oxygen diffusion is still effective, but there is sufficient curing power at both ends to strength adhesion joint between two materials by equating the interaction area between polymer and fibre at both interfaces. In contrast to uni-directional photopolymerization, in bi-directional curing, the maximum lateral displacement increases linearly with increasing bridge lengths as illustrated in Fig. 5-12. The new approach did not make significant change corresponding to waveguides with 300 μm long and shorter.

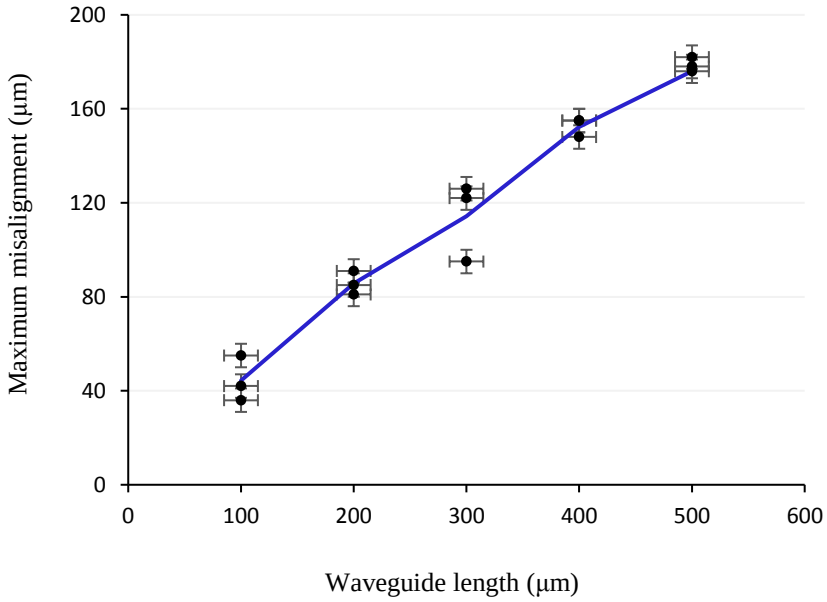

Fig. 5-12: Maximum lateral deflection of various length waveguides before detaching at polymer/fibre interface. Points show three different repeats for each treatment, the line is the mean.

Optical transmission also showed less sensitivity to the waveguide misalignment as the bridge length increased. Fig. 5-13 shows optical loss evolution associated with waveguides under shear strain. Insertion loss of 500 μm long bridges remained below 5 dB until 25 μm misalignment as it is clear from Fig. 5-12.

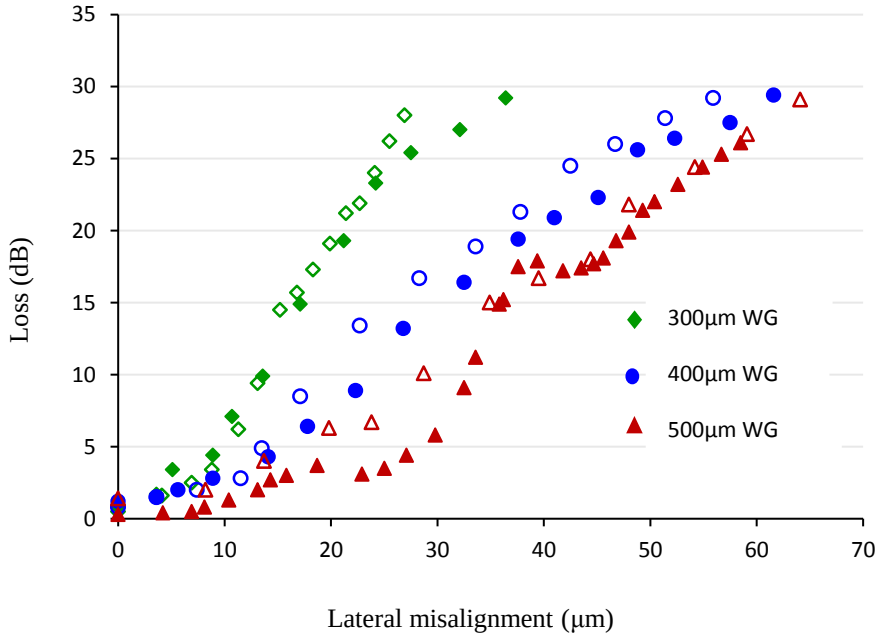

Fig. 5-13: Optical loss development of 300 µm, 400 µm and 500 µm polymer waveguides according to transverse misalignment. Points show two different repeats for each waveguide length.

In addition, bi-directional photopolymerization enables us to break the limitation associated with polymer waveguide length which occurred because of deterioration of the curing beam intensity at the output end. Using the same light source, the self-written waveguide length has been extended to 750 µm as the longest waveguide that could be fabricated by bi-directional irradiation, Fig. 5-14. The limitation here is caused by surface tension rather than the beam intensity, even with heavy lubrication a millimetre long drop can not be deposited. Furthermore the optical transmission efficiency has also been improved, such that insertion loss decreased to 0.58 dB from 1.24 dB in 600 µm long polymer waveguide.

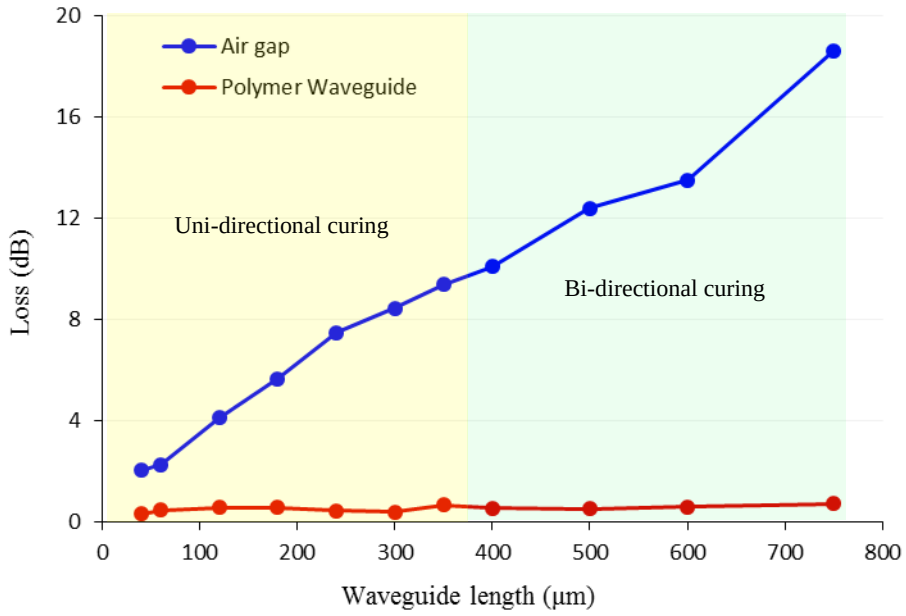

Fig. 5-14: Loss recorded between two aligned fibres with air in between (blue line) compared with loss in a polymer waveguide bridge (red line). Loss averaged from 1500 - 1600 nm, in the single moded region of the fibre. The bridges located in yellow highlighted part are fabricated by uni-directional curing and those located in green highlighted part are fabricated by bi-directional curing.

5.9 Polymer bridges under pure tensile stress

Further mechanical characterization was conducted by putting polymer waveguide under pure tensile strain by elongating polymer channel. Throughout this experiment the joint strength at polymer/fibre interfaces was evaluated by measuring breaking strain. The optical transmission was also investigated as a response to the tensile strain.

5.9.1 Effect of the waveguides' size

To investigate the effect of the polymer waveguide's size on its mechanical properties, three different sets of bridges were fabricated under the same experimental conditions, for instance curing power of 12.8 µW and PETA drop contains Eosin concentration of 0.5wt. %. Exposure time was the only parameter varied to obtain various bridge sizes with different cross-sectional areas as well as different joint areas at the polymer/fibre interfaces. The challenging point in this experiment was the drop's size and shape, since

it is crucial in the polymer channel size through surrounding oxygenation. Short exposure time leads to thinner bridges and vice versa, as shown in Fig. 5-15 (a-c). The three columns are all 300 µm long waveguides which were cured for 5 s, 30 s and 60 s respectively. Then the polymer bridges were longitudinally extended and pictured at every 5 µm step before they detached from fibre.

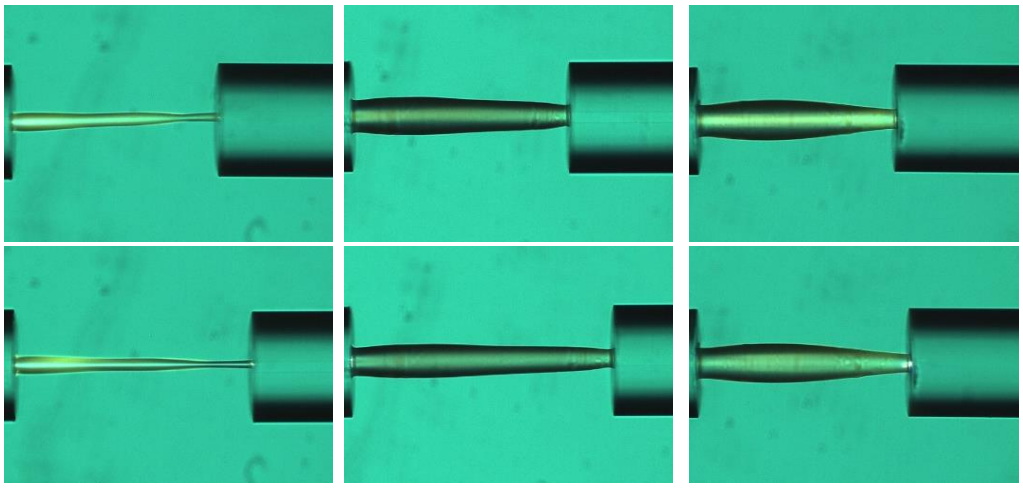

Fig. 5-15: Optical microscope images of 300 µm long polymer bridges fabricated with different exposures at different strain values. a) Thinner bridge cured for 5 s, waveguide diameter at the middle before strain is 12 µm. b) Medium sized bridge cured for 30 s, waveguide diameter at the middle before strain is 32 µm. c) Wider bridge cured for 60 s, waveguide diameter at the middle before strain is 43 µm.

Different bridge sizes showed different maximum tensile strain values, which was not a monotonic trend; strain values were 13%, 23%, and 8% for the thinner to the wider bridges respectively, Fig. 5-16. Although the adhesion interaction area increases at the interfaces as exposure time is extended which in turn increases the adhesion between the two materials, the polymer bulk size also enlarges which results in strengthening of the polymer bulk which results in less elasticity. Consequently the resultant maximum strain before breakage will be determined by the competition between the adhesion joint strength, which cannot be much enlarged beyond some certain value, and the polymer structure size which is to a less extent limited. The straight bridge with medium structure size shows the largest strain value.

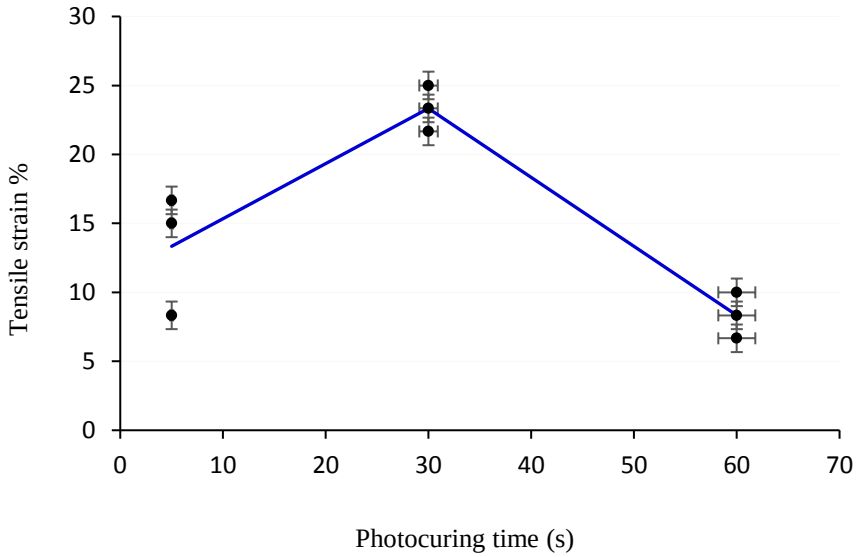

Fig. 5-16: Maximum strain against photocuring time corresponding to the bleached 300 μm waveguides fabricated with the same beam power. Points show three different repeats for each treatment, the line is the mean.

A medium sized waveguide is not only the best mechanically but also optically more efficient. Fig. 5-17 shows the optical transmission under the strain was also examined. The result shows that average insertion loss decreases from 0.75 dB to 0.3 dB for tensile strain in the range between 4% and 7%, then it gradually increases but it does not return back to the value associated with 0% strain. Photobleaching immediately after rinsing results in local temperature raising by exciting the Eosin residuals remained in the waveguide structure as explained in section 4-7, the high temperature elongates the waveguide and causes some bending. The initial tensile stress releases the bending and leads to loss reduction. Then after a certain strain value the applied pulling force starts to exert detaching force at the polymer/fibre interfaces and causes loss increasing again until the polymer detaches.

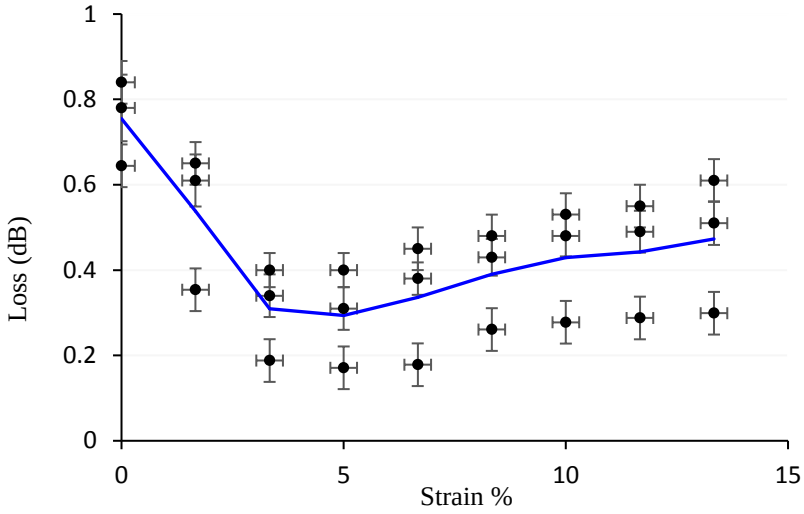

Fig. 5-17: Development of the insertion loss at 1550 nm of a 300 µm long waveguide fabricated with 30 s exposure as a function of tensile strain. Points show three different repeats for each treatment, the line is the mean.

The variation of insertion loss is not restricted to wavelengths where the waveguide is single moded (1550 nm) but also it follows the same pattern of loss variation over the full spectral range (350 nm- 1750 nm), as shown in Fig. 5-18.

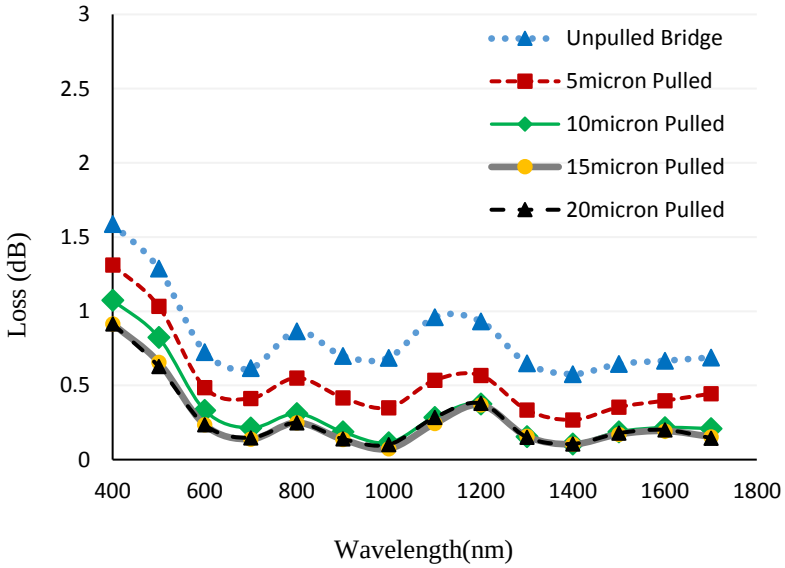

Fig. 5-18: Optical transmission variation of optimum size 300 µm long waveguide under waveguide elongation over a broad spectrum. The waveguide was fabricated from PETA droplet cured for 30 s with beam power of 12.8 µW.

5.9.2 Effect of photobleaching

To investigate the crosslinking degree and conversion rate of polymer structure on the maximum strain value, polymer waveguides were put under tensile strain immediately after rinsing. In the previous case the waveguide was photobleached until the fluorescence weakened (see section 5.9.1) then the stress was applied, but in this experiment the beam was blocked after the rinsing. Waveguides of 300 μm long were fabricated, keeping the same optical and chemical parameters used for medium size waveguide in the previous case. Tensile stress was applied to the polymer bridges when crosslinking is expected to be low [26]. Fig. 5-19 shows an unbleached 300 μm long waveguide under tensile strain. The bright fluorescence indicates that the waveguide is unbleached. The average of maximum tensile strain increased to 32% for three new waveguides, it has increased from 23% for bleached waveguides. The result verifies the hypothesis that the larger the degree of crosslinking and conversion rate the smaller the tensile strain.

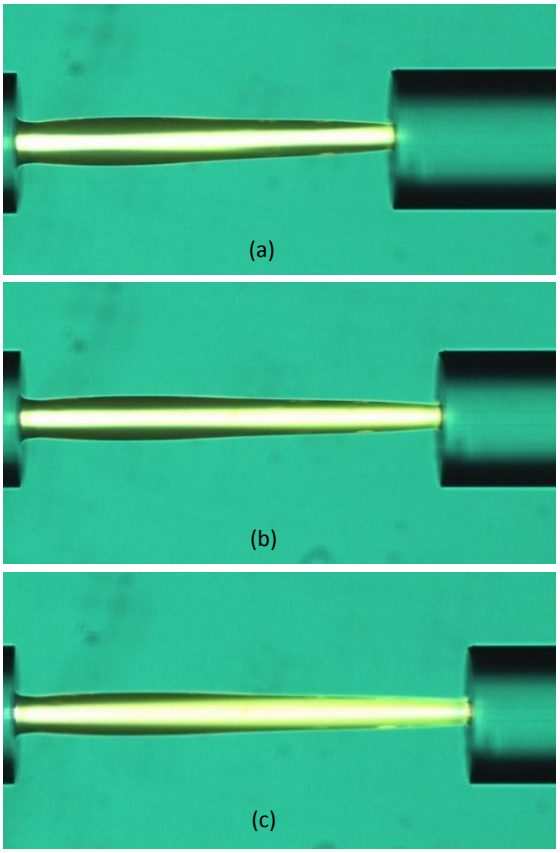

Fig. 5-19: Optical micrographs of 300 μm long waveguide under elongation immediately after rinsing. The waveguide was fabricated from PETA droplet cured for 30 s with beam power of 12.8 μW. a) The waveguide after rinsing. b) Elongated to 345 μm. c) Elongated to 390 μm.

The waveguide waist diameter reduces with tensile strain as illustrated in Figs. 5-19 and 20. The diameter decreases by 10 µm at the centre indicating polymer mechanical flexibility and large stress at interfaces. This phenomenon also shows the impact of adhesion promoter on the self-written polymer waveguide's mechanical and optical performance.

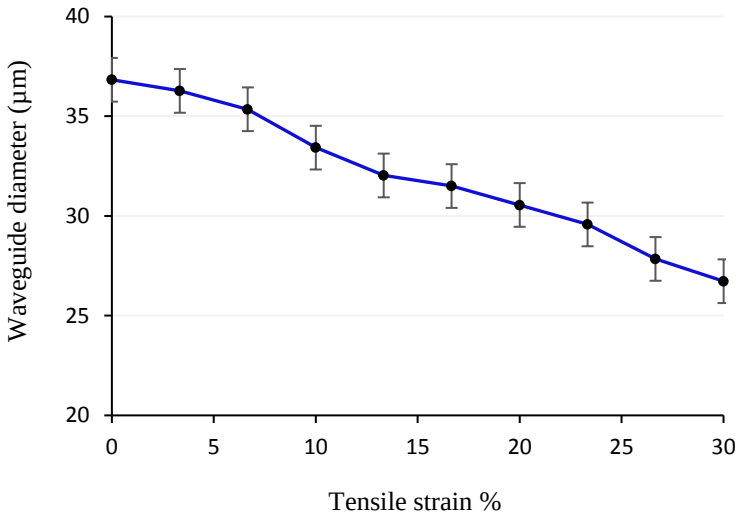

Fig. 5-20: The waist diameter reduction versus tensile strain corresponding to the unbleached 300 µm polymer waveguide shown in Fig. 5-19.

Chapter Six

Optical nonlinearity in self-written polymer waveguides

6.1 Introduction

High transmission materials are vital for electro-optical devices such as ultrafast all optical switches in optical communication systems. Recent advances in this field demands materials with appropriate optical characteristics, for instance strong nonlinearity and low propagation loss. Moreover the material must be efficiently integrated with the system to provide the desired requirements [126]. Self-written polymer waveguides fabricated between two single mode fibres can be a possible entrant for such applications as they can provide high optical transmission and self-alignment with optical fibres [84]. The process is simple and allows us to fabricate waveguides without using sophisticated lithography and precisely positioning an external light source. It also ensures automatic alignment of the polymer channel with the optical fibres [127]. Self-written polymer waveguides have been suggested for some applications such as optical and printed circuit interconnections, splicing, sensing and integrated optical devices [128]. They might be used for nonlinearity applications as well. Here we present a technique to fabricate millimeter long freestanding waveguides with high transmission efficiency to investigate their nonlinear response with a high power short pulse laser. A long interaction length in a polymer waveguide allows self-phase modulation (SPM) features to occur in response to high peak power laser propagation through the polymer structure. The waveguides showed adequate transmission over a broad band from the visible to NIR which also qualifies these polymer microstructures for nonlinearity investigation. None the less it is hard to accurately measure nonlinearity coefficient (γ) and hence nonlinear refractive index (n_2) because not all the optical parameters that are involved with SPM measurement are accurately known. The pulse shape is also one of

the factors which has a significant impact on the output pulse shape and that makes SPM determination difficult. In addition, both the fibre and the waveguide support higher order modes at the laser wavelength which reduce accuracy of assuming some given numbers of modal field distribution and effective area of propagation. In spite of difficulties, we qualitatively demonstrated and measured nonlinear effects occurring in the polymer waveguide through spectral broadening. The effect was also compared with the well known nonlinearity in silica fibre which enables us to measure nonlinearity coefficient (γ) of polymer more presisely.

Nonlinear waveguides have been an interesting field for intense research in the past two decades due to a variety applications in ultra-fast optical switching and supercontinuum generation. Various nonlinear effects have been previously detected in nano- and micro-waveguides such as silicon on insulator [129, 130], silicon nitride [131] silica glass [132] and chalcogenide glass [126], also in crystals [133-135] even in polymer waveguides [136, 137]. Benefiting from its excellent optical transmission and easy fabrication a self-written polymer waveguide is a desirable candidate for nonlinearity investigation. The nonlinear response of such polymer structures mainly occurs because of Kerr effect or third order nonlinear response. The phenomenon implies primarily SPM which may also be accompanied with two photon absorption (TPA) [126, 130].

6.2 Nonlinear optical media

A nonlinear medium is a material in which the optical properties of the material are modified as a result of strong electric field guiding through it [138]. The electromagnetic beam radiates by conventional light sources such as laser driven xenon lamp used to fabricate polymer waveguides is neither monochromatic nor coherent. Intensity of such light sources is small when they propagate through an optical waveguide and their interaction with waveguide material results in familiar phenomena like reflection, scattering, refraction and absorption. Consequently the microscopic properties of the waveguide material remains unchanged since the intensity of guided beam is several orders of magnitude smaller than the intensity of intrinsic electric field in the matter (of the order of 10^9 V/cm). Coherent laser light is sufficiently intense to induce nonlinear effects in a material system. The intensity of electric field associated with high power short pulsed lasers is of order of 10^5 to 10^8 V/cm. It is therefore comparable to interatomic

electric fields in the optical waveguide materials. Beside applied beam intensity the host martial properties are also crucial in how significant the guided beam interacts with the medium. Dielectric materials interact with applied beam through an induced polarization [139].

In linear dielectric medium the relation between polarization density P and applied electric field E is described by:

$$\vec{P} = \epsilon_{\circ}\chi\vec{E} \quad , \tag{6-1}$$

where $\epsilon_{\circ}$ is the permittivity of free space and χ is electric susceptibility of the medium. On the other hand, in nonlinear dielectric media when the applied electric field is strong the former relationship becomes nonlinear and higher order terms involve in the medium polarization and the induced polarization is described by:

$$\vec{P} = \epsilon_{\circ}\chi^{(1)}.\vec{E} + \epsilon_{\circ}\chi^{(2)}:\vec{E}\,\vec{E} + \epsilon_{\circ}\chi^{(3)}\vdots\vec{E}\,\vec{E}\,\vec{E} + \cdots \quad . \tag{6-2}$$

The second order nonlinear term is dominant in materials without centro-symmetry where polarization reverses when electric field is reversed, for instance transparent crystals that allow phase matching such as lithium niobate, potassium dihydrogen phosphate (KDP), and potassium titanyl phosphate (KTP). The nonlinear response of these crystals are used in applications like second harmonic generation. However the second term is zero in optical media possessing centrosymmetric atomic distribution. Therefore in these media the dominant nonlinear term is the third order and the second term is zero [65].

6.3 Optical nonlinearity in Kerr medium

In isotropic and homogeneous optical media, the dominant nonlinear term is the third term when they subjected to high intensity electromagnetic wave are called Kerr media. These materials are called Kerr media and they respond to strong electromagnetic fields through processes such as SPM and third harmonic generation (THG) [65]. Although the

latter requires phase matching [140]. Therefore SPM is the only nonlinear effect that has been investigated in the polymer waveguides reported in chapters 4 and 5. In Kerr media the refractive index in the presence of nonlinear effects is expressed as:

$$\begin{aligned} n(\omega, I) &= n(\omega) + \Delta n \\ &= n(\omega) + n_2 I \ , \end{aligned} \tag{6-3}$$

where $n(\omega)$ is the linear refractive index, n_2 is a medium dependent term called intensity dependent refractive index coefficient or nonlinear-index coefficient related to the third order susceptibility $\chi^{(3)}$ of the medium [61]. It is positive for most of transparent materials [65]. I is the intensity of the pulse. Thus, Δn is proportional to the intensity of the optical field. Also the resultant refractive index $n(\omega, I)$ increases with intensity. The refractive index increment in equ. (6-3) is called optical Kerr effect in which the phase velocity of the wave is a function of its own intensity.

6.4 Nonlinear pulse propagation in Kerr medium

Analysis of high intensity optical signal propagation in self-written polymer waveguide integrated with optical fibres starts from the Maxwell's equations. This is because of the fact that these equations are modified when nonlinearity is taken into consideration. Under nonlinearity condition the displacement current D is determined by:

$$\begin{aligned} \vec{D} &= \epsilon_o \vec{E} + \vec{P} \\ &= \epsilon_o \vec{E} + \vec{P}_{\mathrm{L}} + \vec{P}_{\mathrm{NL}} \ , \end{aligned} \tag{6-4}$$

in which the polarization term includes nonlinear polarization P_{NL} along with linear polarization P_{L}[61]. Therefore the scalar wave equation for isotropic homogeneous dielectric media becomes:

$$\nabla^2 E - \frac{1}{c^2} \frac{\partial^2 E(r,t)}{\partial t^2} = \mu_o \frac{\partial^2 P_{\mathrm{L}}(r,t)}{\partial t^2} + \mu_o \frac{\partial^2 P_{\mathrm{NL}}(r,t)}{\partial t^2} \ , \tag{6-5}$$

where c is the speed of light in vacuum and it relates with ϵ_o and μ_o via $\mu_o \epsilon_o = {}^1/_{c^2}$. Here a relation between the induced polarization P and the electric field E is needed to

complete the picture, as in equ. (6-2). Also it is convenient to separate the fast varying part carrier wave and slowly varying envelope of a pulse with time as the pulse evolves through the waveguide. Consider the nature of evolution of a pulse launched into an optical waveguide in the presence of nonlinearity, it can be more appropriate to work in the frequency domain. Hence electric field is expressed in frequency domain instead of time domain by taking Fourier transform:

$$\tilde{E}(r, \omega - \omega_\circ) = \int_{-\infty}^{+\infty} E(r,t) e^{i(\omega-\omega_\circ)t} dt \quad . \tag{6-6}$$

Thus, the wave equation (6-5), by using equs. (6-2) and (6-4) for P_{L} and P_{NL} can be re-written as:

$$\nabla^2 \tilde{E} \; + \; \epsilon(\omega) k_{\mathrm{o}} \tilde{E} = 0 \quad , \tag{6-7}$$

where

$$\epsilon(\omega) = 1 + \chi_{xx}^{(1)}(\omega) + \epsilon_{NL} \; , \tag{6-8}$$

and

$$\epsilon_{NL} = \frac{3}{4} \chi_{xxxx}^{(3)} |E(r,t)|^2 \; . \tag{6-9}$$

The new dielectric constant can be used to define the refractive index $\tilde{n}$ and the absorption coefficient $\tilde{\alpha}$ in the presence of nonlinearity. Since ϵ_{NL} is intensity dependent then both $\tilde{n}$ and $\tilde{\alpha}$ become intensity dependent as well and they are defined as:

$$\tilde{n} = n + n_2 |E|^2 \; , \qquad \tilde{\alpha} = \alpha \; + \; \alpha_2 |E|^2 \; . \tag{6-10}$$

For conventional waveguides like optical fibre intensity can be expressed as $|E|^2$. Using $\epsilon = \left(\tilde{n} \; + \; i \; {}^{\tilde{\alpha}}/_{2k_o}\right)^2$ with equ. (6-8) and equ. (6-9), the nonlinear index coefficient n_2 and the two-photon absorption coefficient $\tilde{\alpha}$ are given by:

$$\epsilon_{NL} = \frac{3}{8n} \, Re(\chi_{xxxx}^{(3)}) \; , \qquad \alpha_2 = \frac{3\omega}{4nc} \, Im\left(\chi_{xxxx}^{(3)}\right) \; . \tag{6-11}$$

On the other hand, the linear refractive index n and linear absorption coefficient α are related to real and imaginary parts of $\chi_{xx}^{(1)}$ respectively.

To solve the wave equ. (6-7) the method of separation of variables is used. Hence the intensity of the field $\tilde{E}(r, \omega - \omega_\circ)$ is written as a product of the field component in the transverse coordinates of the propagation of wave (r, φ), the component of slowly varying envelope in the z direction $\tilde{A}(z, \omega - \omega_\circ)$, and the fast varying component $e^{i\beta_o z}$

$$\tilde{E}(r, \omega - \omega_\circ) = F(r, \varphi)\tilde{A}(z, \omega - \omega_\circ)e^{i\beta_o z} \quad , \tag{6-12}$$

where β_o is propagation constant. By substituting equ. (6-12) in equ. (6-7) and assuming that second order derivative of the envelope is negligibly small (${\partial^2 \tilde{A}}/{\partial z^2} = 0$), since the rate of spatial evolution is very slow. The following two equations are obtained corresponding to the transverse field and the envelope of the signal [141].

$$\nabla_\perp^2 F + \left[\epsilon(\omega)k_o^2 - \tilde{\beta}^2\right]F = 0 \quad , \tag{6-13}$$

$$2i\beta_o \frac{\partial \tilde{A}}{\partial z} + \left[\tilde{\beta}^2 - \beta_o^2\right]\tilde{A} = 0 \quad . \tag{6-14}$$

The eigenvalue $\tilde{\beta}$ is a function of frequency can be written as:

$$\tilde{\beta}(\omega) = \beta(\omega) + \Delta\beta(\omega) \quad . \tag{6-15}$$

Since the frequency of the signal is narrow, $\tilde{\beta}$ is approximately equal to β_o . Then equ. (6-14) becomes:

$$\frac{\partial \tilde{A}}{\partial z} = i[\beta(\omega) + \Delta\beta(\omega) - \beta_o]\tilde{A} \quad . \tag{6-16}$$

Applying Taylor series expansion around β_o and $\Delta\beta(\omega)$, also taking the inverse Fourier transform of the envelope $\left(\tilde{A}(z, \omega - \omega_\circ) \rightarrow A(z, t)\right)$, then equ. (6-16) becomes:

$$\frac{\partial A}{\partial z} + \beta_1 \frac{\partial A}{\partial t} + \frac{i\beta_2}{2}\frac{\partial A^2}{\partial t^2} + \frac{\alpha}{2}A = i\gamma(\omega_o)|A|^2 A \ , \tag{6-17}$$

where γ is nonlinear parameter and defined by:

$$\gamma(\omega_o) = \frac{n_2(\omega_o)\,\omega_o}{cA_{\text{eff}}}\ , \tag{6-18}$$

and A_{eff} is effective mode area and given by:

$$A_{\text{eff}} = \frac{\left(\iint_{-\infty}^{+\infty}|F(x,y)|^2\,dxdy\right)^2}{\iint_{-\infty}^{+\infty}|F(x,y)|^4\,dxdy}\quad . \tag{6-19}$$

Assuming that the frame of reference is moving with the pulse which has a group velocity of v_g, this assumption requires new time frame corresponding to moving observer. Then new time can be expressed as:

$$T = t - \frac{z}{v_g} = t - \beta_1 z\quad . \tag{6-20}$$

Thus,

$$\beta_1\frac{\partial A}{\partial t} = \beta_1\frac{\partial A}{\partial T}.\frac{\partial T}{\partial t} = \beta_1\left(1-\beta_1 v_g\right)\frac{\partial A}{\partial T} = 0\ , \tag{6-21}$$

therefore equ. (6-17) becomes:

$$\frac{\partial A}{\partial z} + \frac{i\beta_2}{2}\frac{\partial A^2}{\partial T^2} + \frac{\alpha}{2}A - i\gamma(\omega_o)|A|^2A = 0\quad . \tag{6-22}$$

This equation is called the Non-linear Schrödinger equation (NLS) which describes the behaviour of pulse evolution through an optical waveguide in the presence of nonlinear effects. The second term in equ. (6-22) characterizes the group velocity dispersion along the waveguide. The third term represents loss of the waveguide. The last and nonlinear term describes SPM as a result of light-material interaction when high intensity electromagnetic field is launched into the waveguide [140].

Introducing new normalized amplitude $\mathrm{U}(z,T)$ such that the envelope could be written in terms of normalized amplitude as:

$$A(z,T) = \sqrt{P_o}e^{-\frac{\alpha z}{2}}\,\mathrm{U}(z,T)\,. \tag{6-23}$$

Rewriting NLS equation using new amplitude function:

$$\frac{\partial \mathrm{U}}{\partial z} + \frac{i\beta_2}{2}\frac{\partial \mathrm{U}^2}{\partial T^2} = i\frac{e^{-\alpha z}}{L_{NL}}|\mathrm{U}|^2\mathrm{U}\ , \tag{6-24}$$

$$L_{NL} = \frac{1}{\gamma P_o}\ , \tag{6-25}$$

where L_{NL} refers to the characteristic length of a waveguide over which the nonlinearity effect becomes significant.

6.5 Self-phase modulation

When an ultrashort optical pulse propagates through a nonlinear medium, the higher intensity part which is the center part of the pulse faces a higher refractive index of the medium, whereas the lower intensity part or the edges meet a lower refractive index. This intensity dependent local index of refraction results in the nonlinear phenomenon known as SPM. The effect leads to a spectral broadening of the pulse while the temporal shape is unchanged also the intensity profile of the pulse does not change. The spectral broadening of the optical pulse without a corresponding change in the temporal width causes frequency chirping. For polymer waveguide used here nonlinear refractive index is positive. Therefore the leading edge of the pulse is red shifted and the trailing edge is blue shifted with respect to the center frequency of the pulse. This pulse broadening generates new frequencies which lead to further temporal broadening in the presence of dispersion. SPM causes a chirping with lower frequencies in leading edge and higher frequencies in the trailing edge. Contrary to SPM, chirping caused by linear dispersion in the anomalous dispersion regime leads to higher frequencies to travel faster than lower frequencies. Thus, in the existence of mutual compensation of dispersion and SPM a pulse can propagate through the waveguide without significant distortion assuming the waveguide is lossless. Such undistorted signal guiding is called soliton and it is an important application of nonlinearity effect [61, 141].

Considering the nonlinear Schrödinger equation under a condition that we can ignore group velocity dispersion (GVD), in the other words dispersion length is much longer than the optical waveguide length ($L_D \gg L$), one can propose that SPM is the only phenomenon that responsible of spectral broadening providing a condition nonlinear length is shorter than the waveguide length ($L > L_{NL}$).

Regarding polymer waveguides as the channel is too short, then we can neglect the second term on the left hand side, hence equ. (6-24) becomes:

$$\frac{\partial \mathrm{U}}{\partial z} = i\frac{e^{-\alpha z}}{L_{NL}}|\mathrm{U}|^2\mathrm{U} \quad . \tag{6-26}$$

Describing U to be a function of envelope $\mathrm{V}(z,T)$ and nonlinear phase function ϕ_{NL} as $\mathrm{U}(z,T) = V(z,T)e^{i\phi_{NL}}$ and equating real and imaginary parts:

$$\frac{\partial \mathrm{V}}{\partial z} = 0 \ , \qquad \frac{\partial \phi_{NL}}{\partial z} = \frac{e^{-\alpha z}}{L_{NL}}|\mathrm{V}|^2 \quad . \tag{6-27}$$

Equ. (6-27) shows the fact that the amplitude of the pulse remains unchanged with length z, but the phase varies with distance hence we can write:

$$\mathrm{V} = \mathrm{U}(z,T) = \mathrm{U}(0,T) \quad , \tag{6-28}$$

$$\phi_{NL} = \frac{|\mathrm{U}(0,T)|^2}{L_{NL}}\left[\frac{1-e^{-\alpha z}}{\alpha}\right] = |\mathrm{U}(0,T)|^2\ \frac{L_{\mathrm{eff}}}{L_{NL}} \quad . \tag{6-29}$$

The length of the optical waveguide over which the nonlinear effects on pulse propagation may be witnessed is denoted as L_{eff}. The maximum amount of phase change that can occur over this length is given by:

$$\phi_{NL_{max}} = \frac{L_{\mathrm{eff}}}{L_{NL}} = \gamma P_o L_{\mathrm{eff}} \quad , \tag{6-30}$$

The nonlinear phase varies with time as pulse propagates through the waveguide. The time dependence of phase implies that instantaneous frequency across the pulse will be different from the central frequency. The frequency difference is given by:

$$\Delta\omega(T) = -\frac{\partial \phi_{NL}}{\partial T} = -\left(\frac{L_{\text{eff}}}{L_{NL}}\right)\frac{\partial |\mathrm{U}(0,T)|^2}{\partial T} \quad . \tag{6-31}$$

Spectral broadening as a result of SPM is a frequency modification of propagated pulse through the optical waveguide and it occurs as a result of the time dependence of ϕ_{NL}. For a chirped pulse, SPM may lead to either spectral broadening or spectral narrowing depending on the way where the pulse is chirped. However for unchirped pulse broadening will always take place [141]. Furthermore, SPM and hence spectral broadening also depends on the several parameters of the guided pulse as well as structural and optical properties of the waveguide.

6.6 Nonlinearity response of polymer waveguides

Polymer materials generally show higher nonlinear response than silica glass usually used for fibre optics. The magnitude of n_2 is typically very small and of order of (10^{-16} cm^2/W and 10^{-8} cm^2/W) for glass and polymer materials respectively [140]. These magnitudes are very small and can be ignored in the bulk material, but over a small cross-sectional and long length in a fibre cable it might reach some value that could not be ignored because the effect is an accumulative phenomenon over substantial length of optical waveguide. As n_2 is several orders of magnitude larger in polymer than in silica glass, nonlinear effects in polymer structures such as self-written polymer waveguides integrated with fibre optics are anticipated even over short lengths in the range of less than a millimeter to few millimeters.

Laser pulse power is the most crucial parameter to enhance nonlinearity in polymer waveguides. Fundamentally nonlinear effect in bulk polymer materials is very weak, regardless of how much power applied on the material. Even though the average of coupled power into the SMF fibre and then to polymer waveguide is in the range of hundred milliwatts, it is still induce considerable nonlinear effect. The effect appears because the polymer channel is extended between the cores of fibres and has a small

diameter, therefore intensity acquires a value of order of MW/cm^2 [142]. Intensity of this order together with low insertion loss leads to an efficient nonlinear interaction. The effective area of the guiding channel is influential in the nonlinear parameter γ (equ. (6- 30)), so needs to be known for the polymer bridges. In standard single mode fibre the wave is guided mostly in the core region as determined in propagation characteristics of step-index waveguide in chapter 3. Therefore the effective area is approximately equivalent to the core area. However the physical diameter of the polymer waveguide is larger than the core of the fibre, but the overlap integral of fundamental mode between the fibre and polymer must be close to unity because the observed insertion loss is very small.

Because of the significant contribution of effective area in nonlinearity it should be reduced if possible. Although narrowing down the bridge's diameter might increase the value of nonlinearity coefficient, but it causes increased loss as it reduces the overlap integral. Moreover thinner bridges were found not to be able to handle high power as launching average pulse power of about 120 mW breaks polymer bridge, as shown in Fig. 6-1. Therefore coupling high power and reducing waveguide diameter become associated with waveguide damage and high loss.

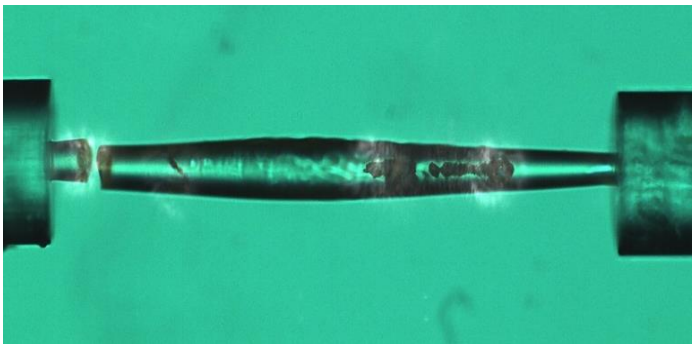

Fig. 6-1: 500 µm PETA polymer waveguide cured by xenon lamp then illuminated by high beam power pulsed laser. Local temperature has increased and broke the channel from several points, the beam emerged from right hand fibre.

The characteristic dispersion length and nonlinear length are decisive whether one can consider ignore dispersion effect or nonlinear effect. For polymer waveguides and optical fibre in the range of 1.5 m one can dismiss the effect of dispersion and only consider the effect of nonlinearity throughout SPM phenomenon [140]. It is therefore most appropriate

to use the longest polymer bridges possible to increase the nonlinear coefficient without being worried about declining optical transmission efficiency.

6.7 Fabrication method of millimeter polymer bridge

To construct a freestanding millimetre long waveguide two main barriers need to be eliminated. Firstly, the light beam power declines considerably at the tail of bridges when curing was done from one fibre resulting in deteriorated surface and a fragile polymer channel as mentioned in section 4.10.1. This was overcome in chapter 5 by coupling both fibres to the light source and curing from both fibres. Secondly, the fibre sizes and monomer viscosity do not allow one to put drops longer than 750 μm even with heavy lubrication. This limitation was eliminated by inserting the fibres into capillaries (ID/OD 300/1000 μm) to grab larger drops. The capillaries also served advantageously by diminishing the impact of oxygen quenching by increasing the diffusion length of surrounding oxygen from the drop/air interface to the polymerization reaction site. The experimental setup for polymer waveguide fabrication was the same as used in Fig. 5-10. Initially the fibre ends were treated by adhesion promoter for 20 min. Then each fibre was put inside a capillary to hold a bigger drop and hence a longer liquid bridge before curing. The pre-polymerization processes is the same as explained in bidirectional curing polymer bridge fabrication in section 5.7. Before curing the input power was reduced and then the long-pass filter was removed to trigger photopolymerization as shown in Fig. 6- 2(a). Then the curing power was gradually increased until the two beams unified at the middle of the deposited droplet and the reaction progress was monitored by taking repeated pictures, Fig. 6-2 (b-e).

Waveguide bridge formation takes a few seconds, but full formation of robust channel needs about 5-10 min of photocuring depending on the waveguide length, desired cross section and oxygen quenching condition. The remaining uncured monomer was rinsed off using ethanol, leaving an exposed polymer waveguide bridge rigidly attached between the fibre ends as an extension of the fibre cores, as shown in Fig. 6-2(f).

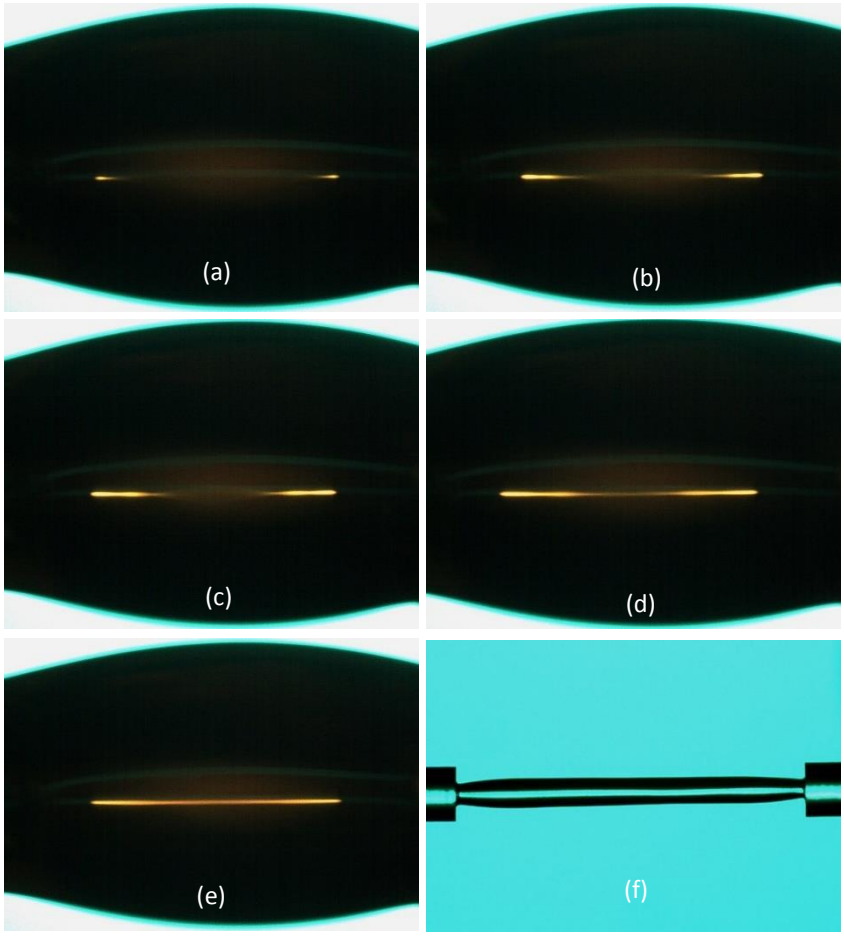

Fig. 6-2: Optical microscope images of a 1.2 mm length photopolymer waveguide writing. a) Photopolymerization triggered, then at b) 2.5 s, c) at 8.5 s, d) 15 s, e) 2 min, and f) after rinsing.

For polymer bridges up to 600 µm long a constant illumination was used during fabrication, whereas for millimeter range waveguides constant exposure led to a bridge which was thinner at the vicinity of the fibres and became wider toward the middle. The phenomenon also reported by Yamashita *et al*. through an investigation includes long waveguides at the end of multimode fibre [109]. The phenomenon is likely because of that when the curing beam comes out from the fibre it will polymerize the liquid at the vicinity of the fibre's core very quickly, and the writing beam will be strongly confined within converted part. Then as polymerization develops far from the fibre ends the previously solidified part of the waveguide absorbs some power. The mitigated beam will slow down the polymerization rate and the refractive index conversion rate, hence the refractive index evolution extends toward the edges of the enlarged beam which also

helped by the drop size that makes oxygen diffusion length relatively longer. Therefore to deal with this obstacle also to fabricate stable and more uniform shaped bridge the photocuring power was adjusted during the photopolymerization reaction. The curing power was increased gradually until the two beams combined at the midpoint leaving polymerization progress to obtain proper bridge with smooth surface as in Fig. 6-2(f). Observing the two beams meeting in the centre (Fig. 6-2(e)) does not mean a proper bridge has been formed. Intensity weakening as both curing beams advance through the PETA droplet causes incomplete polymerization and a nonuniform surface at the centre of the bridge as shown in Fig. 6- 3(a). The uneven surface is zoomed in in Fig. 6-3(b) which appears as corrugated features indicating weak polymerization.

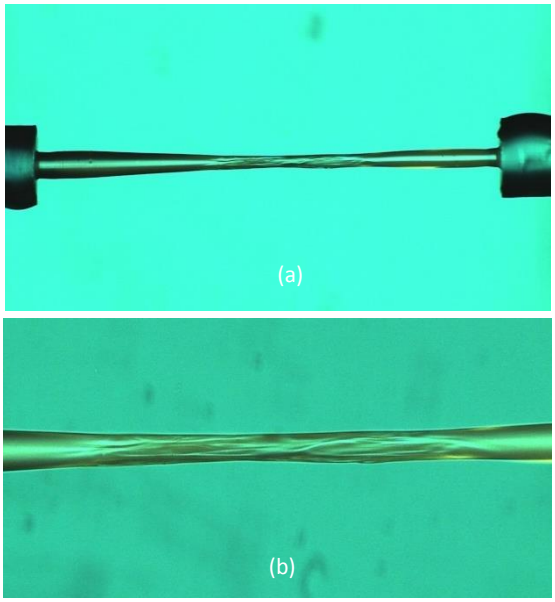

Fig. 6-3: a) Optical microscope images of a 1.3 mm long waveguide rinsed after two beams met at the midpoint after 2 min from polymerization initiation. b) Deteriorated region, intensity of writing beam declined at about 0.5 mm from the fibre ends.

The surface deterioration can be overcome by extending illumination for several minutes after the two beams meeting. This was assisted by the long diffusion length of oxygenation particularly at the centre because of the size of the droplet. In contrast, the similar surface morphology fault seen in chapter 4 did not vanish when the fibres were not inserted into capillaries no matter how long photocuring was extended after bridge formation.

6.8 Optical transmission of millimeter waveguides

Long polymer bridges showed excellent optical transmission. Fig. 6-4 shows insertion loss spectrum of 1 mm air gap and the polymer waveguide, referenced to the transmission of plain fibre between the source and OSA. There are some features associated with a sudden increase of loss beyond 1600 nm which was not observed for waveguides below 750 µm [84]. The absorption of the Eosin between 400 and 550 nm is also clearly visible. The absorption peak becomes higher and higher as waveguide length increases because there will be larger amount of unbleached photoinitiator left in the bridge structure. The peak associated with 400 µm bridge is 2 dB as shown in Fig. 4-10, but it increases to 5 dB with 1 mm waveguide. Except the aforementioned abrupt features, the final polymer waveguide bridge shows little residual absorption and a low loss ~1 dB across the whole spectral range.

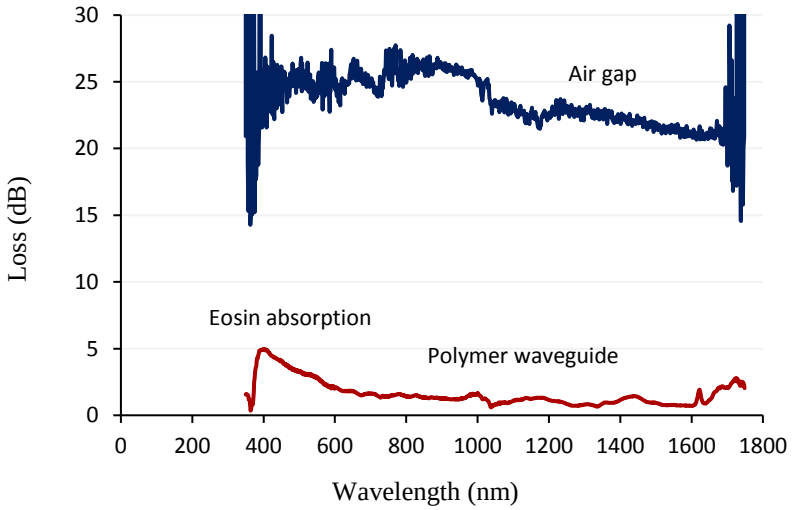

Fig. 6-4: Loss as a function of wavelength associated with 1mm air gap and polymer waveguide fabricated from PETA droplet contained 0.5 wt. % Eosin, and the it photocured for 8 min. Then the rinsed bridge illuminated for 15 min to allow extra photobleaching to maximize optical transmission.

The high transmission efficiency and strong mechanical characteristics of long polymer waveguides are mainly attributed to the new techniques used in fabrication

process such as adhesion promoter, bidirectional curing, and embedding fibre ends in the capillaries. The new approach also leads to rectifying the surface morphology deteriorations which previously resulted in relatively rapid increase in loss with 500 µm and 600 µm bridges [84]. A 1 mm long waveguide showed loss of 0.8 dB at 1550 nm. Fig. 6-5 is the extension of the same trend shown in Figs. 4-11 and 5-14, where the polymer bridge length is almost doubled by using capillaries.

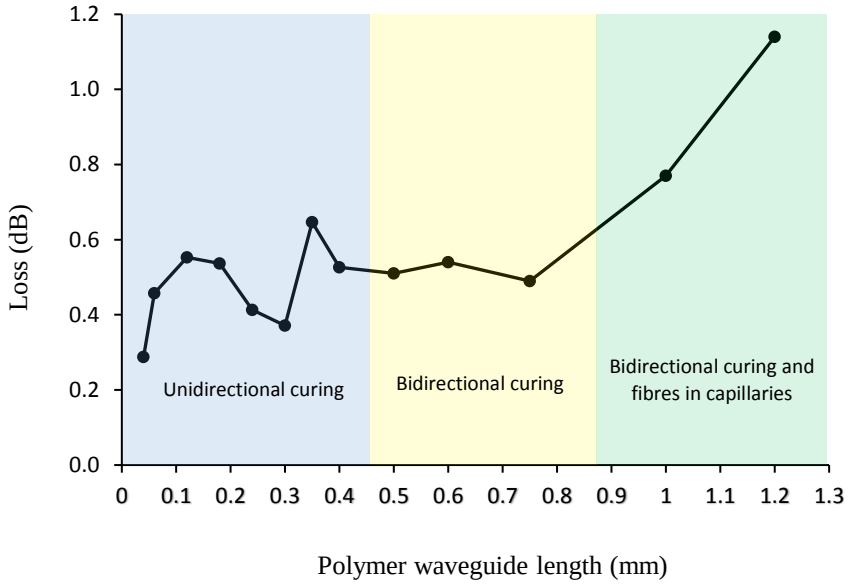

Fig. 6-5: Loss development of polymer waveguides as a function of waveguide length. Data taken from spectra as in Fig. 6-4 averaged from 1500 –1600 nm, in the single moded region of the fibre.

To show the details of loss development associated with polymer waveguide the loss of air gap excluded as it monotonically increases with the gap length. the loss has been kept under 1 dB up to 1 mm waveguide length and it only reached 1.1 dB with a 1.2 mm waveguide. The insertion loss increased by only 0.8 dB when the waveguide length increased from 0.04 mm to 1.2 mm, in the spectral region where the fibre is single moded. At other wavelengths the attenuation was similar, even at shorter wavelengths where the fibre is multimode. For each waveguide length the lowest loss was targeted, and at least two to three low-loss waveguides were fabricated, with the better loss presented in Fig. 6- 5. The fabrication process also showed very high reproducibility alongside the excellent optical and mechanical performances, particularly with new fabrication procedures.

6.9 Spectral broadening in polymer waveguides

To observe a spectral broadening, a transform limited pulses from a laser (*Fianium* – femtopower ultrafast laser 1064 nm) were propagated through a polymer waveguide as shown in Fig. 6-6. The laser emits 220 fs pulses at a wavelength of 1064 nm, with an average power of 80 mW and repetition rate of 10 MHz. The incident power was varied with half wave plate and polarizer. The power was measured in front of the waveguide and the coupled peak power was calculated considering coupling efficiency of 55%. Then the light was launched into an SMF 28e fibre by an objective lens and the pulse evolution was monitored from the other end by an OSA. To minimize the nonlinearity caused by fibre itself we used 1.5 m of fibre, which was the minimum possible length to fabricate waveguide in between two pieces also to couple the input fibre with pulsed laser after waveguide fabrication. This physical length (L) is also shorter than the dispersion length (L_D) for silica fibre which is about 3 m when a pulse of 220 fs at 1064 nm propagate through the fibre.

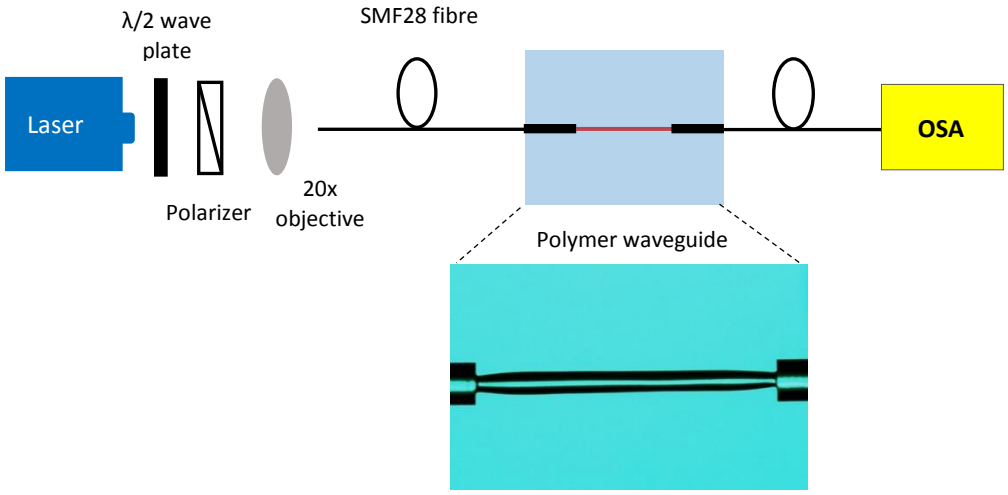

Fig. 6-6: Experimental setup of propagating high power pulsed laser through a polymer waveguide to investigate spectral broadening.

Fig. 6-7 shows pulse evolution at three different beam powers corresponding to 1.5 m of plain fibre and 1.2 mm polymer waveguide integrated with a 1.5 m total length of fibre.

Considerable spectral broadening was observed when the beam propagated through the polymer bridge in each power level. The outer set of spectra correspond to the polymer waveguide, which shows that spectrum has been significantly broadened by polymer channel compared to the plain silica fibre which is represented by the inner set of spectra. This is remarkable as the polymer length is 1000 times less than the fibre length, indicating the strength of the polymer nonlinearity. The comparison confirms that the nonlinearity coefficient of the polymer waveguide is at least thousand times higher than that of silica fibre.

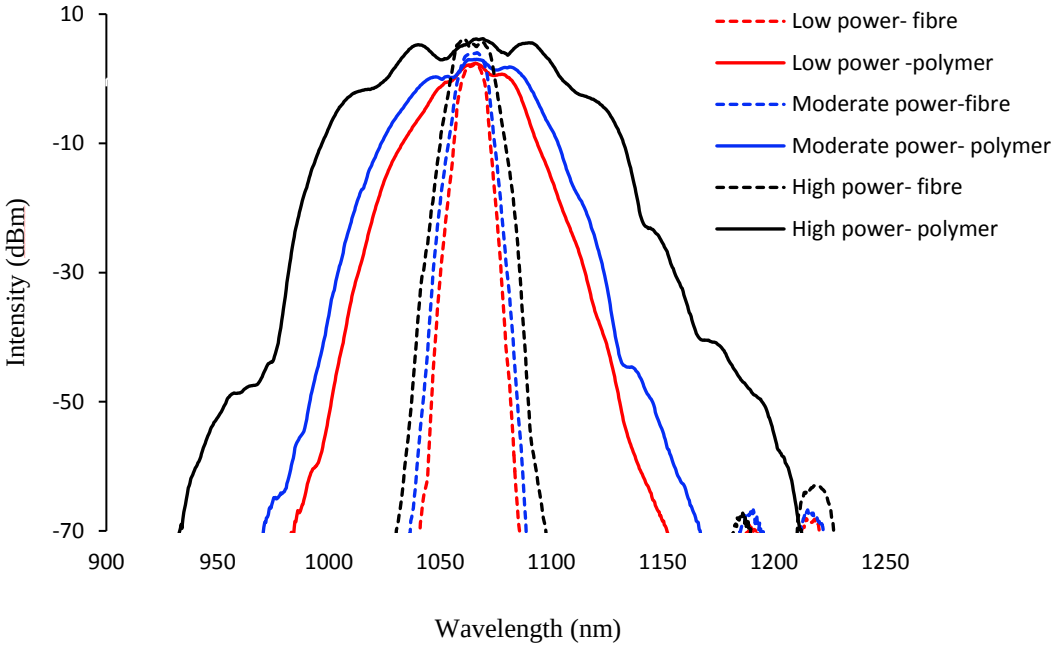

Fig. 6-7: Optical spectra and intensity dependence of spectral broadening associated with the short pulse laser passing through 1.5 m long plain fibre (inner set- dashed lines) and 1.2 mm polymer waveguide fabricated between two fibres of 1.5 m total length (outer set- solid lines).

Figs. 6-8 and 6-9 show spectral evolution in linear scale corresponding to the logarithmic scale shown in Fig. 6-7 in four different peak power levels. The spectra have broadened as the peak power increased in both the fibre and the polymer waveguide. The broadening was accompanied by development of oscillatory characteristic in the output spectra [143]. The origin of this oscillatory features can be attributed to frequency chirp induced by the time dependence of SPM. Therefore there will be two points of the same instantaneous frequency in the pulse but different phase. The phase difference

consequently, causes constructive or destructive interference between the two points that essentially manifest two waves of the same frequency [141]. The multipeak features associated with the polymer channel are more obvious compared with that of the plain fibre which originated from the interference of the chirped frequency components induced by SPM.

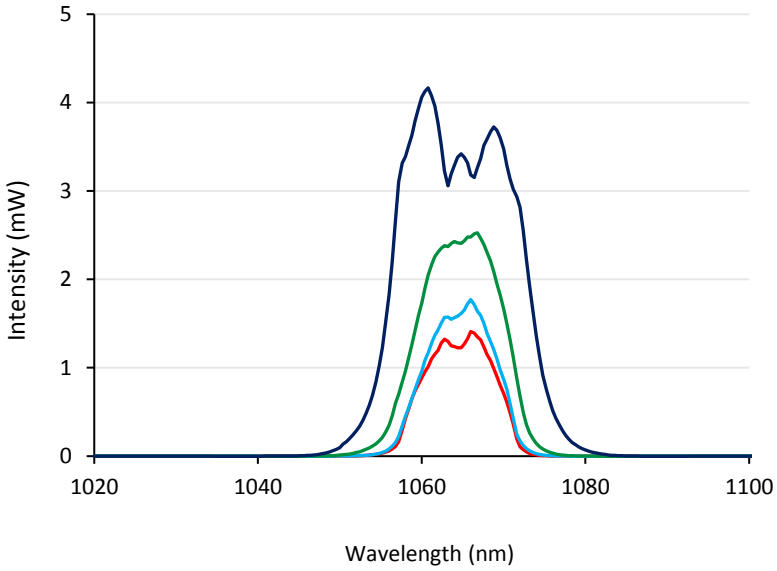

Fig. 6-8: Spectrum evolution associated with 1.5 m plain fibre as a result of increasing coupled peak power through following steps (3, 3.5, 6 and 13 kW). As the coupled power is increased the spectrum broadens due to self-phase modulation effect.

From Fig. 6-9 the full-width at half maximum (FWHM) of the pulse spectrum increases as peak coupled power increases from 3 kW to 11 kW which is a clear indication of spectral broadening induced by SPM under the nonlinearity response of the polymer structure. SPM induces new frequency generation as a consequence of temporal phase shifting of the incident ultrashort pulses, assuming that group velocity dispersion can be neglected due to the fact that waveguide length (L) is shorter than dispersion length (L_{D}) [144]. Furthermore, spectral broadening induced by the SPM is directly proportional to the effective nonlinear coefficient γ, peak power and effective length of the waveguide. Qualitatively speaking the nonlinear coefficient associated with the polymer material is much higher than that of silica fibre as it is clear from Figs. 6-7 and 6-8, because the oscillatory features are obvious in the polymer bridge which indicates the maximum

phase shift occurred in the polymer is larger than that of the plain fibre. Consider the highest power, the maximum phase shift can be estimated to be about 2.5π, compared with the standard phase shift occurred in the plain fibre by propagating Gaussian pulse through it presented in ref. [141]. Therefore using equ. (6-30) we can calculate γ to be in the range of 800-1300 W^{-1} km^{-1} which is about three orders of magnitude larger than that of silica fibre. This range of nonlinearity in polymer waveguides was also reported elsewhere. Chon *et al*. investigated SPM in polymer waveguide fabricated by spinning a PMMA-styrene-acrylonitrile matrix doped with squarylium dye onto a silver-ion-exchanged single-mode (at λ = 1.5 μm) waveguide in BK7 glass. The measured value of nonlinear refractive index of the polymer matrix was three orders of magnitude greater than that of silica fibre [137].

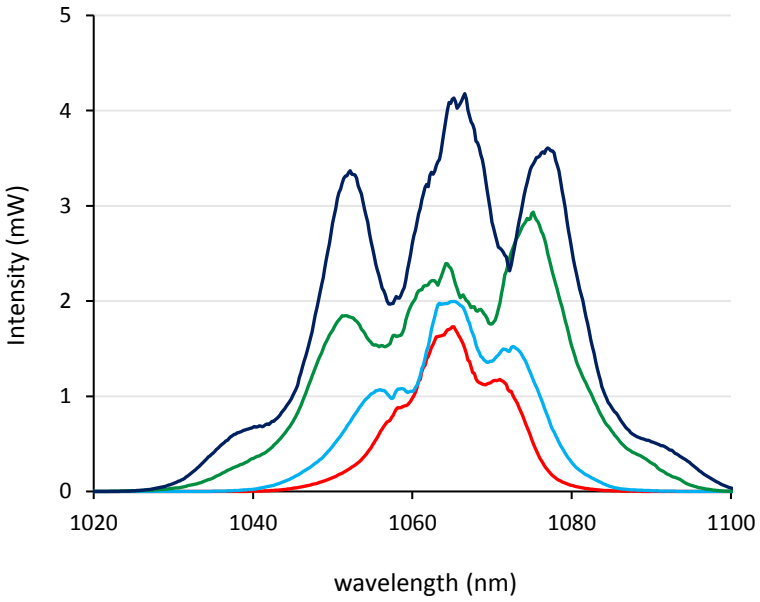

Fig. 6-9: Spectral broadening of transmitted light with the coupled peak power increased (3, 4.5, 7 and 11kW) observed for polymer waveguide of 1.2 mm length waveguide has transmission loss of 1.1 dB.

Any effort here to calculate the nonlinearity coefficient in the polymer waveguide will be a qualitative measurement because many crucial parameters in the calculation are not well known and several approximations have been employed. For instance the input pulse shape is significant such that equations used here assumed that the pulse is Gaussian which cannot be completely guaranteed. Moreover the fibre supports higher order modes

at the pulse wavelength, hence the beam profile in the polymer waveguide is not simple to determine. Never the less, the results are promising to investigate further nonlinearity measurements in this polymer structures by doping them with particles which can improve the nonlinear properties further.

Chapter Seven

Conclusion and Future work

7.1 Conclusion

Free radical photopolymerization was implemented to polymerize liquid monomers. Acrylate monomers undergo polymerization by illuminating them with high intensity UV light or extend their curing sensitivity to visible by adding appropriate photoinitiators and coinitiators. The incident light excites photoinitiator molecules to higher energy states which derive free radicals by reaction with an electron donor coinitiator amine. The reactive species open carbon-carbon double bonds by adding to nearby monomer molecules to form combined free radicals. Then polymer chains are generated by adding more monomer molecules.

Polymer waveguides were fabricated from an acrylate based three compound system (PETA) and commercial adhesives (NOAs) by using self-written technique. For the first time the fabrication process involved spatially controlled photopolymerization of a liquid monomer drop deposited between two fibres using a broadband incoherent light source. Curing by a broadband incoherent laser driven xenon lamp showed some advantages over conventional monochromatic laser curing. Firstly, it provides a beam profile more like Gaussian beam at the end of optical fibre which leads to uniform single structure. Secondly, the wide spectrum was employed to investigate optical transmission efficiency of the polymer waveguides over the spectral range (350 – 1750 nm) rather than at single wavelength.

Waveguides were optically characterized as an interconnecting bridge between two single mode optical fibres. The particular technological goal worked on was to address the lack of long (> 500 μm) freestanding polymer waveguide between two single mode fibres in literature. The fabrication process showed high reproducibility, although polymer bridges were fragile at the polymer to fibre interfaces and the adhesion bonding

between two different materials was weak. About one third of the bridges did not survive rinsing. A part from the mechanical deficiency, polymer waveguides up to 600 µm long showed high optical transmission with less than 1.2 dB loss (and less than 0.5 dB over 400 µm) over a broad spectral region from the visible to the near infrared. Some limitations prevented extending polymer waveguide length beyond 600 µm. The main one was the curing power from the light source was not sufficient to cure bridges longer than 600 µm because the beam intensity reduction caused some undesired morphological effects on the surface of the waveguide and lead to increasing loss. The other limitation was the size of the fibre which only allows them to hold a monomer drop which could only be extended to about 750 µm.

In order to improve chemical bonding at the polymer/fibre interfaces adhesion promoter was used to modify the fibre ends before photopolymerization. The adhesion promoter with methoxysilyl groups react with the fibre by covalently binding to –Si-O-H groups on the silica surface. On the other side the methacrylate tail of the adhesion promoter polymerizes with the PETA system. The treatment showed a profound effect on the polymer bridges' mechanical performance such that the bridges not only resisted aggressive rinsing but also showed high flexibility to transverse misalignment and tensile stress. Furthermore, the photocuring was done bi-directionally from both fibres instead of uni-directional curing from one fibre. Bi-directional illumination resulted in more uniform waveguides and improved the quality of bridges morphologically as well as optically. It enabled us to extend the waveguide lengths to 750 µm with insertion loss less than 1 dB. The new approach lead to improve the polymer/ fibre interaction area from both interfaces it also caused maximum lateral misalignment to increase from 120 µm to 170 µm for 400 µm long waveguides. The optical transmission of polymer waveguides was also improved under tensile stress such that the loss of 300 µm waveguide reduced from 0.8 dB to 0.3 dB after applying a strain of 5 %. The polymer channels also showed higher tensile strain before damage while they had less crosslinking i.e. when the waveguide was not completely photobleached after rinsing the maximum strain increased from 23% to 32%.

Adhesion promoter and bidirectional curing significantly improved mechanical properties of self written waveguides, but fibre diameter still remained main obstacle to extend the bridge length to millimetre ranges. Therefore to fabricate longer bridges the fibre ends were inserted into glass capillaries with dimensions ID/OD 300/1000µm,

which allowed a deposited droplet to be extended to about 3 mm. However available curing power only allowed us to fabricate polymer waveguides up to 1.2 mm with optical loss about 1.1 dB. Such high transmission alongside with millimetre effective length and small effective area can qualify polymer waveguides to show some nonlinear response under high power ultra short pulsed lasers. A 1.2 mm polymer waveguides were illuminated with pulsed laser ($\lambda = 1064$ nm, $\tau = 220$ fs) and the output spectrum was broadened remarkably compared with the output from 1.5 m of untreated fibre. The pulse broadening showed that the nonlinearity coefficient of polymer material is about > 1000 times higher than that of silica.

7.2 Future work

The basic demands from polymer waveguides integrated with optical fibres to be implemented in optical system are; easy fabrication and processibility, low loss, high mechanical stability and satisfactory adhesion bonding to optical fibre. The photopolymerization technique provides excellent fabrication tool which facilitate self-alignment and no post polymerization processes are needed. Self-written polymer waveguides showed promising characteristics to be used in real applications. However optical transmission and mechanical properties still require intensive effort to qualify these types of integrated waveguides to be implemented at least in local networking communication and sensing applications. In addition, exploring different raw materials with some pre-polymerization modifications can discover other monomer materials to be used as the backbone of polymer waveguides. In this context, the following steps can be taken to further investigate self-written polymer waveguides, or may upgrade their quality to be used in applications.

- Extending the polymer waveguide length by using high power curing source such as stable supercontinuum light source. This allow the researcher to measure insertion loss more rigorously by using cut-back method and measure the real attenuation of polymer structure to distinguish between that the loss caused by the polymer/ fibre interfaces.

- Using different monomer systems with lower and higher functionality for instance bi- acrylate or tetra-acrylate based transparent monomers to investigate the impact of

crosslinking on the optical transmission. Also using various photoinitiators with different absorption spectral range.

- Purifying monomer or the photopolymerizable solution from lumps and other scattering centres formed during preparation by using fine filters. Or doping the monomer with heavy fluorine to replace some hydrogen atom in C-H bonds.

- Narrow bridges showed high losses compared with the bridges which have diameter larger than that of the core of SMF 28e fibre because of stronger evanescent field associated with smaller diameter waveguides. Cladding narrow bridges with different photopolymerizable system which has refractive index slightly smaller than that of PETA may reduce loss by providing better light confinement.

- Splicing fibres with different sizes by short polymer bridges and compare with the other splicing techniques.

- Integrating polymer structures with different shapes and various radius of curvatures to be used in coupling and imaging applications for instance coupling fibre into light sources, detectors and microchips efficiently.

These steps could improve the optical characteristics of polymer bridges and allow one to expand the research in this field. Also extending the waveguide length improves the nonlinearity response of the waveguide to be implemented in nonlinear optics applications.

References

[1] Y. Koike, and T. Ishigure, "High-Bandwidth Plastic Optical Fiber for Fiber to the Display," *Journal ofLightwave Technology,* vol. 24, no. 12, pp. 4541-4553, 2006.

[2] S. J. Frisken, "Light-induced optical waveguide uptapers," *Optics Letters,* vol. 18, pp. 1038-1037, 1993.

[3] R. Bachelot, A. Fares, R. Fikri, D. Barchiesi, G. Lerondel, and P. Royer, "Coupling semiconductor lasers into single-mode optical fibers by use of tips grown by photopolymerization," *Optics Letters,* vol. 29, no. 17, pp. 1971-1972, 2004.

[4] Z. Sedaghat, A. Rumyantseva, A. Bruyant, S. Kostcheev, S. Blaize, S. Jradi, R. Bachelot, and A. Monmayrant, "Near-field optical imaging with a nanotip grown on fibered polymer microlens," *Applied Physics Letters,* vol. 100, no. 3, pp. 033107(1-3), 2012.

[5] Herbert Sturmer, J. Michael Kohler, and T. M. Jovin, "Microstructured polymer tips for scanning near-field optical microscopy," *Ultramicroscopy* vol. 71, pp. 107-110, 1998.

[6] S. Jradi, O. Soppera, and D. J. Lougnot, "Fabrication of polymer waveguides between two optical fibers using spatially controlled light-induced polymerization," *Applied Optics,* vol. 47, no. 22, pp. 3987-3993, 2008.

[7] J. Missinne, S. Beri, M. Dash, S. Samal, P. Dubruel, J. Watte, and G. Van Steenberge, "Curing kinetics of step-index and graded-index single mode polymer self-written waveguides," *Optical Materials Express,* vol. 4, no. 7, pp. 1324-1335, 2014.

[8] K. Yamashita, E. Fukuzawa, H. Okada, and K. Oe, "Fiber-to-fiber optical gain of polymer-based amplifier with self-written active waveguide," *Japanese Journal of Applied Physics,* vol. 48, no. 10, pp. 1024061-1024064, 2009.

[9] A. Günther, A. B. Petermann, U. Gleissner, T. Hanemann, E. Reithmeier, M. Rahlves, M. Meinhardt-Wollweber, U. Morgner, and B. Roth, "Cladded self-written multimode step-index waveguides using a one-polymer approach," *Optics Letters,* vol. 40, no. 8, pp. 1830- 1833, 2015.

[10] K. Ikemura, and T. Endo, "A review of the development of radical photopolymerization initiators used for designing light-curing dental adhesives and resin composites," *Dental Materials Journal,* vol. 29, no. 5, pp. 481-501, 2010.

[11] J. P. Fouassier, and J. Lalevee, *Photoinitiators for Polymer Synthesis: Scope, Reactivity and Efficiency*, Weinheim: Wiley, 2012.

[12] R. Schwalm, *UV Coatings: Basics, Recent developments and new application*, Amsterdam: Elsevier Science, 2006.

[13] R. Kimmich, and N. Fatkullin, "Polymer Chain Dynamics and NMR," *NMR, 3D Analysis, Photopolymerization*, Advances in Polymer Science 170, A. Abe, ed., New York: Springer 2004.

[14] J. P. Fouassier, *Photoinitiation, Photopolymerization, and Photocuring: Fundamentals and Applications*, Munich: Hanser Publishers, 1995.

[15] H. J. Hageman, "Photoinittors for free radical polymerization," *Progress in Organic Coatings, ,* vol. 13, pp. 123 - 150, 1985.

[16] Y. Yagci, S. Jockusch, and N. J. Turro, "Photoinitiated polymerization: Advances, challenges, and opportunities," *Macromolecules,* vol. 43, no. 15, pp. 6245-6260, 2010.

[17] R. Tripathy, J. V. Crivello, and R. Faust, "Photoinitiated polymerization of acrylate, methacrylate, and vinyl ether end-functional polyisobutylene macromonomers," *Journal of Polymer Science Part A: Polymer Chemistry,* vol. 51, no. 2, pp. 305-317, 2013.

[18] A. K. O'Brien, and C. N. Bowman, "Modeling Thermal and Optical Effects on Photopolymerization Systems," *Macromolecules,* vol. 36, pp. 7777-7782, 2003.

[19] D. J. Dyer, "Photoinitiated Synthesis of Grafted Polymers," vol. 197, pp. 47-65, 2006.

[20] H. F. Gruber, "Photoinitiators for free radical polymerization," *Progress in Polymer Science,* vol. 17, pp. 953-1044, 1992.

[21] R. Suriano, M. Levi, E. Emilitri, C. Momo, and S. Turri, "Fabrication of Sealed μ-Channels Through a Fast and Reliable Photopolymerization Process," *Macromolecular Materials and Engineering,* vol. 296, no. 7, pp. 666-676, 2011.

[22] K. Dietliker, R. Hüsler, J. L. Birbaum, S. Ilg, S. Villeneuve, K. Studer, T. Jung, J. Benkhoff, H. Kura, A. Matsumoto, and H. Oka, "Advancements in photoinitiators-Opening up new applications for radiation curing," *Progress in Organic Coatings,* vol. 58, no. 2-3, pp. 146-157, 2007.

[23] J. V. Crivello, and E. Reichmanis, "Photopolymer Materials and Processes for Advanced Technologies," *Chem. Mat.,* vol. 26, no. 1, pp. 533-548, 2014.

[24] K. D. Belfield, and J. V. Crivello, "Preface," *Photoinitiated Polymerization*, ACS Symposium Series K. D. Belfield and J. V. Crivello, eds., Washington DC: American Chemical Society, 2003.

[25] D. Dendukuri, P. Panda, R. Haghgooie, J. M. Kim, T. A. Hatton, and P. S. Doyle, "Modeling of Oxygen-Inhibited Free Radical Photopolymerization in a PDMS Microfluidic Device," *Macromolecules,* vol. 41, no. 22, pp. 8547-8556, 2008.

[26] G. Odian, *Principles of Polymerization*, Fourth ed., New Jersy: John Wiley 2004.

[27] T. Scherzer, W. Knolle, S. Naumov, and L. Prager, “Investigations on the Photoinitiator-free Photopolymerization of Acrylates by Vibrational Spectroscopic Methods,” *Macromolecular Symposia,* vol. 230, no. 1, pp. 173-182, 2005.

[28] J. Kabatc, and K. Jurek, "The Comparison of the Photoinitiating Ability of the Dyeing Photoinitiating Systems Acting via Photoreducible or Parallel Series Mechanism," *Molecular Photochemistry-Various Aspects*, S. Saha, ed., pp. 243-264: InTech, 2012.

[29] N. S. Allen, “Photoinitiators for UV and visible curing of coatings: Mechanisms and properties,” *Journal of Photochemistry and Photobiology A: Chemistry,* vol. 100, no. 1-3, pp. 101-107, 1996.

[30] J. P. Fouassier, X. Allonas, J. Laleve´e, and C. Dietlin, "Photoinitiators for Free Radical Polymerization Reaction," *Handbook of photochemistry and photophysics of polymer materials* N. S. Allen, ed., pp. 351-420, New Jersy: John Wiley, 2010.

[31] R. Schwalm, *UV Coatings Basics, Recent Developments and New Applications* Elsevier Science, 2006.

[32] A. Ibrahim, L. Stefano, O. Tarzi, H. Tar, C. Ley, and X. Allonas, “High-performance photoinitiating systems for free radical photopolymerization. Application to holographic recording,” *Photochem Photobiol,* vol. 89, no. 6, pp. 1283-1290, 2013.

[33] I. Capek, “On photoinduced polymerization of acrylamide,” *Designed Monomers and Polymers,* vol. 17, no. 4, pp. 356-363, 2014.

[34] J. V. Crivello, “A new visible light sensitive photoinitiator system for the cationic polymerization of epoxides,” *Journal of Polymer Science Part A: Polymer Chemistry,* vol. 47, no. 3, pp. 866-875, 2009.

[35] C. Barner-Kowollik, P. Vana, and T. P. Davis, "The Kinetics of Free Radical Polymerization," *Handbook of Radical Polymerization*, K. Matyjaszewski and T. P. Davis, eds., pp. 187-262, New Jersey: Wiley, 2002.

[36] J. G. Drobny, *Radiation Technology for Polymers*, Second ed., Florida: CRC Press, 2010.

[37] M. F. Perry, and G. W. Young, “A Mathematical Model for Photopolymerization From a Stationary Laser Light Source,” *Macromolecular Theory and Simulations,* vol. 14, no. 1, pp. 26-39, 2005.

[38] B.D. Malhotra, *Handbook of Polymers in Electronics*, UK: Rapra Technology, 2002.

[39] H. Cao, E. Currie, M. Tilley, and Y. C. Jean, "Oxygen Inhibition Effect on Surface Properties of UV-Curable Acrylate Coatings," *Photoinitiated Polymerization*, ACS Symposium Series K. D. Belfield and J. V. Crivello, eds., pp. 152-164, Washington DC: American Chemical Society, 2003.

[40] K. Taki, Y. Watanabe, H. Ito, and M. Ohshima, “Effect of Oxygen Inhibition on the Kinetic Constants of the UV-Radical Photopolymerization of Diurethane Dimethacrylate/Photoinitiator Systems,” *Macromolecules,* vol. 47, no. 6, pp. 1906-1913, 2014.

[41] A. K. O'Brien, and C. N. Bowman, “Impact of Oxygen on Photopolymerization Kinetics and Polymer Structure,” *Macromolecules,* vol. 39, no. 7, pp. 2501-2506, 2006.

[42] E. Andrzejewska, “Photopolymerization kinetics of multifunctional monomers,” *Progress in Polymer Science,* vol. 26, pp. 605-665, 2001.

[43] C. Decker, D. Decker, and F. Morel, "Light Intensity and Temperature Effect in Photoinitiated Polymerization," *Photopolymerization Fundamentals and Applications*, ACS Symposium Series A. B. Scranton, ed., pp. 63-80, Washington DC: American Chemical Society, 1997.

[44] B. Falk, S. M. Vallians, and J. V. Crivello, “Monitoring Photopolymerization Reactions with Optical Pyrometry,” *Journal of Polymer Science: Part A: Polymer Chemistry,* vol. 41, pp. 579-596, 2003.

[45] C. P. Jiang, Y. M. Huang, and C. H. Liu, “Dynamic finite element analysis of photopolymerization in stereolithography,” *Rapid Prototyping Journal,* vol. 12, no. 3, pp. 173-180, 2006.

[46] S. K. Moorjani, B. Rangarajan, and A. B. Scranton, "Effect of Viscosity on the Rate of Photosensitization of Diaryliodonium Salts by Anthracene," *Photopolymerization Fundamentals and Applications*, ACS Symposium Volume A. B. Scranton, ed., pp. 95-106, Washington DC: American Chemical Society, 1997.

[47] K. Makino, Y. Akimoto, K. Koike, A. Kondo, A. Inoue, and Y. Koike, “Low Loss and High Bandwidth Polystyrene-Based Graded Index Polymer Optical Fiber,” *Journal of Lightwave Technology, ,* vol. 31, no. 14, pp. 2407-2412, 2013.

[48] K. Okamoto, *Fundamentals of optical waveguides*, 2nd ed., Amsterdam: Elsevier 2006.

[49] A. W. Snyder, and J. D. Love, *Optical Waveguide Theory*, Boston: Kluwer Academic, 1983.

[50] G. P. Agrawal, *Fiber Optic Communication Systems*, 4th ed., New Jersy: Wiley, 2010.

[51] R. G. Hunsperger, *Integrated Optics: Theory and Technology*, 6th ed., New York: Springer, 2009.

[52] A. Ghatak, *Optics*, New York: McGraw-Hill, 2010.

[53] A. D. Ryer, *Light Measurement Handbook*, USA: International light Inc., 1997.

[54] X. C. Tong, "Advanced Materials for Integrated Optical Waveguides," *Springer Series in Advanced Microelectronics*, K. Itoh, ed., Springer, 2014.

[55] O. Ziemann, J. Krauser, P. E. Zamzow, and W. Daum, *POF Handbook: Optical Short Range Transmission System*, 2nd ed., Berlin: Springer, 2008.

[56] L. Ibbotson, *The Fundamentals of Signal Transmission: In Line, Waveguide, Fibre and Free Space*, London: Elsevier, 1999.

[57] K. Thyagarajan, and A. Ghatak, *Fiber Optic Essentials*, New Jersey: Wiley, 2007.

[58] N. J. Cronin, *Microwave and Optical Waveguides*: IOP Publishing, 1995.

[59] http://www.riwoodward.com/wp-content/uploads/2015/06/fibre_modes.jpg.

[60] A. K. Ghatak, and K. Thyagarajan, *Contemporary Optics*, 1st ed., New York: Plenum Press, 1978.

[61] Ajoy Ghatak, and a. K. Thyagarajan, *Introduction to fiber optics*, Cambridge: Cambridge University Press, 1998.

[62] P. L. Chu, "Recent Development of a Polymer Optical Fiber and its Applications," *Guided Wave Optical Components and Devices: Basics, Technology and Applications* B. P. Pal, ed., pp. 27-40, Amsterdam: Elsevier, 2006.

[63] H. M. Lee, W. Y. Hwang, M. C. Oh, H. Park, T. Zyung, and J. J. Kim, "High performance electro-optic polymer waveguide device," *Applied Physics Letters,* vol. 71, no. 26, pp. 3779-3781, 1997.

[64] W. Groh, "Overtone absorption in macromolecules for polymer optical fibers," *Macromolecular Chemistry and Physics,* vol. 189, no. 12, pp. 2861–2874, 1988.

[65] B. E. A. Saleh, and M. C. Teich, *Fundamentals of Photonics*, 2nd ed., New York: Wiley, 2007.

[66] D. Kato, "Light coupling from a stripe-geometry GaAs diode laser into an optical fiber with spherical end," *Journal of Applied Physics,* vol. 44, no. 6, pp. 2756-2758, 1973.

[67] H. M. Presby, A. F. Benner, and C. A. Edwards, "Laser micromachining of efficient fiber microlenses," *Applied Optics,* vol. 29, pp. 2692-2695, 1990.

[68] G. Eisenstein, and D. Vitello, "Chemically etched conical microlenses for coupling single-mode lasers into single-mode fibers," *Applied optics,* vol. 21, no. 19, pp. 3470, 1982.

[69] M. Hocine, R. Bachelot, C. Ecoffet, N. Fressengeas, P. Royer, and G. Kugel, "End-of-fiber polymer tip: manufacturing and modeling," *Synthetic Metals,* vol. 127, no. 1-3, pp. 313-318, 2002.

[70] R. Bachelot, S. Blaize, C. Pang, A. Bruyant, and P. Royer, "Polymer-Tipped Optical Fibers," *Fiber and Integrated Optics,* vol. 27, no. 6, pp. 542-558, 2008.

[71] S. Jradi, O. Soppera, D. J. Lougnot, R. Bachelot, and P. Royer, "Tailoring the geometry of polymer tips on the end of optical fibers via control of physico-chemical parameters," *Optical Materials,* vol. 31, no. 4, pp. 640-646, 2009.

[72] T. Monro, C. M. De Sterke, and L. Poladian, "Catching light in its own trap," *Journal of Modern Optics,* vol. 48, no. 2, pp. 191-238, 2001.

[73] A. S. Kewitsch, and A. Yariv, "Self-focusing and self-trapping of optical beams upon photopolymerization," *Optics Letters,* vol. 21, no. 1, pp. 24-26, 1996.

[74] A. Espanet, C. Ecoffet, and D. J. Lougnot, "PEW: Photopolymerization by evanescent waves. II. Revealing dramatic inhibiting effects of oxygen at submicrometer scale," *Journal of Polymer Science: Polymer Chemistry,* vol. 37, no. 13, pp. 2075-2085, 1999.

[75] S. Shoji, S. Kawata, A. A. Sukhorukov, and Y. Kivshar, "Self-written waveguides in photopolymerizable resins," *Optics Letters,* vol. 27, no. 3, pp. 185-187, 2002.

[76] C. Pang, F. Gesuele, A. Bruyant, S. Blaize, G. Lérondel, and a. P. Royer, "Enhanced light coupling in sub-wavelength single-mode silicon on insulator waveguides," *Optics Express,* vol. 17, pp. 6939-6945, 2009.

[77] H. Wang, K.-S. Lee, S. Li, L. Jin, S.-K. Lee, Y. Wu, Y.-H. Cho, and J. Cai, "Fabrication of CdSe–ZnS nanocrystal-based local fluorescent aperture probes by active polymerization of photosensitive epoxy," *Optics Communications,* vol. 281, no. 6, pp. 1588-1592, 2008.

[78] R. Bachelot, C. Ecoffet, D. Deloeil, P. Royer, and D.-J. Lougnot, "Integration of micrometer-sized polymer elements at the end of optical fibers by free-radical photopolymerization," *Applied Optics,* vol. 40, no. 32, pp. 5860-5871, 2001.

[79] M. Hocine, N. Fressengeas, G. Kugel, C. Carre, D. J. Lougnot, R. Bachelot, and P. Royer, "Modeling the growth of a polymer microtip on an optical fiber end," *Journal of the Optical Society of America B: Optical Physics,* vol. 23, no. 4, pp. 611-620, 2006.

[80] C. Ecoffet, A. Espanet, and D. J. Lougnot, "Photopolymerization by Evanescent Waves: A New Method to Obtain Nanoparts," *Advanced Materials,* vol. 10, no. 5, pp. 411-414, 1998.

[81] K. Dorkenoo, A. van Wonderen, H. Bulou, M. Romeo, O. Cregut, and A. Fort, "Time-resolved measurement of the refractive index for photopolymerization processes," *Applied Physics Letters,* vol. 83, no. 12, pp. 2474-2476, 2003.

[82] A. O'Brien, and C. Bowman, "Impact of oxygen on photopolymerization kinetics and polymer structure," *Macromolecules,* vol. 39, no. 7, pp. 2501-2506, 2006.

[83] B. Pinto-Iguanero, A. Olivares-Perez, and I. Fuentes-Tapia, “Holographic material film composed by Norland Noa 65 adhesive,” *Optical Materials,* vol. 20, no. 3, pp. 225-232, 2002.

[84] P. Mohammed, and W. Wadsworth, “Long, free-standing polymer waveguides fabricated between single mode optical fiber cores,” *Journal of Lightwave Technology,* vol. 33, no. 20, pp. 4384-4389, 2015.

[85] T. M. Monro, C. Martijn de Sterke, and L. Poladian, “Self-writing a waveguide in glass using photosensitivity ” *Optics Communications,* vol. 119, pp. 523-526, 1995.

[86] S. K. Anthony, and Y. Amnon, “Nonlinear optical properties of photoresists for projection lithography,” *Applied Physics Letters,* vol. 68, pp. 455, 1996.

[87] S. N. Mensov, and Y. V. Polushtaytsev, “On the efficiency of optical joining of fibres in a photopolymerisable composition,” *Quantum Electronics,* vol. 37, no. 9, pp. 881-884, 2007.

[88] K. Dorkenoo, O. Crégut, L. Mager, F. Gillot, C. Carre, and A. Fort, “Quasi-solitonic behavior of self-written waveguides created by photopolymerization,” *Optics Letters,* vol. 27, no. 20, pp. 1782-1784, 2002.

[89] C. Ecoffet, and D. J. Lougnot, “Light-induced self-writing welding of optical fiber,” *Journal of Lightwave Technology,* vol. 28, no. 8, pp. 1278-1283, 2010.

[90] U. Streppel, P. Dannberg, C. Wächter, A. Bräuer, and R. Kowarschik, “Formation of micro-optical structures by self-writing processes in photosensitive polymers,” *Applied Optics,* vol. 42, no. 18, pp. 3570-3579, 2003.

[91] L. Tong, F. Zi, X. Guo, and J. Lou, “Optical microfibers and nanofibers: A tutorial,” *Optics Communications,* vol. 285, no. 23, pp. 4641-4647, 2012.

[92] F. Gu, L. Zhang, X. Yin, and L. Tong, “Polymer Single-Nanowire Optical Sensors,” *Nano Letters,* vol. 8, no. 9, pp. 2757-2761, 2008.

[93] K. Ramanathan, M. A. Bangar, M. Yun, W. Chen, N. V. Myung, and A. Mulchandani, “Bioaffinity Sensing Using Biologically Functionalized Conducting-Polymer Nanowire,” *Journal of the American Chemical Society,* vol. 127, pp. 496-497, 2005.

[94] Y. Soeda, T. Enomoto, and O. Mikami, "Self-written waveguide technology with light-curable resin enabling easy optical interconnection," 2013, pp. 1-4.

[95] C. Bin, K. Kyoji, S. Okihiro, K. Manabu, T. Masaaki, M. Takayuki, and K. Toshikuni, “A three-dimensional polymeric optical circuit fabrication using a femtosecond laser-assisted self-written waveguide technique,” *Applied Physics Letters,* vol. 92, pp. 253302, 2008.

[96] K. Yamashita, E. Fukuzawa, A. Kitanobou, and K. Oe, “Self-written active waveguide for integrated optical amplifiers,” *Applied Physics Letters,* vol. 92, pp. 051102(1-3), 2008.

[97] J. Yang, M. B. J. Diemeer, G. Sengo, M. Pollnau, and A. Driessen, "Nd-Doped Polymer Waveguide Amplifiers," *Journal of Quantum Electronics,* vol. 46, no. 7, pp. 1043-1050, 2010.

[98] H. Li, Y. Dong, P. Xu, Y. Qi, C. Guo, and J. T. Sheridan, "Beam self-cleanup by use of self-written waveguide generated by photopolymerization," *Optics letters,* vol. 40, no. 13, pp. 2981, 2015.

[99] S. Shoji, and S. Kawata, "Optically-induced growth of fiber patterns into a photopolymerizable resin," *Applied Physics Letters,* vol. 75, no. 5, pp. 737-739, 1999.

[100] K. D. Dorkenoo, F. Gillot, O. Crégut, Y. Sonnefraud, A. Fort, and H. Leblond, "Control of the refractive index in photopolymerizable materials for (2+1)D solitary wave guide formation," *Physical review letters,* vol. 93, no. 14, pp. 143905, 2004.

[101] R. J. Black, S. Lacroix, F. Gonthier, and J. D. Love, "Tapered single-mode fibres and devices Part 2. Experimental and theoretical quantification," *IEE Proceedings J - Optoelectronics,* vol. 138, no. 5, pp. 355-364, 1991.

[102] G. Brambilla, V. Finazzi, and D. Richardson, "Ultra-low-loss optical fiber nanotapers," *Optics express,* vol. 12, no. 10, pp. 2258-2263, 2004.

[103] G. Yongmin Jung, D. J. Brambilla, and D. J. Richardson, "Efficient higher-order mode filtering in multimode optical fiber based on an optical microwire," in Asia Optical Fiber Communication and Optoelectronic Shanghai, China, 2008, pp. 1-3.

[104] O. Soppera, C. Turck, and D. J. Lougnot, "Fabrication of micro-optical devices by self-guiding photopolymerization in the near IR," *Optics Letters,* vol. 34, no. 4, pp. 461-463, 2009.

[105] S. Liu, M. R. Gleeson, J. Guo, and J. T. Sheridan, "Optical characterization of photopolymers materials: theoretical and experimental examination of primary radical generation," *Applied Physics B,* vol. 100, no. 3, pp. 559-569, 2010.

[106] H. Haiying, A. Majumdar, and J. S. Cho, "Fabrication and evaluation of hybrid silica/polymer optical fibre sensors for large strain measurement," *Transactions of the Institute of Measurement and Control,* vol. 31, no. 3-4, pp. 247-257, 2009.

[107] U. Streppel, P. Dannberg, Ch. Wachter, A. Brauer, and R. Kowarschik, "Formation of micro-optical structures by self-writing processes in photosensitive polymers," *Applied Optics,* vol. 42, no. 18, pp. 3570-3579, 2003.

[108] S. N. Mensov, Y. V. Polushtaitsev, E. M. Dianov, M. I. Belovolov, and V. B. Makhalov, "Visible radiation-induced connection of single-mode IR fibres in a photopolymerising composition," *Quantum Electronics,* vol. 38, no. 12, pp. 1142-1146, 2008.

[109] T. Yamashita, M. Kagami, and H. Ito, “Waveguide shape control and loss properties of light-induced self-written (LISW) optical waveguides,” *Journal of Lightwave Technology,* vol. 20, no. 8, pp. 1556-1562, 2002.

[110] N. Hirose, T. Yoshimura, and O. Ibaragi, "Optical solder effects of self-written waveguides in optical circuit devices coupling." pp. 223-228.

[111] Q. Sun, K. Ueno, and H. Misawa, “In situ investigation of the shrinkage of photopolymerized micro/nanostructures: the effect of the drying process,” *Optics letters,* vol. 37, no. 4, pp. 710-712, 2012.

[112] K. Yamashita, T. Kuro, K. Oe, K. Mune, K. Tagawa, R. Naitou, and A. Mochizuki, “Fabrication of self-written waveguide in photosensitive polyimide resin by controlling photochemical reaction of photosensitizer,” *Applied Physics Letters,* vol. 85, no. 18, 2004.

[113] H. Jung, D. Keum, and K.-H. Jeong, “Laser induced self-aligned microlens and waveguide arrays using a self-writing process in a photosensitive polymer resin,” in International Solid-State Sensors, Actuators and Microsystems Conference, Colorado, USA, 2009, pp. 497-500.

[114] T. Shioda, N. Watanabe, H. Ozawa, and O. Mikami, “Effects of dye on formation and properties of light-induced self-written waveguide,” *Japanese Journal of Applied Physics, Part 2: Letters,* vol. 43, no. 8 A, pp. L1023-L1025, 2004.

[115] H. E. Williams, D. J. Freppon, S. M. Kuebler, R. C. Rumpf, and M. A. Melino, “Fabrication of three-dimensional micro-photonic structures on the tip of optical fibers using SU-8,” *Optics express,* vol. 19, no. 23, pp. 22910, 2011.

[116] K. W. Cheng, M. A. Uddin, H. P. Chan, and S. C. Chan, “Optical alignment tolerances in double-side irradiated self-written waveguide-induced fiber arrays packages,” *Optics Communications,* vol. 283, no. 13, pp. 2669-2675, 2010.

[117] H. Huang, A. Majumdar, and J. S. Cho, “Fabrication and evaluation of hybridsilica/polymer optical fibre sensors forlarge strain measurement,” *Transactions of the Institute of Measurement and Control,* vol. 31, no. 3/4, pp. 247-257, 2009.

[118] T. Matsui, T. Yamashita, and M. Kagami, “Improvement in positioning accuracy of light-induced self-written polymeric optical waveguide using an optical solder effect,” *Japanese Journal of Applied Physics, Part 2,* vol. 45, no. 37-41, pp. 1033-1035, 2006.

[119] T. Yoshimura, M. Iida, and H. Nawata, “Self-aligned optical couplings by self-organized waveguides toward luminescent targets in organic/inorganic hybrid materials,” *Optics Letters,* vol. 39, no. 12, pp. 3496-3499, Jun 15, 2014.

[120] T. Yoshimura, and M. Seki, “Simulation of self-organized parallel waveguides targeting nanoscale luminescent objects,” *Journal of the Optical Society of America B,* vol. 30, no. 6, pp. 1643, 2013.

[121] S. N. Mensov, and Y. V. Polushtaytsev, "Formation of Nonrectilinear Waveguide Structures upon the Interaction of Counterpropagating Beams in Photopolymerizable Media," *Laser Physics,* vol. 18, pp. 424-429, 2008.

[122] S. J. Marshall, S. C. Bayne, R. Baier, A. P. Tomsia, and G. W. Marshall, "A review of adhesion science," *Dental Materials,* vol. 26, no. 2, pp. 11-16, 2010.

[123] D. J. dos Santos, and G. F. Batalha, "Failure criterion for adhesively bonded joints using Arcan´s experimental method," *Polímeros,* vol. 24, no. 4, pp. 441-445, 2014.

[124] T. A. Birks, I. Gris Sanchez, S. Yerolatsitis, S. G. Leon-Saval, and R. R. Thomson, "The photonic lantern," 2015.

[125] S. G. Leon-Saval, A. Argyros, and J. Bland-Hawthorn, "Photonic lanterns: a study of light propagation in multimode to single-mode converters," *Optics express,* vol. 18, no. 8, pp. 8430, 2010.

[126] J. M. Laniel, N. Hô, R. Vallée, and A. Villeneuve, "Nonlinear-refractive-index measurement in As 2 S 3 channel waveguides by asymmetric self-phase modulation," *Journal of the Optical Society of America B: Optical Physics,* vol. 22, no. 2, pp. 437-445, 2005.

[127] A. Jemal, M. Ben Belgacem, S. Kamoun, M. Gargouri, K. Dorkenoo, A. Barsella, and L. Mager, "Electro-optic phase modulation in light induced self-written waveguides propagated in a 5CB doped photopolymer," *Optics Express,* vol. 21, no. 2, pp. 1541-1546, 2013.

[128] T. Yoshimura, J. Roman, Y. Takahashi, W. C. V. Wang, M. Inao, T. Ishitsuka, K. Tsukamoto, S. Aoki, K. Motoyoshi, and W. Sotoyama, "Self-organizing lightwave network (SOLNET) and its application to film optical circuit substrates," *IEEE Transactions on Components and Packaging Technologies,* vol. 24, no. 3, pp. 500-509, 2001.

[129] M. A. Foster, A. C. Turner, J. E. Sharping, B. S. Schmidt, M. Lipson, and A. L. Gaeta, "Broad-band optical parametric gain on a silicon photonic chip," *Nature,* vol. 441, no. 7096, pp. 960, 2006.

[130] G. W. Rieger, K. S. Virk, and J. F. Young, "Nonlinear propagation of ultrafast 1.5 μm pulses in high-index-contrast silicon-on-insulator waveguides," *Applied Physics Letters,* vol. 84, no. 6, pp. 900-902, 2004.

[131] J. Levy, A. Gondarenko, M. A. Foster, A. Turner-Foster, A. L. Gaeta, and M. Lipson, "CMOS-compatible multiple-wavelength oscillator for on-chip optical interconnects," *Nature Photonics,* vol. 4, no. 1, pp. 37-40, 2010.

[132] A. Pasquazi, Y. Park, J. Azaña, F. Légaré, R. Morandotti, B. E. Little, S. T. Chu, and D. J. Moss, "Efficient wavelength conversion and net parametric gain via four wave mixing in a high index doped silica waveguide," *Optics express,* vol. 18, no. 8, pp. 7634, 2010.

[133] E. Y. M. Teraoka, D. H. Broaddus, T. Kita, A. Tsukazaki, M. Kawasaki, A. L. Gaeta, and H. Yamada, "Self-phase modulation at visible wavelengths in nonlinear ZnO channel waveguides," *Applied Physics Letters,* vol. 97, no. 7, 2010.

[134] H. Ono, and I. Saito, "Characterization of self-phase modulation in liquid crystals on dye-doped polymer films," *Japanese Journal of Applied Physics, Part 1: Regular Papers and Short Notes and Review Papers,* vol. 38, no. 10, pp. 5971-5976, 1999.

[135] K. Dolgaleva, W. C. Ng, L. Qian, J. S. Aitchison, M. C. Camasta, and M. Sorel, "Broadband self-phase modulation, cross-phase modulation, and four-wave mixing in 9 mm long AlGaAs waveguides," *Optics letters,* vol. 35, no. 24, pp. 4093-4095, 2010.

[136] A. Jemal, M. B. Belgacem, S. Kamoun, M. Gargouri, K. D. Dorkenoo, A. Barsella, and L. Mager, "Electro-optic phase modulation in light induced self-written waveguides propagated in a 5CB doped photopolymer," *Optics Express,* vol. 21, no. 2, pp. 1541-1546, 2013.

[137] J. C. Chon, and A. R. Mickelson, "Fabrication and characterization of a third-order nonlinear organic-polymer composite glass waveguide: a self-phase modulator," *Applied Optics,* vol. 33, no. 30, pp. 6935-6941, 1994.

[138] R. W. Boyd, *Nonlinear Optics*, 3rd ed., Amsterdam: Academic Press, 2008.

[139] H. Abramczyk, *Introduction to Laser Spectroscopy*, New York: Elsevier, 2005.

[140] T. Schneider, *Nonlinear Optics in Telecommunications*, 1st ed., New York: Springer, 2004.

[141] G. Agrawal, *Nonlinear Fiber Optics*, 4th ed., Burlington: Elsevier Science, 2010.

[142] J. A. Buck, "Nonlinear effects in Optical fibers," *Fiber optics handbook fiber, devices, and systems for optical communications* M. Bass and E.W. Van Stryland, eds., New York: McGraw-Hill, 2002.

[143] C. Y. Tai, J. S. Wilkinson, N. M. B. Perney, M. C. Netti, C. E. Cattaneo, J. J. Finlayson, and J. J. Baumberg, "Determination of nonlinear refractive index in a Ta2O5 rib waveguide using self-phase modulation," *Optics Express,* vol. 12, no. 21, pp. 5110-5116, 2004.

[144] Y. Y. Lin, C. L. Wu, W. C. Chi, Y. J. Chiu, Y. Hung, A. K. Chu, and C. K. Lee, "Self-phase modulation in highly confined submicron Ta2O5 channel waveguides," *Optics express,* vol. 24, no. 19, pp. 21633-21641, 2016.